THE ATMOSPHERE OF VENUS

V. I. MOROZ

Space Research Institute, Academy of Sciences, Moscow, U.S.S.R.

(Received 9 March, 1981)

Abstract. The investigations of Venus take a special position in planetary researches. It was just the atmosphere of Venus where first measurements *in situ* were carried out by means of the equipment delivered by a space probe (Venera 4, 1967). Venus appeared to be the first neighbor planet whose surface had been seen by us in the direct nearness made possible by means of the phototelevision device (Venera 9 and Venera 10, 1975).

The reasons for the high interest in this planet are very simple. This planet is like the Earth by its mass, size and amount of energy obtained from the Sun and at the same time it differs sharply by the character of its atmosphere and climate.

We hope that the investigations of Venus will lead us to define more precisely the idea of complex physical and physical-chemical processes which rule the evolution of planetary atmospheres. We hope to learn to forecast this evolution and maybe, in the far future, to control it.

The last expeditions to Venus carried out in 1978 – American (Pioneer-Venus) and Soviet (Venera 11 and 12) – brought much news and it is interesting to sum up the results just now. The contents of this review are:

1. The planet Venus – basic astronomical data.
2. Chemical composition.
3. Temperature, pressure, density (from 0 to 100 km).
4. Clouds.
5. Thermal regime and greenhouse effect.
6. Dynamics.
7. Chemical processes.
8. Upper atmosphere.
9. Origin and evolution.
10. Problems for future studies.

Here we have attempted to review the data published up to 1979 and partly in 1980. The list of references is not exhaustive. Publications of special issues of magazines and collected articles concerning separate space expeditions became traditional last time. The results obtained on the Soviet space probes Venera 9, 10 (the first publications) are collected in the special issues of *Kosmicheskie issledovanija* (**14**, Nos. 5, 6, 1975), analogous material about Venera 11, 12 is given at *Pis'ma Astron. Zh.* (**5**, Nos. 1 and 5, 1978), and in *Kosmicheskie issledovanija* (**16**, No. 5, 1979). The results of Pioneer-Venus mission are represented in two Science issues (**203**, No. 4382; **205**, No. 4401) and special issue of *J. Geophys. Res.* (1980). We shall mention some articles to the same topic among previous surveys: (Moroz, 1971; Sagan, 1971; Marov, 1972; Hunten *et al.*, 1977; Hoffman *et al.*, 1977) and also the books by Kuzmin and Marov (1974) and Kondrat'ev (1977). Some useful information in the part of ground-based observations may be found in the older sources (for example, Sharonov, 1965; Moroz, 1967). For briefness we shall use as a rule the abbreviations of space missions names: V4 instead of Venera 4, M10 instead of Mariner 10 and so on. The first artificial satellites of Venus in the world (orbiters Venera 9 and 10) we shall mark as V9-O, V10-O unlike the descent probes V9, V10. Fly-by modules of Venera 11 and Venera 12 we shall mark as V11-F and V12-F. Pioneers descent probes – Large (Sounder), Day, Night and North – will be marked as P-L, P-D, P-Ni, P-No, orbiter as P-O, and bus as P-B.

1. The Planet Venus – Basic Astronomical Data

Basic astronomical data which is useful as reference material is collected in Table I. We shall discuss two questions in more detail because they are important for our

Space Science Reviews **29** (1981) 3–127. 0038–6308/81/0291–0003 $18.75.

TABLE I

The main astronomical data

Major semiaxis, AU.	0.723 332
Eccentricity	0.006 787
Inclination of the orbital plan to ecliptic	3°23′40″
Siderial period of revolution	$224\,701^{d}$
Sinodial period of revolution	583.92^{d}
Radius of the solid surface, km	6052[a]
Mass, g	$(4.871 \pm 0.004)\,10^{27}$
Relation of the mass of the Sun to the mass of Venus	$408\,523.9 \pm 1.2$[b]
Relation of the mass of Venus to the mass of the Earth	0.815 03
Average density, $g\ cm^{-3}$	5.24
Gravity acceleration on the surface, $cm\ s^{-2}$	887.0
Escape velocity, $km\ s^{-1}$	10.4
Period of rotation	243.01 ± 0.03^{d} [c, d]
Duration of the solar day	116.7^{d}
Equatorial inclination	$2.6 \pm 0.5°$ [d]
Solar flux on the orbit of Venus, $W\ m^{-2}$	2600 ± 25[e]
Integral Bond albedo	0.75 ± 0.03[f]
Effective temperature of the planet, K	231 ± 7[f]
Temperature of the surface, K	735 ± 3
Atmospheric pressure by the surface, atm	90 ± 2

[a] From ground-based radar and simultaneous M5 trajectory measurements/radar (Anderson *et al.*, 1968). Radar experiments on Pioneer orbiter give averaged radius of 6051.3 km for 80% of the planetary surface (Pettengill *et al.*, 1980).
[b] Howard *et al.* (1974).
[c] 'Reverse' rotation.
[d] Shapiro *et al.* (1974).
[e] For the average distance from the Sun 0.7233 AU and solar constant 1.95 $cal\ cm^{-2}\ min^{-1}$ ($1360\ W\ m^{-2}$).
[f] See Section 5.1.

topic: (a) axial rotation of the planet, (b) radiation of Venus as a celestial body. Further (c) we shall represent the list of space probes in use for the investigation of Venus.

A. *The Axial Rotation* of Venus has four particularities:

(1) The direction of axial rotation is unusual: it is clock-wise looking from the north pole whereas all the other planets of the solar system and the Sun itself rotate in the opposite direction. In the same direction all the planets move along their orbits. So the direction of Venusian axial rotation is known as 'reverse'.

(2) The speed of axial rotation is small. The periods of rotation ($P_a = 243^{d}$) and of revolution ($P_s = 225^{d}$) are close. It gives the duration of the solar day ($P_t = 117^{d}$) as roughly equal to half of P_a (and P_s) because

$$\frac{1}{P_t} = \frac{1}{P_a} + \frac{1}{P_s} \tag{1.1}$$

in the case of reverse rotation. Day and night are long on Venus. However we shall

see later that it doesn't lead to big daily variations of the atmospheric parameters (see Sections 3 and 5).

(3) The inclination of the equator to the plane of the orbit is small and so the change of seasons is absent on Venus.

(4) The siderial rotation period corresponds to the resonance with the relative motion of the Earth and Venus almost exactly: in the inferior conjunction (during the maximal approach of both planets) Venus turns to the Earth by the same side. It is necessary to have $P_a = 243.16^d$ for the exact resonance but apparently the true period is slightly less (Shapiro *et al.*, 1979).

The atmosphere of the planet doesn't permit us to observe the surface in the optical region, but it is transparent for radio waves. Data about the rotation of the planetary solid body are obtained as the result of radar measurements which have been done in the U.S.A. and the U.S.S.R. over the last 20 years.

During visual observations of Venus by means of a telescope the planetary disk seems to be very homogeneous. However, rather contrasting details are revealed on the photographs in the ultraviolet region ($\lambda \simeq 0.35$ μm). It is possible to determine the period of rotation on the base of such details' motion. The period is about 4^d, much less than radar measurements give. The contradiction is solved simply if we suppose that the ultraviolet details are the clouds and their apparent speed of motion is determined by the wind and not by the planetary rotation. We shall return to this question in Sections 4 and 6.

B. *The Spectrum* of the outgoing radiation of Venus (as with every planet) has two maxima. The first (shortwavelength) is corresponding to the reflected solar emission and the second (longwavelength) to the thermal radiation of the planet. Stellar magnitude and albedo are the main planetary radiation parameters in the region of reflected solar emission. The most reliable measurements of the visual magnitude of Venus (Müller, 1893; Danjon, 1949; Knuckles *et al.*, 1961; Irvine, 1968) are in good accordance. Recalculations of these magnitudes in comparison to Johnson's photometric system give average

$$V(1, 0) = 4^m.51 \pm 0.08 \tag{1.2}$$

for distance 1 a.e. to the Sun and Earth from the planet and for phase angle $\alpha = 0$. Accordance in the Bond albedo is even better. The above mentioned four works give an average value of

$$A_B(V) = 0.83 \pm 0.04\,. \tag{1.3}$$

This is the Bond albedo for the wavelength $\lambda = 0.55$ μm.

Observational data concerning the spectral reflectivity of Venus in the different wavelength regions are presented in Figure 1. We attempted to evaluate the spectral dependence of the Bond albedo from these data. We supposed that the phase integral is linearly coupled with the relative geometric albedo and found this couple

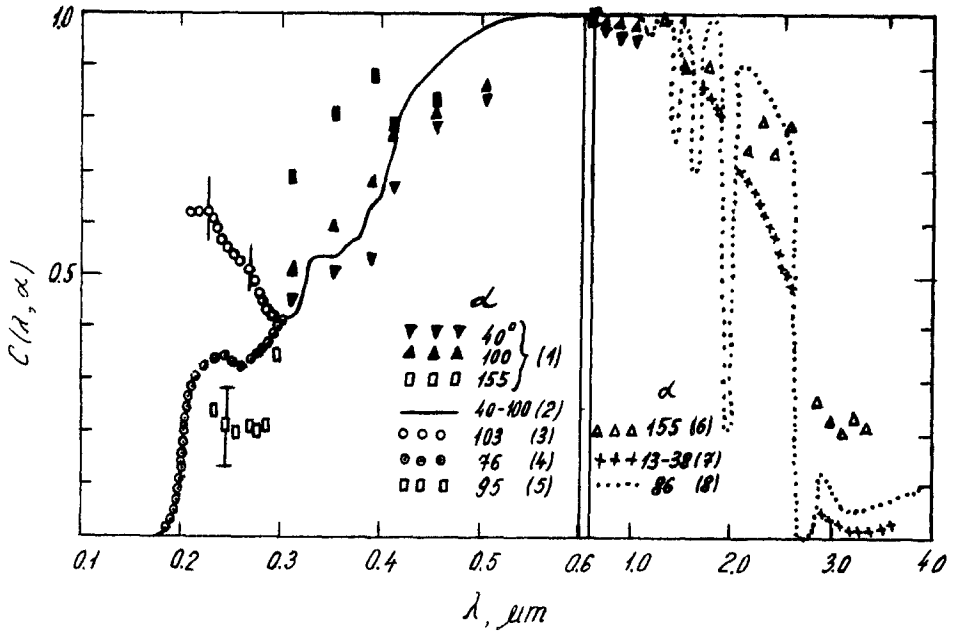

Fig. 1. Spectral reflectance of Venus. Relative geometric albedo – $C(\lambda, \alpha)$ according to various observations: (1) Irvine (1968), (2) Barker *et al.* (1975), (3) Anderson *et al.* (1969), (4) Wallace *et al.* (1972), (5) Evans (1967), (6) Sinton (1963), (7) Moroz (1964), (8) Pollack *et al.* (1978).

from Irvine's (1968) measurements. The relative geometric albedo $C(\lambda, 50) = p(\lambda, 50)/p(0.55, 50)$ in the region 0.3–1.2 μm for $\alpha = 50°$ was taken from the observations of Barker *et al.* (1975) and was extrapolated outside of this region on the basis of a few other observations. The spectral dependence of the Bond albedo obtained by this procedure is presented in Figure 2. The relative geometric albedo $C(\lambda, 50)$ used in the calculations is also presented there.

It is possible to remark on the next main properties of the spectral reflectance of Venus:

(1) Bond albedo is large (>0.6) in the broad spectral region from 0.4 to 2.5 μm. The largest part of the solar energy (84%) is inside this interval. This is the reason why integral albedo is also large:

$$A_I = \frac{\int_0^\infty A_B(\lambda) S(\lambda)\, d\lambda}{\int_0^\infty S(\lambda)\, d\lambda} = 0.74 \pm 0.04\,. \tag{1.4}$$

Here $S(\lambda)$ is the distribution of energy in the solar spectrum. Measurements of the outgoing planetary thermal radiation lead to a little larger value (0.76–0.79, see Section 5).

(2) Albedo is relatively low at short wavelengths ($\lambda < 0.4$ μm) and long wavelengths ($\lambda > 2.5$ μm). Both depressions are smooth, and probably are the results of absorption in the condensation phase (the substance of clouds' particles).

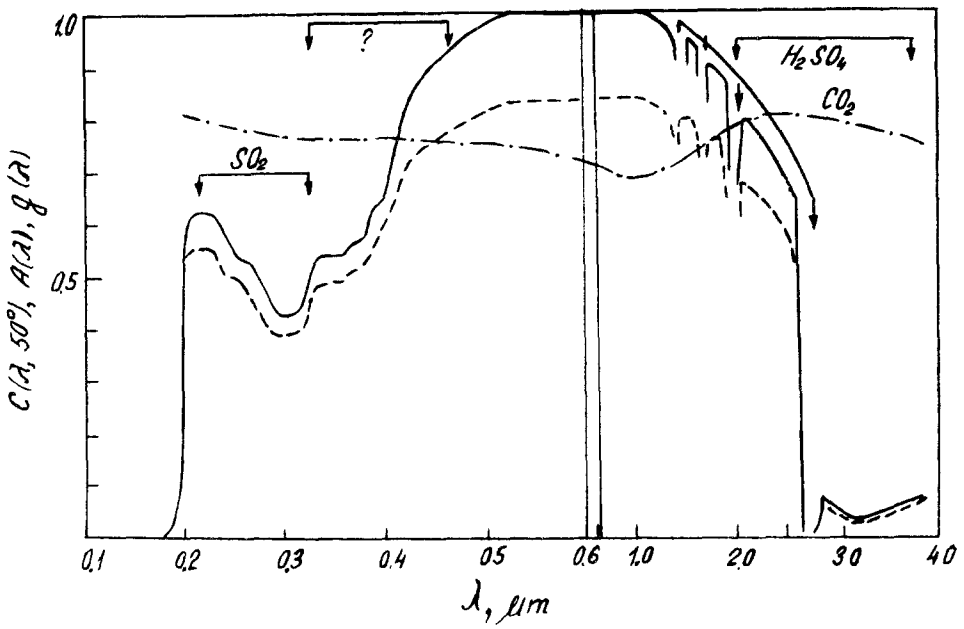

Fig. 2. 'Standard' $C(\lambda, \alpha)$ curve – full line. This curve was used for calculation of the spectral Bond albedo A_B (dashed line). Dot–dashed line is the factor of anisotropy of scattering for the upper part of the clouds (D-layer – see Table XIV and XVII).

The small gaseous constituent SO_2 gives additional absorption in the spectral region $\lambda < 0.32$ μm (Barker *et al.*, 1979).

(3) There are noticeable phase variations. In the regions $\lambda < 0.4$ μm and $\lambda > 1.5$ μm, reflectivity $C(\lambda)$ is ordinarily larger for big phase angle than for the small one. Except for phase dependence there are some irregular variations. Such irregularities are very strong in ultraviolet (0.2–0.3 μm, see Figure 1). Taranova (1977) observed a variation of less amplitude in the near infrared (1.5–2.5 μm).

A few groups of the strongest CO_2 bands are shown on $C(\lambda)$, $A_B(\lambda)$ curves. They have complicated structures which is known in great detail with the spectral resolution about 0.1 cm^{-1}. The influence of CO_2 bands on the integral albedo A_I is not very important because the most intense bands are on the wavelengths $\lambda > 1.2$ μm and only 20% of solar energy is emitted there.

'Reflected' solar radiation goes into space after the scattering in the atmosphere, and one of the consequences of scattering is some polarization. Polarization depends on the phase angle α and wavelength λ. Curves of equal polarizations for Venus in the coordinates α and $1/\lambda$ are presented in Figure 3. These curves are based on the results of measurements of the integral polarization of Venus in 10 wavelengths (Coffeen and Gehrels, 1969) and were used for the determination of some of the physical properties of cloud particles (see Section 4).

A_I is a part of solar energy which is reflected by planets. Part 1-A_I is absorbed and reradiated in the thermal infrared. The observational data concerning the

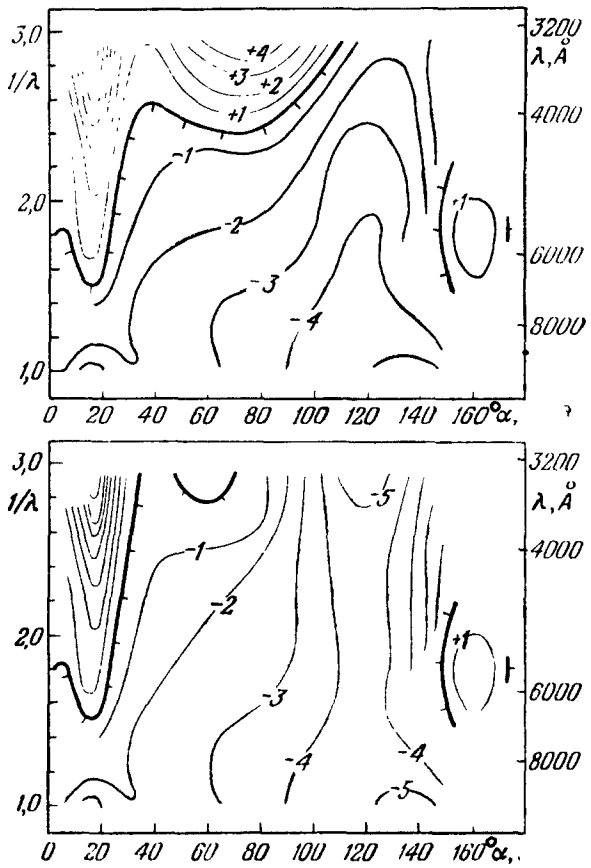

Fig. 3. Integral polarization of Venus as phase angle α and inverse wavelength λ^{-1} function (Coffeen and Gehrels, 1969).

thermal radiation of Venus is presented in Figures 4, 5, and 6. The average disk brightness temperature is raised from approximately 220 to 240 K between 8 and 20 μm and is almost constant to within a few hundred microns. $T_B \simeq 300°$ about wavelength 1 mm. The maximum of the thermal emission spectral distribution is near $\lambda = 12$ μm and the effective temperature of Venus is

$$T_e = 231 \pm 7 \text{ K}. \tag{1.5}$$

Brightness temperature is noticeably raised toward the centimeter wavelength and its typical value for diapason 3–15 cm is 620–650 K. Now it is well known that the reasons for such an unusual spectral dependence of $T_B(\lambda)$ are the high temperature of the Venusian surface and the high thermal opacity of the atmosphere for $\lambda < 1$ cm. We can see the surface of the planet only in radiowaves. The high brightness temperature of Venus was discovered in 1956 (Mayer *et al.*, 1958) and its nature was the subject of debate over the next 10 years. The straightforward explanation (high kinetic temperature of the surface and low atmosphere) was

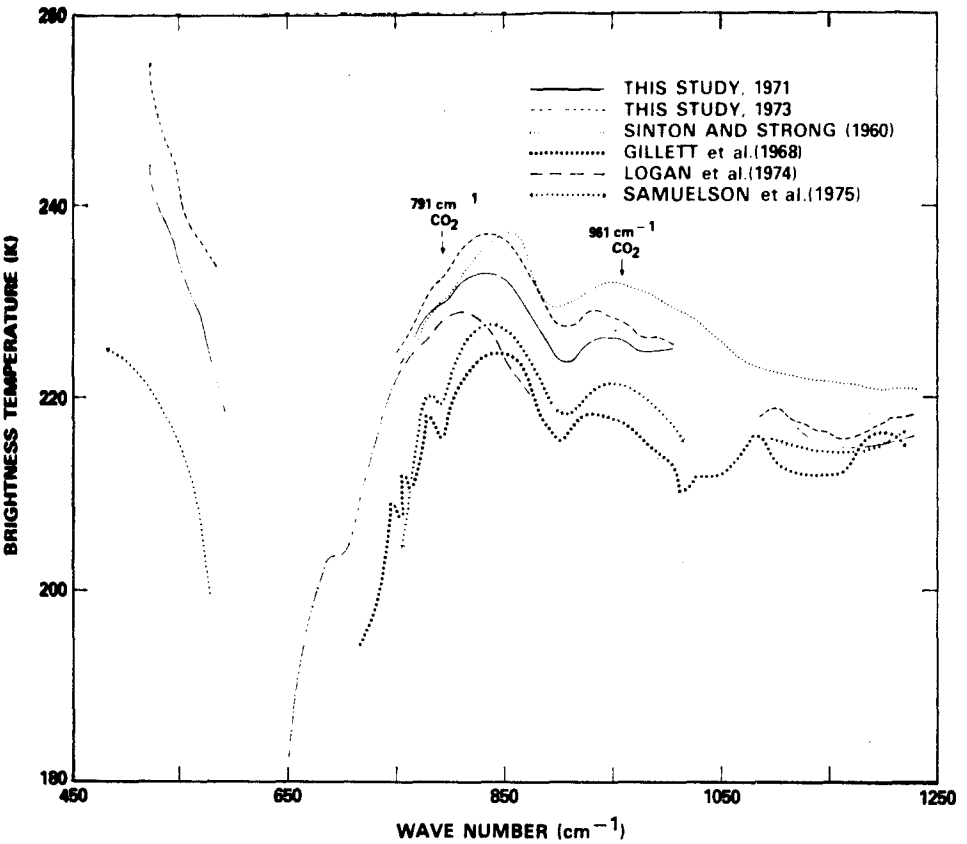

Fig. 4. Thermal radiation of Venus spectrum in the region 8–20 μm according to the observations of Kunde *et al.* (1977). Other observations are represented for the comparison.

proposed almost at the first. However, before the triumph of Venera 4 which translated information immediately from the hot Venusian atmosphere, not all scientists were in agreement with such an explanation. It was considered as very probable (Walker and Sagan, 1966; Moroz, 1967) but not adopted finally.

We discussed only the average disk brightness temperature measured when the radiation of all the disk is received by the detector device. The spatial and angle structure of the outgoing radiation field (day–night, etc.) will be reviewed in Section 5, but we can remark now that the space and time inhomogeneities of Venus' radiation fields are relatively small. Differences in the infrared brightness temperature between different regions of the planet are not more than 20° in ordinary cases and very seldom rise to 40°. On radiowavelengths there are no observable differences between the day and the night side of the planet within the limits of error (which are however of the order of a few tens of degrees for most observations).

C. *The List of space probes* which were used for the investigation of Venus is given in Table II. The most important results were obtained by means of sounders and

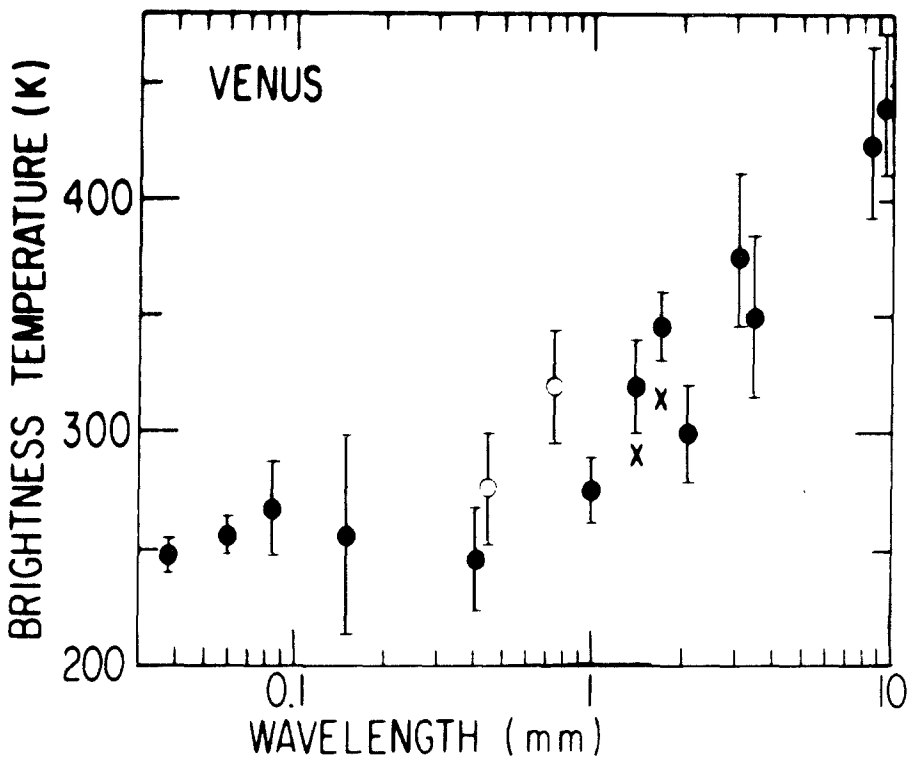

Fig. 5. Thermal radiation of Venus spectrum in submillimeter and millimeter ranges (survey diagram from the article by Whithcomb *et al.* 1979).

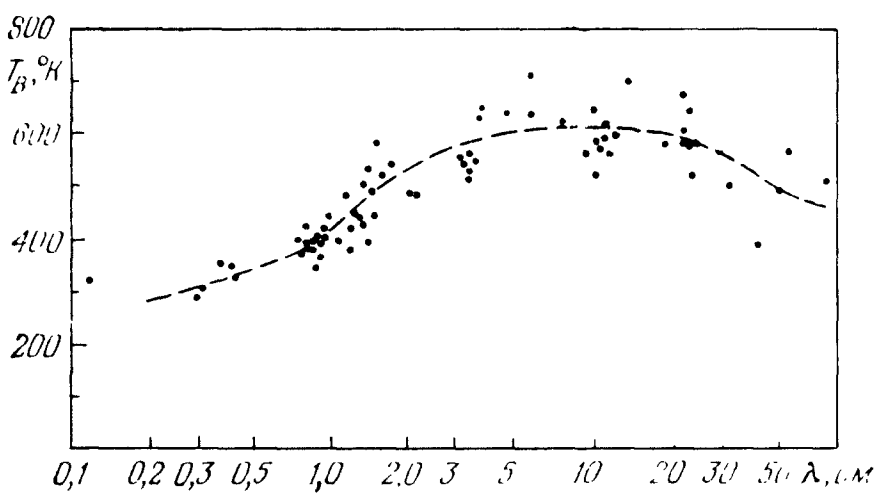

Fig. 6. Radioemission of Venus spectrum in centimeter and decimeter ranges. Typical errors of brightness temperature measurements corresponding to separate points from 50 to 100° are represented.

TABLE II

The list of space probes used for studies of Venus

Name of mission	Type of mission	Launch	Arrival	What was measured
Mariner-2	fly-by[a] (35 000 km)	26.8.62	14.12.62	Infrared and radio brightness temperature, magnetic field.
Venera-4	descent probe	12.6.67	18.10.67	T, P, ρ (on altitudes 55–25 km), abundance of CO_2, N_2, O_2, H_2O, wind.
	+ fly-by			Lα and O I 1300 Å (resonance emissions).
Mariner-5	fly-by (4000 km)	14.6.67	19.10.67	Radio occultation, Lα.
Venera-5	descent probe	5.1.69	16.5.69	T, P (on altitudes 55–20 km), abundances of CO_2, N_2, O_2, H_2O, wind.
Venera-6	descent probe	10.1.69	17.5.69	The same.
Venera-7	lander	17.7.70	15.12.70	T (between 55 km and surface).
Venera-8	lander	26.3.72	22.7.72	T, P, abundance NH_3, flux of solar scattered radiation (between 55 km and surface), wind, *K*, *U*, *Th* abundance in the ground.
Mariner-10	fly-by (5800 km)	3.11.73	5.2.74	UV-imaging of the clouds, IR T_B, UV-spectrum, radio occultation.
Venera-9	lander	8.6.75	22.10.75	In the atmosphere T, P, chemical composition (mass-spectrometer and narrow-band photometer), solar flux, clouds (nephelometer and photometers), wind. On the ground: imaging of the surface, density of ground, *K*, *U*, *Th*.
	+ orbiter (1545 km)			Imaging of the clouds, IR T_B narrow-band photometry between 0.4 and 2.5 μm, polarimetry, spectrum of night-glow, Lα, radio occultation, solar wind, interaction, magnetic field.
Venera-10	lander + orbiter (1665 km)	14.6.75	25.10.75	The same as Venera-9.
Pioneer-Venus	Orbiter (150 km)	20.5.78	4.12.78	Imaging of clouds, IR thermal sounding, UV-spectrum, polarimetry, radio occultation, upper atmosphere's in situ measurements (drag, neutral and ionic composition, T_e, n_e).
Pioneer-Venus	'Multiprob' (large probe + 3 small probes + bus)	8.8.78	9.12.78	T, P, ρ, solar and planetary fluxes, chemical composition (mass-spectrometer and gas-chromatograph), clouds (particle size spectrometer and nephelometer).

(*continued on next page*)

Table II (continued)

Name of mission	Type of mission	Launch	Arrival	What was measured
Venera-11	lander	9.9.78	25.12.78	T, P, ρ, chemical composition (mass-spectrometer), spectrum of scattered solar radiation, thunderstorms, clouds (nephelometer).
	+fly-by (40 000 km)			UV-spectrum
Venera-12	lander	12.9.78	21.12.78	T, P, ρ, chemical composition (mass-spectrometer and gas-chromatograph), spectrum of scattering solar radiation, clouds (composition).
	+fly-by (40 000 km)			UV-spectrum.

[a] For fly-by probes and orbiters the minimal distance to the surface is given.

landers – Venera 4 was first (1967) and Venera 11, 12 were the last (1978). American probes Pioneer-Venus arrived on Venus only 11 years after V4.

There were two generations of Soviet descent probes: the first – from V4 to V8 and the second from V9 to V12. The probes of the first generation could provide measurements which had relatively limited possibilities (instrument weights, information as to volumes etc.) but gave some basic information about atmosphere – the main components, temperature and pressure profiles. Radiolink was very simple – immediately from the probe to Earth.

The descent probes of the second generation were built for much more delicate experiments, for example such as optical imaging of the surface, precise chemical analysis by mass-spectrometers and gas chromatographs, investigations of atmospheric optical properties. They can survive and work on the surface for a relatively long time – about 1 hour. Radiolink is provided through retranslator – satellite or fly-by probe, which makes it possible to transmit much more information. Most atmospheric measurements were begun at a height of about 60 km nearly at the moment of opening of the main parachute; and the time between the switch-on of the instrument and landing is also about 1 hour. Artificial satellites of Venus ('orbiters') were used of course not only for retranslation of sounders informations but also for scientific measurements. Orbiters V9-O and V10-O were the first artificial satellites of Venus. The first optical panoramas of the Venusian surface were translated through its radiosystems.

A rich complex of scientific possibility was given by the first American Venus expedition (Pioneer-Venus). It contained four descent probes – one large with the fullest set of experiments and three smaller with limited sets. Pioneer's sounders provided almost simultaneous measurements in the different parts of the planet.

None of the American probes were adapted for a soft landing but one of them survived on the surface for about half an hour. A huge mass of scientific information was obtained from P-O (Pioneer-orbiter). An important peculiarity of P-O is its very low periastre altitude.

The coordinates of the places of landing for all the Soviet and American sounders are presented in Table III.

TABLE III

Descent probes locations[a]

Probe[b, c]	Day	Latitude	Longitude	Local solar time	Solar zenith angle
Venera-4	18.10.67	19°	38°	4:40	
Venera-5	16.5.69	−3	18	4:12	
Venera-6	17.5.69	−5	23	4:18	
Venera-7	15.12.70	−5	351	4:42	
Venera-8	22.7.72	−10	335	6:24	84.5 ± 2.5°
Venera-9	22.10.75	31.7	290.8	13:12	33
Venera-10	25.10.75	16.0	291.0	13:42	27
Pioneer:					
Large probe	9.11.78	4.4	304.0	7:38	65.7
North probe	9.11.78	59.3	4.8	3:35	108.0
Day probe	9.11.78	−31.7	317.0	6:46	79.9
Night probe	9.11.78	−28.7	56.7	0:07	150.7
Bus	9.11.78	−37.9	290.9	8:30	60.7
Venera-11	25.11.78	−14	299	164	20
Venera-12	21.11.78	−7	294	157	25

[a] Planetographic coordinates for Venus (*Transaction of IAU*, Vol. 14B, D. Reidel Publ. Co., Dordrecht, Holland, 1971) is defined by North Pole right ascension and declination: $\alpha_{1950} = 273.0$; $\delta_{1950} = 66.0$. Central meridian (observed from the Earth) 320° in 6^h 20 June 1964 (JD 2 438 566.5), period 243.0. Slightly different coordinates for the North Pole were used for the localization of American probes ($\alpha_{1950} = 273.3$; $\delta_{1950} = 67.3$).

[b] Abramovich *et al.* (1976, 1979).

[c] Colin (1979b).

2. Chemical Composition

Almost fifty years ago Adams and Dunham (1932) identified carbon dioxide in the atmosphere of Venus. However only measurements on V4 (Vinogradov *et al.*, 1968) definitely proved that CO_2 is the most abundant constituent of the Venusian atmosphere. Much later in 1978 such refined experiments as measurements of noble gases and their isotopes were provided. In this section we shall review the methods (2.1.) – very briefly – and experimental results (2.2.)–(2.7.) of studies of the atmosphere of Venus's chemical composition.

2.1. Methods of measurements

The following methods were used for experimental investigation of the chemical composition:

(1) spectroscopy of the outgoing radiation,
(2) gas analysis by means of specific chemical reactions,
(3) mass-spectrometry,
(4) gas-chromatography,
(5) optical spectroscopy in the deep layer of the atmosphere.

The first method is the classical remote sensing approach which was used most widely in ground-based observations. The next four are in situ methods. Method (2) was used on the V4, V5, V6, and V8. The first attempt at mass-spectrometry was made on V9, V10, but new scientific results were obtained later – on P-L, P-B, P-O, V11, and V12 (1978). Gas-chromatographs provided some chemical measurements on board P-L and V12 and optical spectrometers on V11, V12. Table IV gives the

TABLE IV

Methods of investigations of the chemical composition of the low atmosphere

Method	Components (which really were studied)	Available altitudes (km)	Sensitivity	Remarks
Measurements on descent probes:				
(a) Mass-spectrometry	CO_2, N_2, He, Ne, Ar, Kr	0–60	0.01–1 ppm	Only in situ method for isotopic analysis.
(b) gas-chromatography	CO, SO_2, H_2O_2	0–60	10 ppm	
(c) optical spectrometry	H_2O, O_2, S_3	0–60	10^{-2}–10 ppm	High sensitivity owing to large optical path.
(d) specific chemical reactions	CO_2, N_2	0–60	10^3 ppm	
Spectroscopy of the outgoing radiation:				
(a) absorption spectroscopy (ground-based, fly-by, orbiters)	CO_2, CO, SO_2 H_2O, HCl, HF	65–75	10^{-2}–1 ppm	Resolution power $\lambda/\Delta\lambda$ to 10^6. Bands of CO_2, CO, H_2O, HCl, HF were observed in the near IR, SO_2 in the near UV, CO also on microwaves (λ 2.6 mm).
(b) emission spectroscopy (fly-by, orbiters)	O_2	80	?	Qualitative identification.

brief summary of estimations of the possibilities of the different methods. Examples of the ground-based optical (near-infrared) spectrum are given in Figure 7 and examples of mass-spectra (V11) in Figure 8.

Experience of the Pioneer and the last Venera mission demonstrated that it is very useful to have simultaneous measurements by different methods on the descent

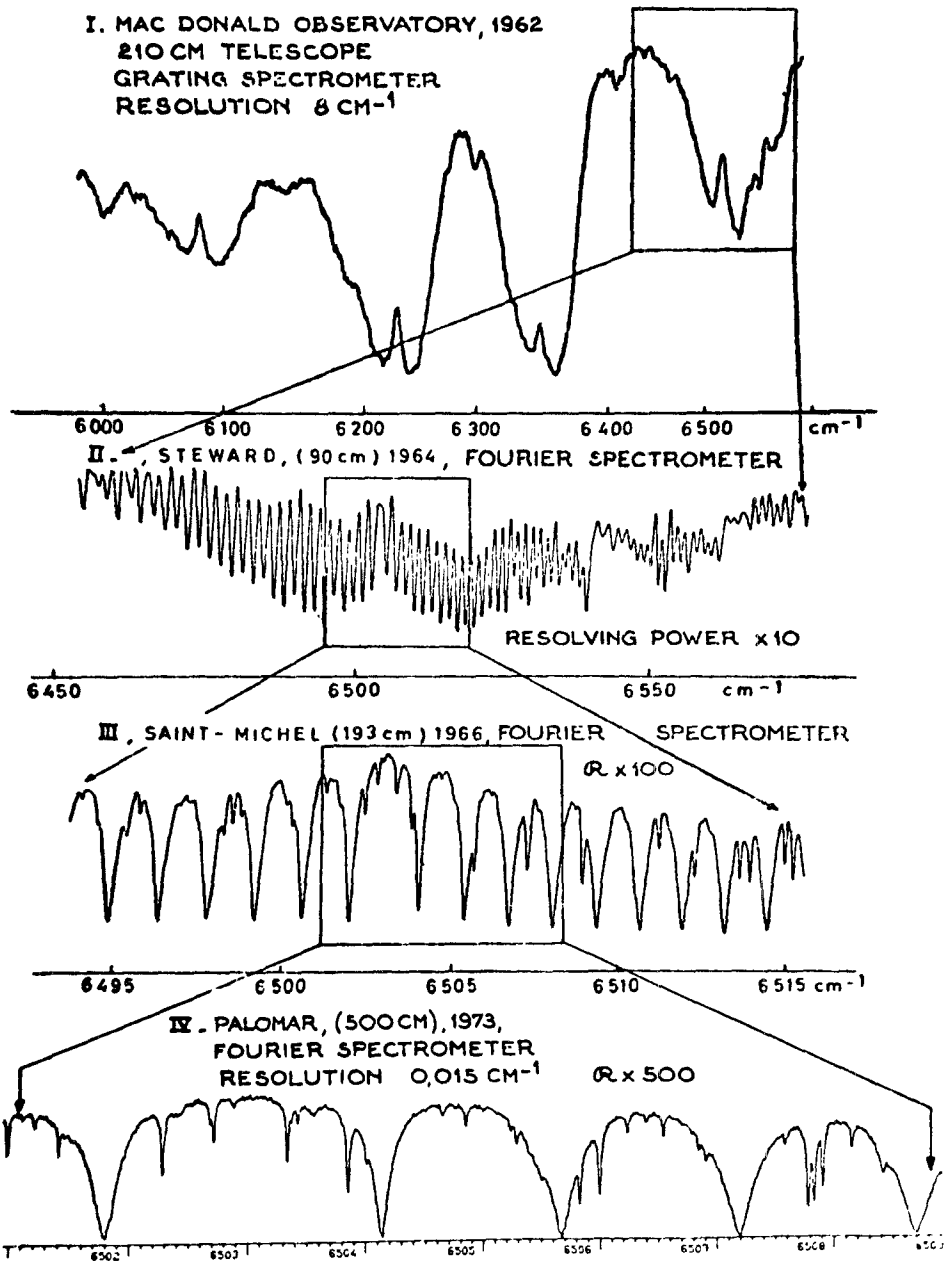

Fig. 7. Spectra of Venus in the near infrared region (Connes and Michel, 1975). The same region about 1.6 μm is shown with different resolution. The upper registrogram is obtained with a diffraction spectrometer, three of the rest – by means of Fourier-spectrometers. Its application provided fantastic progress in the resolution. The spectrum of Venus with 0.1 cm^{-1} resolution in the region 1–2.5 μm is represented in the atlas (Connes *et al.*, 1969).

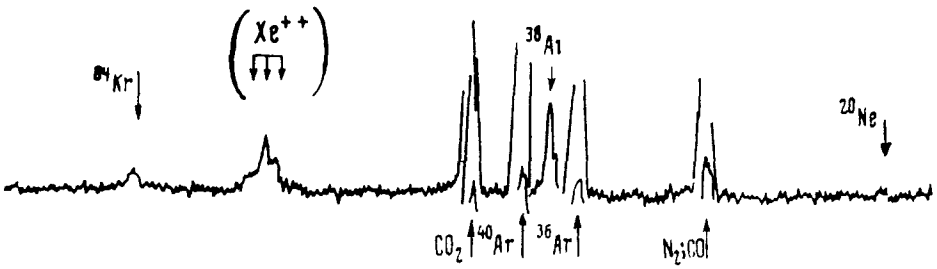

Fig. 8. The fragment of mass-spectrum (raw data) obtained on V11 (Istomin *et al.*, 1979b). Argon peaks are seen well. Discontinuities in the curves correspond to the moments of sensitivity switching.

probes. For example, the mass-spectrometer can't measure CO against a strong background of N_2 ($\mu = 28$ for both molecules) but the gas chromatograph can. Both instruments provided measurements of the full abundance of Ar, but the mass-spectrometer gives additionally very important measurements of isotopic ratios. Some optically active constituents (H_2O, S_3) can be measured by the optical spectrometer with much better sensitivity than by other instruments (for example measurements of S_3 are practically inaccessible for other instruments by the sensitivity available in practice).

2.2. General Summary of the Experimental Data

There are 12 gases which were undoubtedly identified in the low atmosphere of Venus: CO_2, N_2, H_2O, CO, HCl, HF, SO_2, S_3, He, Ne, Ar, and Kr. Data concerning the abundances of these gases are listed in Table V. Carbon dioxide and nitrogen are the main constituents, all of the rest are small constituents with the mixing ratio of less than 0.1%.

Table VI contains the list of gases for which only the upper limits are known. Two molecules in Table VI – O_2 and NH_3 – are in a doubtful position, because some authors published positive identifications, but others gave only hard upper limits, which are in contradiction with such identifications.

Table VII summarizes data about the isotopic relation deduced from ground-based infrared spectroscopy and mass-spectrometry. References and some comments are given in the footnotes. In the next sections we shall additionally discuss data about the most important constituents. Readers can find a useful critical review of chemical experiments on board the Soviet and American descent probes of 1978 in the paper of Hoffman *et al.* (1980b).

2.3. CO_2 and N_2. The Mean Molecular Weight

The mixing ratio of both gases is now known with a precision of about 1%. It is possible to accept as average values

$$f_{CO_2} = 0.965 \pm 0.010 \tag{2.1}$$

$$f_{N_2} = 0.035 \pm 0.010\,. \tag{2.2}$$

For the calculation of the mean molecular weight the other constituents are not important. Its value is

$$\tilde{\mu} = 43.5 \pm 0.2 . \tag{2.3}$$

The surface atmospheric pressure is about 90 atm. (see Section 3). Consequently the partial pressure of nitrogen is nearly 3.3 atm.: 4 times more than on the Earth.

2.4. H_2O

Water is the most abundant volatile constituent on the Earth. If one were to evaporate (of course, mentally) the Earth's hydrosphere the water vapor atmosphere would have a surface pressure of about 300 atm. The temperature on Venus is high enough to have all free water in the atmosphere: however, the surface partial pressure of H_2O is much less than 1 atm. The real lack of free water in the atmosphere is outside all doubt, but quantitative evaluations from different measurements are in strong disagreement. The most important are the measurements in the lower layers of atmosphere – at altitudes below 10–15 km, because the main part of the atmospheric mass is located here.

The first in situ measurements of water vapor were provided by V4, V5, and V6 (Vinogradov *et al.*, 1970). The measured values of mixing ratio were

$$10^{-3} < f_{H_2O} < 10^{-2} \tag{2.4}$$

at altitudes of about 50 km. Much later Andrejchikov (1978) published measurements of V5, V6 at lower altitudes. This data has large experimental errors but there is some tendency towards a decreasing of the mixing ratio between heights of 50 and 20 km.

On V9, V10 there was the first attempt to use the optical measurements of H_2O water bands in the deep layer of the Venusian atmosphere (Moroz *et al.*, 1976). The experiment was much improved on the V11 and V12. A spectrophotometer with continuous scanning of the spectrum in the region 4500–12 000 Å was used there (Moroz *et al.*, 1979a, b, 1980; Ekonomov *et al.*, 1979). Examples of measured spectra are presented in Figure 9. The intensities of H_2O band λ 9500 and 8200 Å (very clearly visible in these spectra) bring us to the much lower evaluations of H_2O content:

$$f_{H_2O} \simeq 2 \times 10^{-5} \tag{2.5}$$

in the lower 10–15 km layer and

$$f_{H_2O} \simeq 2 \times 10^{-4} \tag{2.6}$$

at the level of the clouds. Precision of these data is evaluated at a factor of 2.

The gas chromatograph on V12 gave an upper limit of $f_{H_2O} < 10^{-4}$ below 42 km in accordance with the optical measurements. The mass-spectrometer on V11, V12 (Isomin *et al.*, 1980) demonstrated in the mass $\mu = 18$ some excess (above level O^{18}

TABLE V

Gases which are definitely identified (volume mixing ratios)

Gas	Ground-based spectrometry (60–70 km)[a]	V4, 5, 6 specific chemical reactions (20–55 km)[g]	V9, 10 mass-spectrometer 0–60 km and narrow-band photometer 20–40 km	V11, 12			Pioneer-Venus			
				mass-spectrometer 0–23 km[j]	gas-chromato-graph 0–42 km[k]	optical spectro-meter 0–60 km	mass-spectrometer on P-L 0–60 km [n, s]	gas-chromato-graph on P-L 55, 42 and 22 km [p, s]	mass-spectrometer on P-B	UV-spec-trometer on P-O[r]
CO_2	from 0.7 to 2.7 km atm.	0.95 ± 0.02	0.982[h]	0.955 ± 0.005	0.975 ± 0.003	—	0.955 ± 0.002	0.964 ± 0.003	—	—
N_2	—	0.05 ± 0.02	0.018[h]	0.040 ± 0.003	0.025 ± 0.003	—	0.045 ± 0.002	0.341 ± 0.002	—	—
H_2O	from 10^{-6} to 10^{-4} [b]	10^{-3}–10^{-2}	$\sim 3 \times 10^{-4}$ [i]	$\sim 10^{-4}$	$\leqslant 10^{-4}$	2×10^{-5} on 0 km on 50 km [l]	$< 10^{-3}$	$< 6 \times 10^{-4}$ 5×10^{-3} 1.36×10^{-3}	—	—
CO	$(4.5 \pm 1.0) \times 10^{-5}$ [c] $(5.1 \pm 0.1) \times 10^{-5}$ [e]	—	—	—	$(2.8 \pm 0.7) \times 10^{-5}$	—	—	3×10^{-5} 3×10^{-5} 2×10^{-5}	—	—
HCl	6×10^{-7} [d] $(4.2 \pm 0.7) \times 10^{-7}$ [e]	—	—	—	—	—	—	—	—	—
HF	5×10^{-9} [d]	—	—	—	—	—	—	—	—	—
SO_2	from 2×10^{-8} to 5×10^{-7} [f]	—	—	$< 10^{-4}$	$(1.30 \pm 0.35) \times 10^{-4}$	—	$< 10^{-5}$ on 55 km $< 3 \times 10^{-4}$ on 24 km	$(1.85^{+3.50}_{-1.56})$	—	$\sim 4 \times 10^{-5}$ cm atm.

S_3	—	—	—	—	—	$\sim 10^{-10}$ (m)	—	—	—	—
He	—	—	—	—	—	—	—	—	$(2^{+2}_{-1}) \times 10^{-5}$ (s)	—
Ne	—	—	—	from 1×10^{-5} to 1.5×10^{-5}	—	—	$(1.5^{+2}_{-1}) \times 10^{-5}$	$(4.3^{+6}_{-4}) \times 10^{-6}$	—	—
Ar	—	—	(h)	$(1.5\pm0.1) \times 10^{-4}$	$(4\pm1) \times 10^{-5}$	—	$(7^{+5}_{-3}) \times 10^{-5}$	—	$<9\times10^{-6}$ (q)	—
Kr	—	—	—	from 5×10^{-7} to 8×10^{-7}	—	—	$<2\times10^{-6}$	—	—	—

(a) Evaluations of abundances CO_2 are shown called 'equivalent paths' above the upper boundary of the clouds in the simple reflection model of the band formation (Young, 1972). Maximal values correspond to weak bands (0.78 μm); minimal mentioned here to moderate (1.05 μm). For strong bands (1.6 μm) the values are less (Moroz, 1967a). Mixing ratios are given for the rest in this column.
(b) See Section 2.4.
(c) Connes *et al.* (1967).
(d) Connes *et al.* (1968).
(e) Young (1972).
(f) Barker *et al.* (1979).
(g) Vinogradov *et al.* (1968a, b, 1970).
(h) Surkov *et al.* (1978).
(i) Ustinov and Moroz (1978).
(j) Istomin *et al.* (1979a, b, 1980).
(k) Gelman *et al.* (1979a, b).
(l) Moroz *et al.* (1979a, b, 1980).
(m) San'ko (1980); thermodynamic calculations show that abundance of S_2 is of an order of two more.
(n) Hoffman *et al.* (1979a, b, 1980).
(p) Oyama *et al.* (1980); for H_2O and CO mixing ratios are presented for three altitudes, for the rest – at 22 km.
(q) Mauersberger *et al.* (1979). Extrapolation from 135 km to the low atmosphere with some model of the profile of eddy diffusion coefficient.
(r) Stewart *et al.* (1979a).
(s) von Zahn *et al.* (1979a); Hoffman *et al.* (1980).

TABLE VI

Upper limits of abundances gases, for which there are no positive identifications or strong disagreements in the identifying problems[a]

Gas	Ground-based spectroscopy 60–70 km [b]	UV-spectroscopy (OAO) 60–70 km [b, c]	Radio-astronomy –60 km [d]	Specific chemical reaction V4, 5, 6, 8	Gas-chromatograph V12 0–42 km [e]	Optical spectrometer on V11, 12 0–60 km [f]	Mass-spectrometer on P-L [g]	Gas chromatograph P-L[h]		
								52 km	42 km	22 km
H_2	—	—	—	—	—	—	—	2×10^{-4}	7×10^{-5}	10^{-5}
O_2	2×10^{-6} [i]	—	—	10^{-3} [i]	2×10^{-5}	5×10^{-5}	3×10^{-5}	$(4.4^{+2.5}_{-3})\times10^{-5}$	$(1.6^{+0.7}_{-0.1})\times10^{-5}$	—
O_3	—	3×10^{-9}	—	—	—	—	—	—	—	—
Cl_2	—	—	—	—	—	10^{-7}	—	—	—	—
Br_2	—	—	—	—		10^{-10}	—	—	—	—
C_3O_2	5×10^{-7} [k]	10^{-7}	—	—	—	—	—	—	—	—
H_2S	2×10^{-4} [l]	10^{-7}	—	—	—	—	—	4×10^{-5}	10^{-5}	2×10^{-6}
COS	10^{-8} [m]	—	—	—	—	—	3×10^{-6}	4×10^{-5}	10^{-5}	2×10^{-6}
NH_3	5×10^{-8} [m]	10^{-7}	10^{-5}	$(10^{-4}$–$10^{-3})$[n]	—	—		—	—	—
NO	—	10^{-6}	—	—	—	—	—	—	—	—
NO_2	—	10^{-8}	—	—	—	5×10^{-10}	—	—	—	—
N_2O_4	—	4×10^{-8}	—	—	—	—	—	—	—	—
N_2O	4×10^{-5} [p]	—	—	—	—	—	—	2×10^{-4}	7×10^{-5}	10^{-5}
CH_4	10^{-6} [m]	—	—	—	—	—	—	10^{-5}	3×10^{-6}	6×10^{-7}
C_2H_2	10^{-6} [m]	—	—	—	—	—	—	—	—	—
C_2H_4	3×10^{-5} [p]	—	—	—	—	—	—	2×10^{-5}	7×10^{-6}	10^{-6}
C_2H_6	2×10^{-5} [p]	—	—	—	—	—	—	2×10^{-5}	7×10^{-6}	10^{-6}
C_3H_8	—	—	—	—	—	—	—	9×10^{-5}	3×10^{-5}	5×10^{-5}

CH_3F	10^{-6} [q]	—	—	—	—	—	—	—	—	—
CH_3Cl	10^{-6} [q]	—	—	—	—	—	—	—	—	—
HCN	10^{-6} [q]	—	—	—	—	—	—	—	—	—
HCHO	—	10^{-6}	—	—	—	—	—	—	—	—
CH_3CHO and aldehydes of the higher order	—	10^{-6}	—	—	—	—	—	—	—	—
CH_3COCH_3 and cations of the higher order	—	10^{-6}	—	—	—	—	—	—	—	—

[a] Mixing ratios are given in parentheses, if the corresponding reference announces some positive identification but other measurements do not confirm it. All values without parentheses are upper limits.
[b] Values in these columns suppose the simple reflection model of band formation.
[c] Owen and Sagan (1972).
[d] Smirnova and Kuzmin (1974).
[e] Gel'man *et al.* (1979a, b).
[f] Moroz *et al.* (1979a), upper limit of O_2 is added.
[g] Hoffman *et al.* (1980b).
[h] Oyama *et al.* (1980).
[i] Traub and Carleton (1974). Some publications about the positive identification of O_2 lines in the Venus spectra are known (Prokof'ev and Petrova, 1963; Prokof'ev, 1965, 1967), but without quantitative evaluations. There are no confirmations by other authors.
[j] Vinogradov *et al.* (1970).
[k] Cruikshank and Still (1967).
[l] Cruikshank (1967).
[m] Kuiper (1968, 1969).
[n] Surkov *et al.* (1973).
[p] Moroz (1964).
[q] Connes *et al.* (1967).

TABLE VII
Isotopic ratios

	Venus				Earth
	Ground-based spectroscopy [a]	Mass-spectrometry			
		V11, 12	P-L[c]	P-O[d]	
$^{13}C/^{12}C$	$\simeq 10^{-2}$	$(1.12 \pm 0.02) \times 10^{-2}$ [b]	$\leqslant 1.2 \times 10^{-2}$	$\simeq 10^{-2}$	1.1×10^{-2}
$^{18}O/^{16}O$	$\simeq 2 \times 10^{-3}$	—	$(2.0 \pm 0.1) \times 10^{-3}$	$\simeq 2 \times 10^{-3}$	2.04×10^{-3}
$^{17}O/^{16}O$	—	—	—	$\simeq 4 \times 10^{-4}$	3.7×10^{-4}
$^{3}He/^{4}He$	—	—	$< 3 \times 10^{-4}$	—	1.4×10^{-6}
$^{22}Ne/^{20}Ne$	—	—	0.07 ± 0.02	—	0.097
$^{20}Ne/^{36}Ar$	—	0.22 ± 0.05[b]	0.19 ± 0.01	—	0.58
$^{36}Ar/^{40}Ar$	—	0.85 ± 0.03[b]	0.98 ± 0.04	~ 1	296
$^{38}Ar/^{36}Ar$	—	0.197 ± 0.010[b]	0.19 ± 0.01	—	0.2
$^{86}Kr/^{84}Kr$	—	[e]	—	—	0.305
$(^{82}Kr + ^{83}Kr)/^{84}Kr$	—	[e]	—	—	0.406

[a] Kuiper (1962).
[b] Istomin *et al.* (1980).
[c] Hoffman *et al.* (1980b).
[d] Niemann *et al.* (1979a).
[e] The same as for the Earth (Istomin, 1980).

if we suppose that O^{18}/O^{16} is the same as on the Earth) which is also in accordance with the optical data in the limits of error of both experiments.

However the gas-chromatograph on P-L (Oyama *et al.*, 1979) provided very different results, nearer to V4–V6 measurements

$$f_{H_2O} = \begin{cases} 1.35 \times 10^{-3} & \text{on 22 km} \\ 5 \times 10^{-3} & \text{on 42 km} \\ < 6 \times 10^{-4} & \text{on 52 km}. \end{cases} \tag{2.7}$$

It is simple to prove that for the mixing ratio measured on V4, V5, V6, and P-L the general view of the optical spectrum of below cloud atmosphere must be very different from that observable from V11 and V12. The two sets of results are incompatible.

There are two possible explanations of this disagreement.

(1) Experiments on V4, V5, V6, and P-L were influenced by some local accumulation of water in the instrument or in the near environment of the probe. Optical spectrometry is not influenced by such a local effect because absorption bands are formed on the path in the order of a few kilometers.

(2) There are real variations of H_2O abundance and profile of mixing ratio. We shall show in Section 5, that high abundance ($f_{H_2O} \simeq 10^{-3}$) in the undercloud

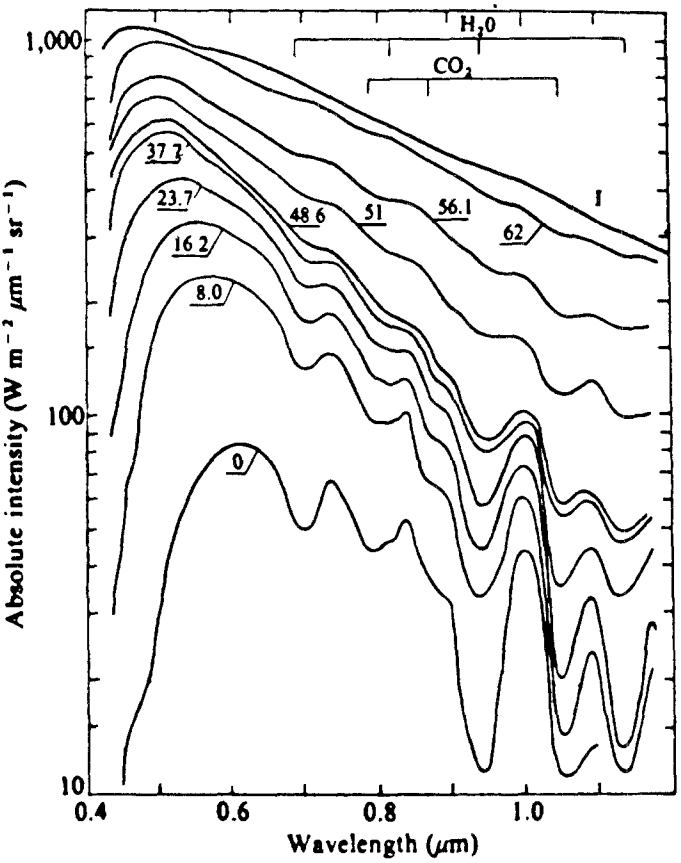

Fig. 9. Spectra of solar radiation scattered in the deep layers of the atmosphere according to spectrophotometer on V11 data (Ekonomov *et al.*, 1979; Moroz *et al.*, 1980). Radiation coming from above is registered. During the descent from the height approximately of 60 km to the surface each 10 s spectrum was registered. Eight typical individual spectra are shown. Figures by the curves indicate the height above the surface in km.

atmosphere is in disagreement with the temperature profiles, measured on Pioneer-probes, and that the second above-mentioned explanation definitely isn't acceptable for the P-L gas-chromatograph's results and isn't probable for V4, 5, and 6.

An additional upper limit on H_2O in the lower atmosphere was given by radioastronomy (for example, Smirnova and Kuzmin, 1974). It was based on the absence of the H_2O absorption line λ 1.35 cm in the radiospectrum. However this upper limit (5×10^{-4}) is not hard enough from the point of view of the last in situ data.

There were many attempts to observe H_2O lines by means of ground-based telescopes and high resolution spectrographs (balloon and aircraft observations also were used). Many observers found only upper limits, sometimes very low (1 micron of precipitated water, in the 'simple reflection' model or $f_{H_2O} \simeq 10^{-6}$, see Fink *et al.*, 1972; Traub and Carlton, 1974). But there are some positive identifications with evaluations from 30 to 100 micron of precipitated water above the clouds (Dollfus,

1963; Belton and Hunten, 1966; Spinrad and Shawl, 1966; Schorn *et al.*, 1969a; Regas *et al.*, 1975; Barker, 1975). Enough long observation programs with some standard procedure (Barker, 1975) demonstrated large variations in f_{H_2O} in time and across the disk, but mixing ratio was always small:

$$1\times10^{-6}<f_{H_2O}<3\times10^{-5}\,. \tag{2.6}$$

These evaluations give the quantity of water in the upper part of the cloud layer. The summary of f_{H_2O} data for different altitudes is presented in Figure 10. There

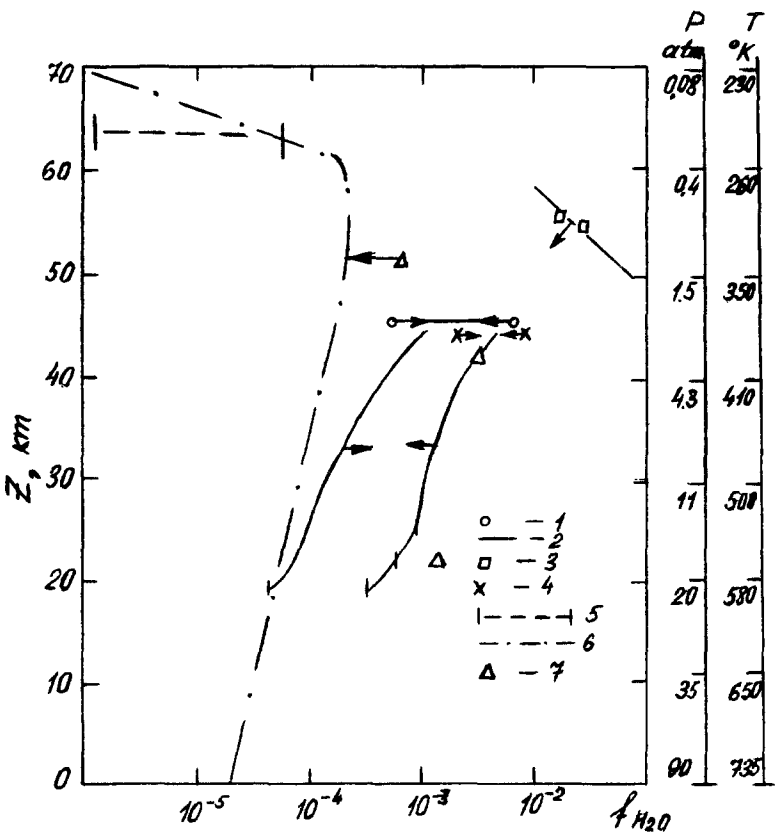

Fig. 10. Vertical profile of H_2O in the atmosphere of Venus. 1 – V4, 2 – V5 (electrolytic method, the interval of probable humidity values is limited by full lines), 3 – V5 (manometric method), 4 – V6, 5 – ground-based observations (limits of variability are shown, Barker, 1975), 6 – the model being in the best agreement with the optical spectrometry in the V11 data (Moroz *et al.*, 1979b), 7 – gaseous chromatograph (Oyama *et al.*, 1979b, 1980). Results obtained on V4, 5, and 6 are given according to Andrejchikov (1978).

are many discrepancies here but the general tendencies are clear: maximum of water abundance at a height of 40–55 km and decrease upwards and downwards from this layer. A possible interpretation of this profile will be discussed in Section 7.

2.5. O_2 AND CO

Dissociation of CO_2 in the upper atmosphere gives oxygen and carbon monoxide (see Sections 7 and 8) and some quantity of these molecules must be transported down by the eddy diffusion. Both gases are very active. In the thermodynamical equilibrium presence of O_2 leads to absence of CO and vice versa (Section 7). But gas-chromatographic experiment on P-L demonstrated presence of both in the low atmosphere of Venus (see Tables V and VI). If both identifications are right, there is no thermodynamical equilibrium in the low atmosphere of Venus. However, identification of O_2 was not confirmed by the chromatograph of V12, which gave only some upper limit. A hard upper limit was found for O_2 from ground-based spectroscopy. At the same time carbon monoxide was identified very firmly by ground-based spectroscopy, which gives

$$f_{CO} \simeq 5 \times 10^{-5}, \tag{2.7}$$

and by both gas-chromatographs (V12 and P-L), which give a little less,

$$f_{CO} \simeq 3 \times 10^{-5}. \tag{2.8}$$

The difference may be real. Measurements on V12 demonstrated some systematic trend of CO abundance between altitudes 36 and 12 km (a decrease of 40%). We should notice that there was no identification of CO in the first publications of American gas-chromatographic results (Oyama *et al.*, 1979a, b). This identification appeared much later in the last version of Pioneer publications (Oyama *et al.*, 1980). This latest paper contained improvements in the abundance data for some other constituents.

2.6. FREE SULFUR AND SULFUR COMPOUNDS

Optical spectra of the solar radiation penetrating in the deep atmosphere (V11 and V12) demonstrated the presence of true absorption in the region $\lambda < 6000$ Å (Moroz *et al.*, 1979a, b, 1980). This absorption appears clearly at an altitude of 35 km and rises to the level $\simeq 15$ km. Lower than 10 km the true absorption coefficient markedly diminishes (Ekonomov *et al.*, 1979). Spectral and altitude dependence of absorption is in accordance with the hypothesis supposing that S_3 and S_4 are the main absorbers between 4500 and 6000 Å. The mixing ratio of S_3 and S_4 must decrease below 10 km as the consequence of thermal dissociation. The most abundant allotropic form of sulfur below 45 km is probably S_2, but in the region 4500–6000 Å much less abundant S_3 and S_4 are more powerful absorbers. The observation of a decrease of absorption coefficient below 10 km is very critical for proposed identification, because it was impossible to choose definitely between sulfur and some other absorbents (Br_2, Cl_2, and NO_2) only on the basis of low resolution spectra. Analysis of the shortwavelength part of the V11 spectrum (San'ko, 1980) bring us to an evaluation of S_3 mixing ratio

$$f_{S_3} \simeq 2 \times 10^{-10}. \tag{2.9}$$

In thermodynamical equilibrium this leads to an S_2 mixing ratio

$$f_{S_2} \simeq 2 \times 10^{-8} . \tag{2.10}$$

If the sum of the mixing ratio of different S_n molecules is independent of altitude, condensation of sulfur starts only at heights 56–57 km and only 10^{-5} g cm^{-2} of elemental sulfur is above this level. But it is not impossible that in the clouds the abundance of the elemental sulfur is much more in the result of some chemical processes which produce sulfur above 50 km (Section 7).

Barker (1979) identified SO_2 bands near 3300 Å in the spectrum of Venus. The mixing ratio SO_2 in the upper part of clouds (altitudes 60–70 km) based on these observations is within the limits

$$2 \times 10^{-8} < f_{SO_2} < 5 \times 10^{-7} . \tag{2.11}$$

SO_2 is much more abundant in the undercloud atmosphere. It was measured by means of the gas-chromatographs of P-L and V12. The two sets of results are in good accordance. The SO_2 mixing ratio below 43 km is

$$f_{SO_2} \simeq 1.5 \times 10^{-4} . \tag{2.12}$$

Probably almost all the sulfur in the low atmosphere of Venus is concentrated in the sulfur dioxide. Chemical reactions with participation of SO_2 and H_2O can be the source of liquid particles of H_2SO_4 in the Venusian clouds (see Sections 4 and 7). Such processes could naturally explain the decrease of f_{SO_2} between 43 and 60 km. One of the important tasks of future experiments is to study the SO_2 profile between these altitudes. There is an upper limit $f_{SO_2} < 10^{-5}$ at the altitude of 55 km (Hoffman *et al.*, 1980).

There were tentative identifications of H_2S and COS traces in the V12 chromatographic records (Gelman *et al.*, 1979a, b) but quantitative evaluations were not published. Oyama *et al.* (1979a, 1980) give only upper limits. The first publication of P-L mass-spectrometric results (Hoffman *et al.*, 1979a) contains data about COS abundance, but later this identification was rejected (Hoffman *et al.*, 1979b). Identification of COS in V9 mass-spectrometric results (Surkov *et al.*, 1978) was apparently also an error.

2.7. Noble Gases and Some Isotopic Ratios

A few mass-spectrometric experiments – on board P-L, P-B, V11, and V12 – provided abundance data for such noble gases as He, Ne, Ar, Kr, and some important isotopic ratios. It was found that relative abundances of ^{36}Ar and ^{40}Ar are very different from the Earth ratio. On Venus

$$^{36}[\mathrm{Ar}]/^{40}[\mathrm{Ar}] \simeq 0.85 \tag{2.13}$$

– approximately 250 times more than on the Earth. There is a strong excess (order of two) of nonradiogenic isotope ^{36}Ar in the ratio of the mass of the isotope to the mass of the planet in comparison to the same ratio for CO_2 and N_2. The main isotopes

of Ne and Kr are nonradiogenic also and these gases demonstrated an excess of the same order of size. Apparently the reason for this strong difference in the abundance of noble gases is connected with some differences in the conditions of formation between the atmospheres of two planets (Section 9).

Isotopic ratio O and C are the same on Venus as on the Earth within the limits of experimental error.

3. Temperature, Pressure, Density (from 0 to 100 km)

A few different methods were used for measurements of thermodynamical parameters of the Venusian atmosphere. We shall discuss here (3.1.) its possibilities, (3.2.) experimental data about atmospheric conditions near the surface, (3.3.) data about altitude profiles of temperature, pressure and density (T, P, and ρ) below 100 km.

3.1. Methods of measurements of T, P, ρ

It is convenient to divide methods of T, P, ρ measurements into two groups: in situ and remote. The first group contains:

(1) measurements by means of meteorological sensors,

(2) measurements of acceleration on the path of the active braking of the probe (drag measurements).

To the second group relate

(1) radio occultations,

(2) stellar occultations photometry,

(3) thermal sounding on the base of spectral analysis of the outgoing radiation spectrum.

There are also rotational temperatures of CO_2 bands and evaluations of the pressure from the linewidths, but these can't give information about the T, P profile of the atmosphere and are useful only for localization of the altitude of the upper clouds. The same is true for broadband measurements of brightness infrared temperature.

In Table VIII there is a comparison of the possibilities of the different methods. The first measurements in situ were provided by the Soviet descent probe V4. The most precise data were obtained by Pioneer multiprobe sounders. In situ methods are very straightforward and we shall discuss in a little more detail only two remote sensing methods: radio occultations and thermal sounding.

3.1.1. *Radio occultations*

If radiowaves from a fly-by probe or an orbiter go through the atmosphere of the planet (it is possible immediately before the occultations of the probe by the planet or after this event), atmospherical refraction leads to phase (frequency) shift, deflexion of the rays and attenuation of the received flux. It is possible from the phase shift (or attenuation) to find the refractivity $N = m - 1$ (m-refractive index)

TABLE VIII

The methods of T, P, ρ measurements

Method or instrument	Immediately measured value	Value obtained after elaboration	Available altitudes km	Typical uncertainty	Remarks
In situ measurements:					
Aneroid pressure sensor	$P(t)$	$T(z)$	0–66	$\Delta P/P \geq 10^{-2}$	(a)
Resistive thermometer	$T(t)$		0–66	$\Delta T \geq 1°$	(a)
Ionization densitometer	(t)	$P(z)$	0–66	$\Delta\rho/\rho \geq 2\times 10^{-2}$	(b)
Accelerometer	$d^2(z)/dt^2$	$\rho(z)$	70–100	$\Delta\rho/\rho \geq 10^{-2}$, $\Delta T \simeq 3°$	(c)
Remote sensing:					
Radio occultation	$\varphi(t)$, dE/dt		40–90	$\Delta P/P \geq 0.05$, $\Delta T \simeq 5°$	(d)
Stellar occultation	dE/dt		110–130	$\Delta P/P \geq 0.05$, $\Delta T \simeq 20°$	(e)
Thermal sounding	$T_B(\nu)$		70–90	$\Delta P/P \geq 0.05$, $\Delta T \simeq 5°$	(f)

(a) t – time, z – altitude. For transition from $P(t)$, $T(t)$ to $P(z)$, $P(z)$ and $\rho(z)$ equations of hydrostatic equilibrium of the thermodynamic state and aerodynamic drag are used; V4 – Avduevsky *et al.* (1968, 1969), V5, 6 – Avduevsky *et al.* (1970), V8 – Marov *et al.* (1973), V9, 10 – Avduevsky *et al.* (1976a), V11 and 12 – Avduevsky *et al.* (1979); Pioneer probes – Seiff *et al.* (1979a, b, 1980).

(b) V4 (Mikhnevich and Sokolov, 1969).

(c) From the equation of motion the density is found, addition of the hydrostatic and state equation give $T(z)$, $P(z)$; V8 – Cheremukhina *et al.* (1974); V9, 10, 11, and 12, Pioneer probes – see remark (a).

(d) ($\varphi(t)$ – phase shift of radiowaves, dE/dt – attenuation of power (see text); M5 – Kliore and Caine (1968), Fjeldbo *et al.* (1971); M10 – Howard *et al.* (1974); V9, 10 – Yakovlev (1976, 1978); P-O – Kliore and Patel (1980).

(e) Analysis of ground-based observations of the occultation of Regul (de Vaucouleur and Menzel, 1960), obtained values of ρ, T do not have good altitude localization.

(f) See text, P-O only (Taylor *et al.* 1979a, b, 1980).

and

$$\rho = \text{const} \times N \tag{3.1}$$

as a function of the altitude. The next step is the determination of $P(z)$ and $T(z)$ profiles using the equation of hydrostatic equilibrium

$$dP = -\rho g\, dz \tag{3.2}$$

and equation of state

$$P = \frac{\rho}{\mu} RT. \tag{3.3}$$

The chemical composition of the atmosphere (main constituents) is supposed to be known. The radiooccultation method didn't work lower than 'critical refraction'

level, for which the radius of the curvature of the ray is equal to the radius of the planet. The altitude of this level is approximately 35 km in the Venusian atmosphere.

As for the propagation of radiowaves through the upper atmosphere ($z > >100$ km), neutral density is too low for this method. However observable refraction may be created by the ionosphere with $n_e > 10^3$ cm^{-3}. Effects of the ionosphere and neutral atmosphere which are separated in the time and phase shifts have opposite signs. This provides an opportunity to study the neutral density and ionospheric electron concentration profiles in the same radio occultation experiment.

The first radio occultations by Venus were observed for M5 and M10 fly-by's. Orbiters V9, V10, and P-O provided many repeated radio occultations on the different latitudes and solar zenith angles. Detailed reviews of the radio occultation method can be found in the books of Yakovlev (1974) and Shutko *et al.* (1979).

In the deep layers of the atmosphere there may be present some additional attenuation connected with the true absorption (for example by cloud particles) and scattering by tropospheric inhomogeneities. The last effect gives fluctuations of the signal and makes it possible to deduce some information about turbulence (Section 6).

With the occultation of a star, whose curve of attenuation depends on the same effect – the refractive divergence of the rays – here the effect is much stronger, because the source is very distant. Attenuations of the order of 2 times correspond to a height of about 120 km for Venus. It is possible to use only a bright star and such observations have been provided only once in the case of Venus – it was occultations of Regul in 1960. A useful review of the problems of star occultation photometry is given in the book of Link (1969).

3.1.2. *Thermal Sounding on the Basis of a Spectral Analysis of the Outgoing Radiation*

The intensity of the thermal planetary radiation on the frequency ν is equal to

$$I(\nu, \mu) = \varepsilon(\nu, \mu)\, B[\nu, T(0)]\, e^{-\tau(\nu, 0)/\mu} + \\ + \frac{1}{\mu} \int_0^\infty B[\nu, T(z)]\, e^{-\tau(\nu, z)/\mu}\, \mathrm{d}\tau, \tag{3.4}$$

where μ – cosine of the emission angle, $\varepsilon(\nu, \mu)$ – emissivity of the surface, $B(\nu, T(z))$ – Plank's function,

$$\tau(\nu, z) = \int_z^\infty \varkappa(\nu, P, T)\, \mathrm{d}z \tag{3.5}$$

– optical depth, $\varkappa(\nu, P, T)$ – volume absorption coefficient, z – altitude. Inside the strong absorption lines (or bands), variations of $\varkappa(\nu, z)$ and $\tau(\nu, z)$ are very strong.

If $\varkappa(\nu, P, T)$ is known and there are enough precise measurements of the spectral profile I, it is possible from Equation (3.4) to find $T(z)$ at some intervals of height.

There are two regions in the spectrum of Venus which are convenient for thermal sounding:

(1) The fundamental band CO_2 λ 15 μm. Measurements of intensities inside this band provide the opportunity of determining the profile of $T(z)$ for altitudes approximately from 65 to 100 km. The lower boundary is defined by clouds. Measurements of such type (in a few frequencies inside 15 mkm band) were provided on P-O.

(2) The edge of the induced rotational and translational band of CO_2 in the radioemission spectrum (Figure 6). Potentially measurements in this region could give full profile between surface and 80 km. However available experimental data (only ground-based) are not precise enough and can't add any useful information to the general bank of data now.

The review of infrared thermal sounding method is given in the Kondrat'ev and Timofeev book (1978).

3.2. Temperature and Pressure Near the Surface

Experimental data concerning atmospheric temperature and pressure near the surface based on the measurements of V8, V9, V10, V11, V12, and Pioneer probes are presented in Table IX. Temperature sensors of Pioneer probes didn't work lower than 11–12 km and Pioneer's surface temperatures mentioned in Table IX are extrapolated data.

TABLE IX

Temperature and pressure near the surface

Probe	Temperature, (K)	Pressure (atm)	Location		Altitude (km)	
			Latitude	Longitude	(d)	(e)
Venera-8[a]	741	93	−12	331		
Venera-9[b]	728	90	31.7	290.8		
Venera-10[b]	737	91	16.0	291.0		
Venera-11[b]	731	91	−14	299		
Venera-12[b]	741	91	−7	294		
Pioneer-Venus[c]:						
North probe	(721)	86.2	4.4	304	+1.0	(−3)
Large probe	(732)	91	59.3	4.8	+0.2	(+3)
Day probe	(733)	91.5	−31.7	317	−0.1	(−7)
Night probe	(732)	94.5	−28.7	56.7	−0.5	(−2)

[a] Marov *et al.* (1973).
[b] Avduevsky *et al.* (1979).
[c] Seiff (1979a); surface temperature was found by extrapolation.
[d] Above reference surface according to radar mapping on P-O (Seiff *et al.*, 1980).
[e] From gravity measurements in the time of landing (Seiff, 1979a). Reality of these data is doubtful.

Different locations can be on the different equipotential levels. It is necessary to know distances to the center of the planet to compare conditions measured in the different places. It is possible to avoid this difficulty by combining profiles obtained by radio occultation and in situ measurements. The occultations profiles give P, T as a function of the distance to the planetary center, and this makes it possible to find the altitudes of in situ measurements above some surface of the constant radius (it can be considered approximately as equipotential). If we choose for this radius value 6052 km, the T, P conditions on this reference surface are the same within the limits of error. The average values are

$$\begin{aligned} T_0 &= 735 \pm 3 \text{ K} \\ P_0 &= \ 90 \pm 2 \text{ atm} . \end{aligned} \tag{3.6}$$

On the basis of radar mapping on P-O, an average planetary radius of 6051.18 km for 80% of the surface was found (Pettengill *et al.*, 1980), not very far from the above-mentioned value. For some regions on the planet there are altitude deviations within the limits ± 7 km from the average radius and this mean, and large local temperature and pressure deviations ($\pm 55°$ and ± 35 atm. correspondingly) are possible. However the data of Table IX demonstrated little variability of the surface values of T, P. There are some ground-based radioastronomical observations (Pechman *et al.*, 1979) which mentioned a systematic positive deviation of T_0 in the polar regions ($\simeq 5°$). Topography is the most probable reason for this effect.

3.3. Vertical profile of T, P, ρ to the altitude 100 km

Examples of some vertical profiles measured by Soviet and American probes are presented in Figures 11–14.

The general view of the $T(z)$ profile is similar to Earth's and Mars' atmospheres. There are in all cases some tropospheres with the relatively large lapse rate and stratomesosphere with a small one. The peculiarity of Venus is the high altitude of the troposphere ($\simeq 60$ km). Below 60 km, the average value of the lapse rate on Venus is

$$\frac{\mathrm{d}T}{\mathrm{d}z} \simeq 8° \text{ km}^{-1} . \tag{3.7}$$

This value is near to the adiabatic lapse rate $(\mathrm{d}T/\mathrm{d}z)_{\mathrm{ad}}$ which is changing between $7.6° \text{ km}^{-1}$ to $10° \text{ km}^{-1}$ at the altitude of 55 km. The adiabatic lapse rate must be supported by strong enough mixing of the atmosphere (for example if there is thermal convection) and is the maximal possible value of the temperature gradient in the free atmosphere. Empirical models of the Venusian atmosphere (Moroz, 1973; Marov and Ryabov, 1974) based on the early results (V4–V8, and M5) supposed an adiabatical lapse rate for all altitudes lower than 55 km. Measurements on V9, V10 do not change the situation. Pioneer probes (Seiff *et al.*, 1979a, b, 1980) proved that the temperature gradient is a little less than adiabatic between 30 and

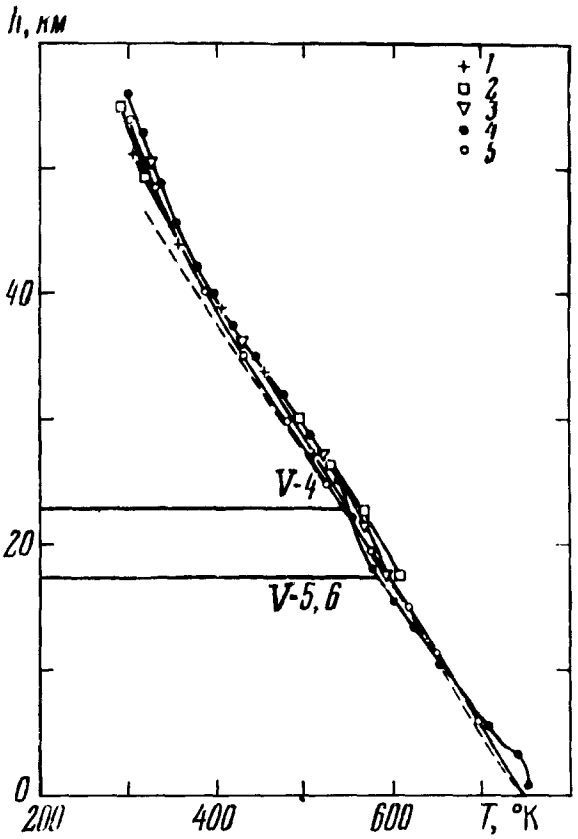

Fig. 11. $T(z)$ profile according to the measurements on the first Soviet space probes: 1 – V4, 2 – V5, 3 – V6, 4 – V7, and 5 – V8 (Kuzmin and Marov, 1974). Horizontal lines – end of measurements for V4 and V5, V6.

50 km approximately. At the same time the adiabatic lapse rate was confirmed for altitudes lower than 30 km and between 50 and 60 km (lower part of the clouds). Seiff *et al.* (1979a) noticed some intervals of altitude with a gradient more than adiabatic ($\Delta T \simeq 1°$) but it is difficult to explain such a positive excess. Theoretical considerations of convective transfer in the free atmosphere admit only much smaller differences.

A sharp decrease in the temperature gradient is observed above 60 km ($T \simeq$ $\simeq$260 K). Its average value is nearly 2.2 K between 60 and 100 km. There is some irregular wave structure with full amplitude 10–20° in the temperature profile at the altitudes >65 km. This wave is marked very clearly on the 'accelerometric' curves (Avduevsky *et al.*, 1979; Seiff *et al.*, 1979a, b, see Figure 12) and, apparently, smoothed on the profiles obtained by means of IR-sounding (Taylor *et al.*, 1979a, b, 1980).

Daily variations are not more than experimental errors ($\simeq 1$ K for Pioneer probes) lower than 45 km. Between 50 and 60 km Pioneer probes demonstrated variations

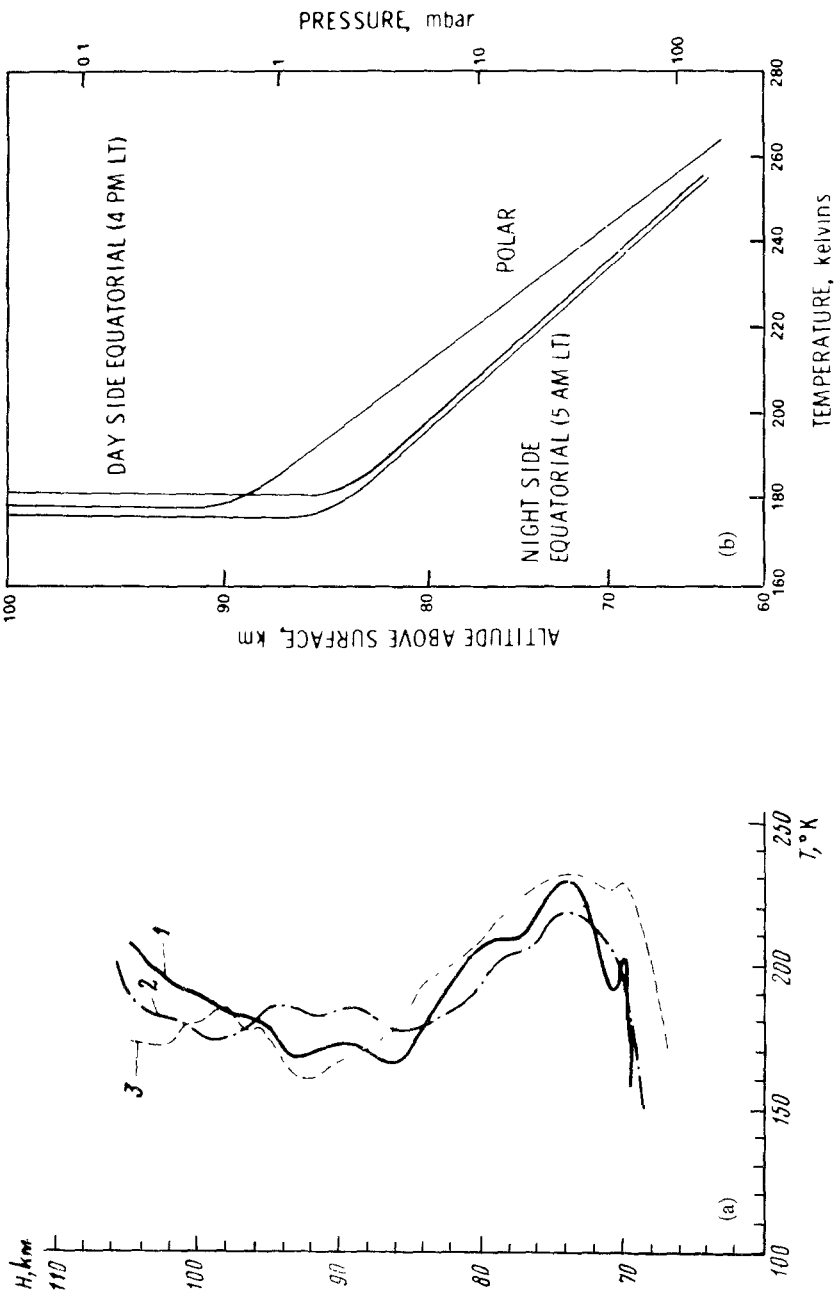

Fig. 12. $T(z)$ profile in the Venusian atmosphere according to the data of accelerometer experiments (a) and the infrared thermal sounding (b). 1 – V11, 2 – V12, 3 – P-No.

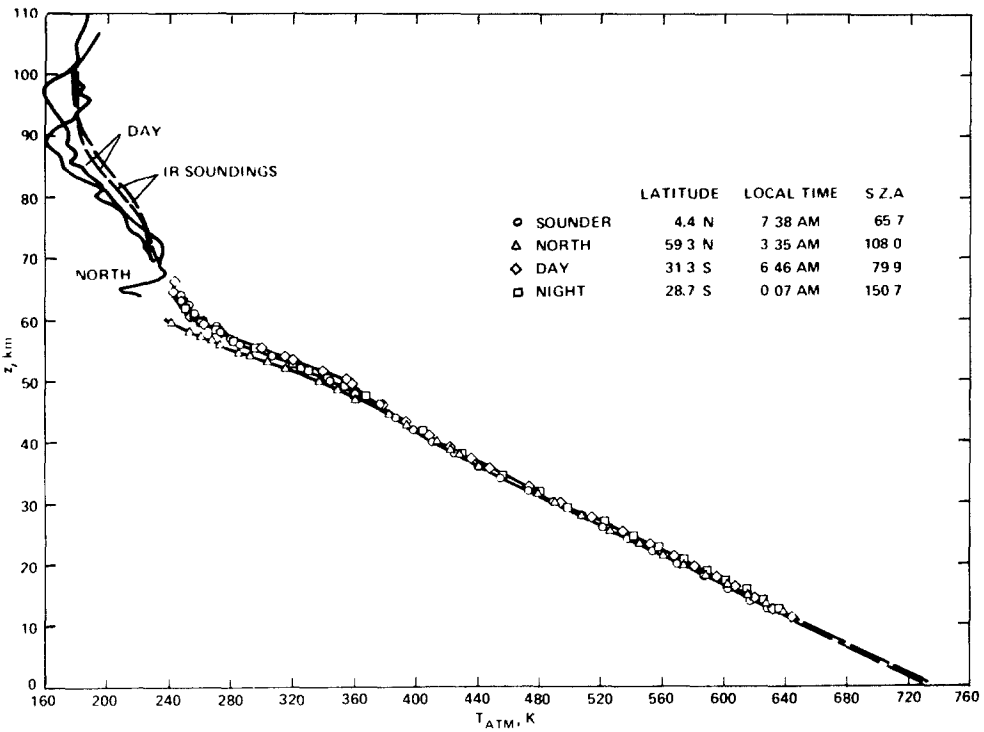

Fig. 13. $T(z)$ profile according to Pioneer probes data (Seiff *et al.*, 1979b).

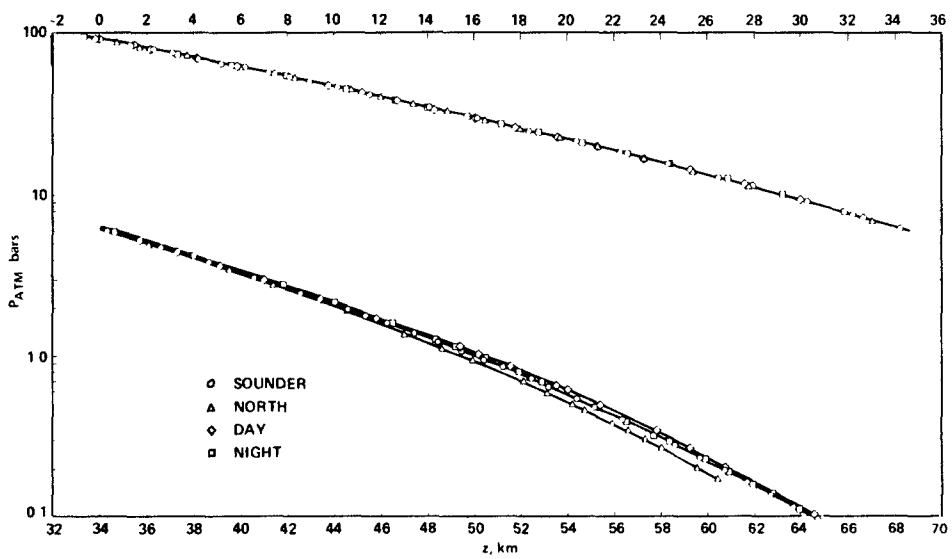

Fig. 14. $P(z)$ profile according to Pioneer probes data (Seiff *et al.*, 1979b).

about 10–15°. Measurements of the P-L and P-D were made in the morning time. Full amplitude of the daily variations is probably more, but it is difficult to admit the amplitude of 50° which was proposed by Avduevsky *et al.* (1976) on the basis of a comparison between V9 and V10 (noon time approximately) and early Soviet probes.

Radio occultations of V9-O and V10-O (Yakovlev *et al.*, 1976, 1978; Kolosov *et al.*, 1978) showed a full amplitude of daily variations of 20–30° at the altitudes 60–80 km. IR-sounding on P-O (Taylor *et al.*, 1979a, b, 1980) demonstrated a full amplitude of 5–10° between the heights of 70 and 90 km. The North Pioneer probe ($\varphi = 59.3°$, $t_\odot = 3^h35^m$) measured temperature lower on 20° than the Night Probe ($\varphi = 28.7°$, $t_\odot = 0^h07^m$) at the altitude 60 km. Lower than 45 km differences between temperature for both probes are practically absent. From IR-sounding it was found that the temperature in the polar regions ($\varphi > 60°$) is on 10–15° more than in the equatorial regions for altitudes of 70–90 km.

The currently empirical model of the Venusian atmosphere is presented in Table X. We used published Pioneer results as the basis but take into account also results of many other missions (V8, V9, V10, V11, V12, radio occultations of M5, M10,

TABLE X

Temperature, pressure and density profiles lower than 100 km (empirical model for low latitudes: $\varphi < 45°$)

Altitude (km)[a]	Average model			Maximal model			Minimal model		
	T (K)	P (atm)	ρ (kg m^{-3})	T (K)	P (atm)	ρ (kg m^{-3})	T (K)	P (atm)	ρ (kg m^{-3})
−6	780			783			777		
−4	765	115.3	79.9	768	117.3	81.3	762	112.9	78.5
−2	750	102.0	72.1	753	104.2	73.4	747	99.8	70.8
0	735	90.0	64.8	738	92.0	66.1	732	89.0	63.7
2	720	79.2	58.3	723	81.0	59.4	717	77.4	57.3
4	705	69.6	52.3	708	71.2	53.3	702	67.9	51.3
6	689	60.9	46.8	692	62.3	47.7	686	59.4	45.6
8	674	53.2	41.8	678	54.4	42.6	670	51.8	41.0
10	658	46.2	37.3	661	47.4	38.0	655	45.1	36.5
12	642	40.1	33.1	645	41.1	33.8	639	39.1	32.4
14	626	34.7	29.4	629	35.6	30.0	623	33.7	28.8
16	609	29.9	26.0	612	30.6	26.5	606	29.0	25.4
18	593	25.6	22.9	596	26.3	23.4	590	24.9	22.4
20	576	21.9	20.1	579	22.5	20.6	573	21.1	19.6
22	560	18.6	17.6	563	19.1	18.0	557	18.0	17.2
24	543	15.7	15.4	546	16.2	15.7	540	15.2	15.0
26	526	13.3	13.4	529	13.6	13.7	523	12.3	13.0
28	509	11.1	11.6	512	11.4	11.8	506	10.7	11.2
30	492	9.23	9.95	495	9.54	10.2	489	8.92	9.67
32	476	7.63	8.51	479	7.90	8.73	473	7.36	8.24
34	460	6.27	7.23	463	6.49	7.44	457	6.04	7.01
36	444	5.12	6.11	447	5.31	6.29	441	4.92	5.92
38	428	4.15	5.13	431	4.31	5.29	425	3.99	4.96

(*continued on next page*)

Table X (continued)

Altitude (km)[a]	Average model			Maximal model			Minimal model		
	T (K)	P (atm)	ρ (kg m^{-3})	T (K)	P (atm)	ρ (kg m^{-3})	T (K)	P (atm)	ρ (kg m^{-3})
40	413	3.34	4.28	416	3.47	4.42	410	3.20	4.14
42	400	2.67	3.53	403	2.78	3.65	397	2.55	3.40
44	387	2.11	2.89	390	2.21	2.99	384	2.02	2.79
46	374	1.66	2.36	378	1.74	2.43	370	1.59	2.27
48	361	1.30	1.91	368	1.36	1.96	355	1.23	1.84
50	347	1.00	1.53	357	1.06	1.57	339	9.45E-1	1.46
52	328	7.64E-1	1.24	338	8.11E-1	1.28	319	7.15E-1	1.19
54	308	5.73E-1	9.87E-1	319	6.14E-1	1.03	300	5.23E-1	9.43E-1
56	289	4.22E-1	7.75E-1	300	4.58E-1	8.11E-1	280	3.90E-1	7.36E-1
58	274	3.05E-1	5.91E-1	285	3.36E-1	6.23E-1	265	2.79E-1	5.58E-1
60	261	2.17E-1	4.41E-1	272	2.42E-1	4.70E-1	252	1.96E-1	4.12E-1
62	250	1.52E-1	3.23E-1	262	1.72E-1	3.50E-1	240	1.35E-1	2.98E-1
64	245	1.05E-1	2.29E-1	257	1.21E-1	2.50E-1	236	9.21E-2	2.08E-1
66	241	7.24E-2	1.58E-1	252	8.49E-2	1.79E-1	232	6.24E-2	1.43E-1
68	236	4.95E-2	1.11E-1	248	5.90E-2	1.25E-1	227	4.20E-2	9.79E-2
70	232	3.36E-2	7.68E-2	243	4.08E-2	8.91E-2	222	2.80E-2	6.69E-2
75	220	1.20E-2	2.90E-2	230	1.59E-2	3.52E-2	210	9.95E-3	2.41E-2
80	208	4.07E-3	1.03E-2	218	5.44E-3	1.32E-2	200	3.09E-3	8.19E-3
85	192	1.27E-3	3.50E-3	202	1.80E-3	4.71E-2	187	9.29E-4	2.63E-3
90	182	3.69E-4	1.07E-3	192	5.55E-4	1.53E-3	175	2.58E-4	7.84E-4
95	187	1.02E-4	3.03E-4	190	2.01E-4	4.53E-4	165	6.61E-5	2.11E-4
100	175	2.72E-5	8.25E-5	190	4.87E-4	1.35E-4	160	1.58E-5	5.26E-5

[a] Above reference level $R = 6052$ km.

V9-O, V10-O). The model is defined for latitudes $\varphi < 45°$. There are 3 versions – mean, maximal and minimal. Deviations of maximal and minimal versions from the average include real variations (daily *et al.*) and also experimental uncertainces. Probable positions of the real values of T, P, ρ are between mean and maximal profile versions for the daytime and between mean and minimal for the night. All three versions presented in Table X are satisfied for Equations (3.1) and (3.2) by $\bar{\mu} = 43.5$.

The deviations defined by the variable wave structure of the stratomesosphere are in general inside of the scattering band of the presented models, besides one exclusion. There is a strong inversion of the temperature at a height of about 70 km near the upper boundary of the cloud layer which was found in a few experiments (accelerometers V11, V12, Avduevsky *et al.*, 1979; accelerometers of Pioneer probes, Seiff *et al.*, 1979a, b, 1980; radio occultation P-OA, Kliore and Patel, 1980). It is expressed on the measured profiles as the minimum of temperature with the depth of some tens of degrees which covers a 3–5 km interval of height. Sometimes this particularity is absent.

Strong refraction effects must be arising in the lower layers of the atmosphere as a consequence of its large density. It was possible to expect on the surface a strong

rise and large removal of the visible horizon in particular. However the photo-panoramas obtained on the surface after V9 and V10 landings don't show it. It is possible to suppose on this basis that in the layer of about 1 m near the surface there is a temperature difference of $\Delta T \simeq 1$ K (Moroz, 1976). Analysis of the conditions in the near-surface layer of the Venusian atmosphere provided by Golitsyn (1978) leads to the same order of ΔT.

4. Clouds

The measurements of the apparent radius of Venus give the values which are 70–80 km larger than the radius of the solid body of the planet (Dollfus, 1972; O'Leary, 1975). The visible radius is determined by the upper boundary of clouds covering the planet. We shall consider here the investigations of aerosol environment in the atmosphere of Venus: (4.1.) methods of measurements, (4.2.) physical properties of aerosols, (4.3.) problem of chemical composition of clouds. In Section (4.4.) data on thunder-storms on Venus will be discussed.

4.1. Methods

The particles in the atmosphere are described by the rather complex system of parameters which may be divided in three groups: I – parameters of the individual particle, II – mean parameters of microvolume, III – parameters of the layer. The diagram which includes the list of most of these parameters and the connections between them is Figure 15. Aerosol environment has direct influence on the propagation of radiation and the most of the methods for measurements of aerosols in the Venusian atmosphere are optical. On the descent probes for the investigations of aerosols the following were used:

(1) photoelectric particle size spectrometry,
(2) nephelometry,
(3) photometry of scattering solar radiation,
(4) X-ray fluorescent spectral analysis.

The remote sensing methods were used at first from the Earth, then from fly-by probes and orbiters:

(1) polarimetry,
(2) photometry,
(3) spectroscopy
} of reflected radiation

(4) infrared radiometry
(5) infrared spectroscopy
} of thermal radiation

Remote sensing gives information on the optical depths $\tau \leqslant 1$ and helps us to study cloud layer only near the upper boundary. Remote sounding of the cloud layer along all the thickness was realized during radio occultation, however it didn't obtain conclusions convincing enough about the physical properties of clouds. Data on the possibilities of each method and references are represented in Tables XI–XIII.

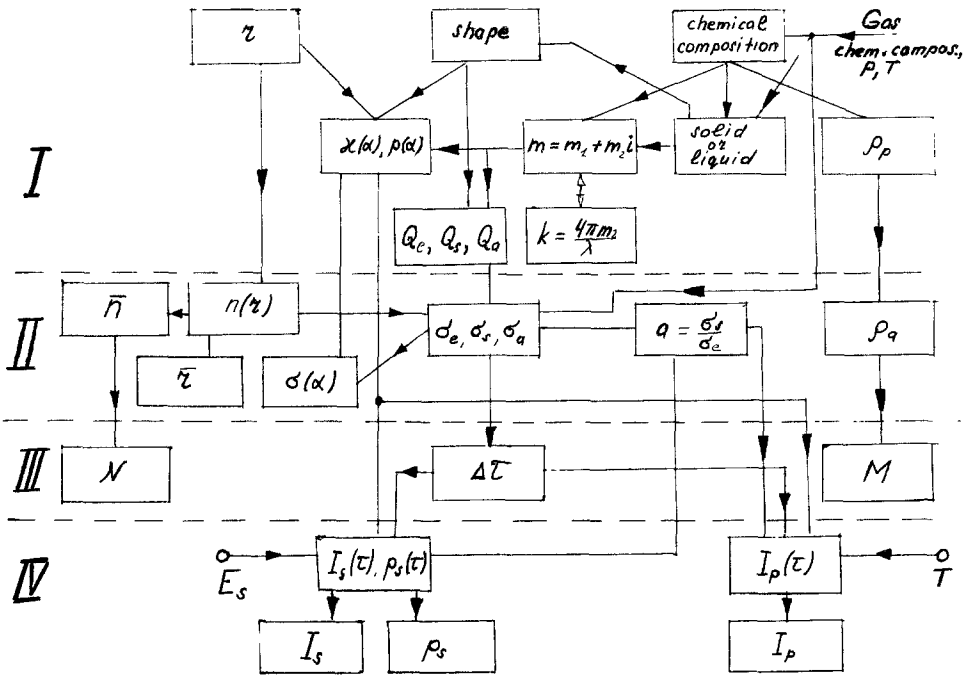

Fig. 15. The physical parameters of the particles, connections between them and also with the radiation field.

(I) Properties of the single particle; r – radius, $\kappa(\alpha)$ – intensity phase function; $p(\alpha)$ – polarization phase function; m_1 – real part of the refractive index, m_2 – imaginary part; ρ_p – density of the particles substance (g cm^{-3}); Q_e, Q_s, Q_a – efficiencies of the extinction, scattering and absorption; k – volume absorption coefficient of the particles substance (cm^{-1}).

(II) Properties of an ensemble of particles; $\bar{n}$ – average number density (cm^{-3}); $n(r)$ – size distribution, $\bar{r}$ – mean radius (for example, the modal which corresponds to the maximum of $n(r)$); σ_e, σ_s, σ_a – volume extinction, scattering and absorption coefficients (cm^{-1}); a – single scattering albedo, ρ_a – volume density of aerosol; $\sigma(\alpha)$ – angle scattering coefficients (cm^{-1} st^{-1}).

(III) Properties of some aerosol layer; N – column number density (cm^{-2}); $\Delta\tau$ – optical thickness, M – mass loading (g cm^{-2}).

(IV) Properties of radiation. $I_s(\tau)$ – solar scattering radiation inside atmosphere, $p_s(\tau)$ – its polarization, $I_p(\tau)$ – planetary thermal radiation, I_s – outgoing solar scattering radiation, p_s – its polarization, I_p – outgoing planetary thermal radiation.

Before 1975 almost all we had known about Venusian clouds was founded on optical ground-based overvations (Table XI). In 1975 on V9, V10 optical sounding of the cloud layer to all depths was carried out by means of a nephelometer (Marov *et al.*, 1976) and two photometers (Avduevsky *et al.*, 1976; Moroz *et al.*, 1976). Important new and more precise data were obtained in the experiments of Pioneer, V11 and V12. Concentration and size-distribution were measured at first on P-L by means of the particle size spectrometer (Knollenberg and Hunten, 1979a, b, 1980), and the first attempt at direct measurement of aerosol chemical composition in clouds was done on V12. A short description of the possibilities of the experiments in situ is represented by Table XII.

TABLE XI

Remote sensing methods for studies of Venusian clouds

Method	Immediately measured parameters	Parameters obtained after elaboration	Which additional data or hypotheses are necessary	Remarks about errors	Main results	Reference
Polarimetry of reflected solar radiation	$p(\alpha, \lambda)$ – polarization phase function and λ dependence; variations on disk	m_1, $\bar{r}$, position of the upper boundary of clouds	Some hypothesis about vertical and horizontal structure of scattering medium (the most simple hypothesis is homogeneity)	$\Delta P/P \simeq 0.1\%$ $\Delta m \simeq 0.02$ $\Delta \bar{r}/r \simeq 0.1$	λ, μm: 0.365; 0.55; 0.99 m_1: 1.46 ± 0.015; 1.44 ± 0.015; 1.43 ± 0.015 $b = 1$, $r^e = 1.05$ μm, $\tau = 1$ at 50 mb	Hansen and Hovenier (1974) [a]
Photometry of reflected solar radiation (a) integral	Stellar magnitudes and photometric phase function $v(\alpha, \lambda)$	Bond albedo $A(\lambda)$, single scattering albedo $a(\lambda)$, scattering phase function	The same	$\Delta v \simeq 0.01^m$ $\Delta A \simeq 0.01$ relative and 0.07^m absolute	$A(\lambda)$, $a(\lambda)$ – see Table XVII and Figure 2 $x_1 = 2.1$	Sobolev (1963) [b]
(b) variation on disk	Distribution of albedo on disk	Vertical structure of upper clouds	—		Two-layer model is necessary: haze above 'main layer'	[c]
Spectrofotometry of reflected radiation (continuous spectrum)	Geometric albedo $p(\alpha)$ for some phase angles	$a(\lambda)$	The same as in the case of polarimetry and photometry	$\Delta P/P \simeq 1$–2% (relative)	$a(\lambda)$ – see Table XVII some limitations on cloud composition	[d]

Table XI (continued)

Method	Immediately measured parameters	Parameters obtained after elaboration	Which additional data or hypotheses are necessary	Remarks about errors	Main results	Reference
Spectroscopy of CO_2 bands (0.78–2.2 μm)	(a) equivalent widths of bands and lines W	σ_s	The same	Evaluation of σ within limits of factor 2	$\sigma_s \simeq 10^{-5}$ cm^{-1}	(e)
	(b) phase dependence of W				(f)	(f)
	(c) local and time variations of W	variations of σ_s or upper clouds boundary			(g)	(g)
	(d) rotational temperatures T_r	Temperature in upper part of clouds		Altitude localization of T and P is not precise	T_r from 230 to 240 K	(h)
	(e) pressure from line widths P_r				P_1 from 30 to 600 mb	Young (1970)
IR-radiometry	Variations of T_B on disk local and time variations	Altitude dependence of σ_a	Temperature profile $T(z)$, $\bar{r}$ and cloud composition	$\Delta T_B \simeq 1°$ $\Delta\sigma_a/\sigma_a \simeq 10\%$ for $0.1 < \tau < 1.5$	T_r from 220 to 240 K for $\tau = 1$ $\sigma_a \simeq 2\times10^{-6}$ cm^{-1} on altitudes 65–70 km ($\lambda \simeq 10$ μm)	(i)
Spectrometry in the middle and long IR (4–100 μm)	Dependence of T_B from wavelength	Altitude dependence of σ_a, $a(\lambda)$, limitations on cloud composition	Temperature profile $T(z)$, $\bar{r}$ and gas composition	$\Delta T_B \simeq 1°$	see Figure 4	(j)

Radio occultation	M (g cm^{-2}) stratification	Some limitations on cloud composition	$M \approx 0.5$ g cm^{-2}	[k]

[a] Mentioned values are based on the ground-based observations given by Coffeen and Gehrels (1969); seel also Gehrels and Samuelsen (1961), Dollfus (1961a), Dollfus and Coffeen (1970). There are some observations in the region 2–5 μm (Landau, 1975). Analysis of the ground-based polarimetric observations was given also by Sobolev (1968), Coffeen (1969), Arking and Potter (1968), Hansen and Hovenier (1974), Kawabata and Hansen (1975), Morozhenko and Yanovitsky (1975), Mukai and Mukai (1979). Results of polarimetric measurements on board P-O by Travis *et al.* (1979a, b) and Kawabata *et al.* (1980).

Results of multiple scattering theory are used for model calculations of the brightness and polarization. Among the useful reference sources are: books of Chandrasekhar (1950), Sobolev (1956, 1972) and reviews of Hunt (1971), Hansen and Travis (1974), Irvine (1975); Rozenberg (1964) and Danielson *et al.* (1969) – the last contain asymptotic formulae which are very effective in the analysis of spectral data.

[b] Ground-based observations – Danjon (1949), Harris (1961), Irvine (1968), analysis – Arking and Potter (1968).

[c] Ground-based observations: Dollfus *et al.* (1975). Interpretation – Bigourd *et al.* (1975), Herman *et al.* (1979). M10 measurements: Murray *et al.* (1974), Hapke (1976), Limaye and Suomi (1976), Devaux *et al.* (1979), Young and Kattawar (1978); V9-O and V10-O: Ksanfomality (1976a), Ksanfomality and Petrova (1978), interpretation see Lestrade (1979), Petrova (1979).

[d] 0.18–0.4 μm (sounding rockets and OAO): Anderson *et al.* (1969), Wallace *et al.* (1972). 0.3–0.6 μm (ground-based observations): Glushneva (1964, 1969), Polozhentseva (1967), Barker and Woodman (1975). 1–4 μm (ground-based observations): Kuiper (1962, 1969), Sinton (1963), Moroz (1964, 1967), Taranova (1977), Martonchik and Beer (1975). Observations on aircraft: Pollack *et al.* (1974, 1975, 1978). V9-O and V10-O: Gnedykh *et al.* (1976). Analysis of the theoretical curve of growth for the medium with the scattering – see Chamberlain (1970), Hansen (1969), Chamberlain and Smith (1970), Regas *et al.* (1975), Young and Kattawar (1976), Kattawar and Young (1977), Sato *et al.* (1977).

[e] Quantity of CO_2 (in the units cm atm) in the photon free path $1 = 1/\sigma_s$ is determined from equivalent widths of CO_2 bands. For example Belton (1968) found $l = 2 \times 10^4$ cm atm. For the effective pressure on the level of formation CO_2 bands $p_e = 200$ mb, this gives $l = 1$ km and $\sigma_s = 10^{-5}$ cm^{-1}. See also Moroz (1967), Kurt and Moroz (1968).

[f] Main peculiarity of the observed phase curve W is the decrease of W by a few times by the raising of the phase angle from 60 to 180°. Such a view of the phase curve means that CO_2 bands are generated not above but inside the clouds, see Chamberlain and Kuiper (1956), Moroz (1967), Barker and Macy (1977).

[g] Spatial variations of W are usually small. However beside some angle effects near the limb and terminator (Gnedykh *et al.*, 1976) in some cases irregular time variations were observed (Cochran *et al.*, 1977), variations with time scale of a few days are possibly the effect of 4^d superrotation (Barker and Perry, 1975; Taranova, 1977) and increase of W at high latitudes (Moroz, 1971).

[h] Chamberlain and Kuiper (1956), Spinrad (1962), Gray (1969), Gray and Schorn (1968, 1969), Schorn *et al.* (1969, 1971, 1975, 1979), Young *et al.* (1969, 1970a, b, 1975, 1977, 1978).

[i] Ground-based observations: Pettit and Nicholson (1924), Sinton and Strong (1960), Sinton (1961), Pettit (1961), Murray *et al.* (1963), Wetphal *et al.* (1965), Moroz *et al.* (1968, 1969), Diner *et al.* (1976), Apt and Goody (1979), Diner and Westphal (1979a, b). M2: Chase *et al.* (1963). M10: Chase *et al.* (1974). V9-O, V10-O: Ksanfomality *et al.* (1976b, c, 1980). P-O: F. W. Taylor *et al.* (1979a, b, 1980). Interpretation: Goody (1965), Pollack and Sagan (1965), Samuelson *et al.* (1975), Ingersoll and Orton (1976), Newman (1975), Taylor (1975), Ksanfomality (1977, 1978b, c; 1980).

[j] Sinton and Strong (1960), Sinton (1961), Gillet *et al.* (1968), Hanel *et al.* (1968), Moroz *et al.* (1969), Hanel *et al.* (1971), Samuelson *et al.* (1975), Kunde *et al.* (1977), Reed *et al.* (1978), Aumann and Orton (1979).

[k] Value of M is given on the base of an interpretation of M10 radio occultation data (Kliore *et al.*, 1979). It is more by an order of two than given by in situ measurements (Table XVI). Some remarks about cloud structure (without quantitative evaluations) are in some other papers devoted to radio occultation data, for example, Yakovlev *et al.* (1978), Kolosov *et al.* (1978).

TABLE XII

The methods of in situ studies of the particulate component of the Venusian atmosphere

Method or instrument	Parameters which are measured immediately (see Figure 15)	Parameters obtained as the result of interpretation	Additional hypotheses by interpretation	Limits of measurements	Remarks about precision	Reference	Interval of altitudes
Photoelectric counter of particles	r, $n(r)$, n, shape[(a)]	σ_e, τ, N, M	m for σ, τ, ρ_p for M	$0.25 < r < 250$ μm altitude resolution ≈100 m	Local concentration in a few subdiapasons of radia precise to 1 particle	The unicle experiment on P-L (Knollenberg and Hunten, 1979a, b, 1980)	66–0 km
Nephelometer							
(a) for back scattering	σ (180°)	m_1, σ	$n(r)$	$\sigma(180) \geq \geq 4 \times 10^{-6}$ m^{-1} sr^{-1} [(b)]	$0.01 < \Delta m_1 < <0.03$	V9, V10 – both versions (Marov *et al.*, 1976, 1978). Version (a) on all four Pioneer probes (Ragent and Blamont, 1979, 1980; Blamont and Ragent, 1979) and V11 (Marov *et al.*, 1979)	62–20 km [(d)]
(b) for a few angle of scattering	$\sigma(\alpha)$, phase function with smoothing	m_1, σ, n, $n(r)$ approximately	—	$\sigma \geq 10^{-4}$ m^{-1} [(c)]	$\Delta\sigma/\sigma \simeq 1\%$ for version (a) and more for version (b)		

In situ photometry of scattering solar light	I(λ)	σ, τ, a	m, $\bar{r}$	$I_\lambda \geqslant 1\ W\ m^{-2}\ m^{-1}\ cr^{-1}$ $\tau \geqslant 0.1$ $1-a \geqslant 9\times10^{-3}$ [e]	$\Delta I_\lambda / I_\lambda \simeq 1\%$ and for absolute value of intensity $\Delta I_\lambda \simeq 20\%$ [e]	see Table XIII	60–0 km
Element composition measurements by means of X-ray fluorescent analysis	ρ_a and M for S, Cl, Hg and other elements	n	$\bar{r}$	$10^{-11}\ g\ cm^{-3}$ for S	?	The unicle experiment on V12 (Surkov *et al.*, 1979)	62–48 km

[a] It is possible to distinguish spherical and nonspherical particles.
[b] For Pioneer nephelometers.
[c] For nephelometer of V9, 10 (version (b)).
[d] Nephelometric measurements on Pioneer probes were started at an altitude of 64.5 km (P-L), 67 km (P-D), 64 km (P-Ni), 61 km (P-No).
[e] Data for spectrophotometer of V11, 12.

TABLE XIII

Photometrical studies in the deep layers of the Venusian atmosphere

Probe	Solar zenith angle	Altitude		Effective wavelength or diapason (μm)	Spectral width of filter $\Delta\lambda$, μm	Angle of vision [a]	Width of angle diapason [b]	Normalized luminance [c]			Conclusions about cloud structure	Reference
		from km	to km					60 km	50 km	0 km		
V8	84°5 ± 2°5	50	0	≈0.7	≈0.2	0	≈60°	—	0.15	0.015	[d]	Avduevsky *et al.* (1973, 1974)
V9	33°	64	0	0.5 –0.56	0.06	0,	40	0.8	0.4 [f]	0.05	Low boundary at 49 km	Avduevsky *et al.* (1976c), Ekonomov *et al.* (1978)
				0.52–0.67	0.15	180,	and					
V10	27°	63	0	0.62–0.70	0.08	≈23 [e]	120° [e]					
				0.70–0.79	0.09							
				0.76–1.06	0.30							
V9	33°	64	0	0.78	0.005	45	15°	0.8	0.5	—	Low boundary at 50 km, local inhomogeneities	Moroz *et al.* (1976)
				0.80								
V10	27°	63	0	0.82								
P-L	65.7°	62	0	0.4–1.0	0.6	27, 60,	5°	0.75	0.42 [g]	0.06	Low boundary at 48 km, a few layers [h]	Tomasko *et al.* (1979a, b)
				0.4–1.8	1.2	83, 102,						
				0.63	0.07	142						
P-L	65.7°	66	0	0.365	0.04	~90	11.5	(0.4)	0.15	? [i]	Low boundary at 48 km, a few layers [h]	Ragent and Blamont (1979, 1980), Blamont and Ragent (1979)
P-D	79.9°	64	0	0.560	0.07			0.75	0.55	?		

V11	20°	64	0	0.45–1.2[j]	from 0.022 to 0.035	0	15°				Low boundary at 49 km, three layers[h]	Moroz *et al.* (1979a, b, 1980)
V12	25°	64	0	0.4–0.6	0.2	angle scanning 0–360°	15°	0.90	0.35	0.08[l]		Ekonomov *et al.* (1979)
				0.6–0.8	0.2							
				0.8–1.3	0.5							
				1.1–1.6[k]	0.6							

[a] Angle between optical axis and vertical (0° – radiation is received from zenith).
[b] Full width at the level 0.5.
[c] Luminance E of horizontal area from up divided by luminance E_s out of the atmosphere. For measurements in the narrow angle isotropy was supposed by evaluation of E.
[d] Measurements were probably started near the low boundary of the clouds. At an altitude of 35 km the derivative dE/dz changed (possibly by some undercloud haze more dense than that observed in the other experiments).
[e] Two wide-angle (120°) channels oriented up and down and one relative narrow angle (40°).
[f] For channel 0.62–0.70 μm.
[g] For channel 0.63 μm.
[h] Layered structure of the clouds gives change of dE/dz.
[i] Reliable evaluation of E are absent because of some infrared leak in the filters.
[j] Spectral measurements with continuous scanning on λ.
[k] Measurements with the four broad-band filters and continuous angle scanning.
[l] E/E_s for $\lambda = 0.7$ μm.

TABLE XIV

Physical parameters of particles in the clouds[a]

Layer or region	Altitude (km)	Temperature (K)	Pressure (atm)	Optical thickness	Mean number density cm^{-3} [b]	Mean diameter m[b]	Refractive index	Hypothesis about composition of particles
	90	182	0.0004		100–500[c]	0.4	?	?
Haze above main clouds E				0.2–1.0				
	70	230	0.03		1–1500	0.4	1.44–1.46[d]	H_2SO_4
Upper cloud layer D				6–8	2–50	2.0		+unknown
	56.5	280			1–300	0.3	1.38–1.42[d]	H_2SO_4
Middle cloud layer C				8–10	2–50	2.5		
					3–10	7.0	?	+unknown
	50.5	340	0.9		1–1200	0.4	1.44[e]	H_2SO_4
Lower cloud layer B				6–12	2–50	2.5		
					3–30	7.0	?	+unknown
	47.5	364	1.4					
Transition region A				0.05–0.1	50–150	0.3 and 2.0[g]	1.44[d]	H_2SO_4 +unknown
	46	374	1.7					
Under cloud haze F_1				0.1–0.2	2–20	0.2	?	?
	31	484	8.5					
Near surface region F_2				[h]				
	0							

[a] Optical thickness, number density and sizes are taken from the paper of Knollenberg and Hunten (1980).

[b] If size distribution is bimodal or trimodal, number density and diameter are given separately for every mode.

[c] Number density in the base of layer E is given. On the altitude 90 km it is less by an order of two (Krasnopolsky, 1979).

[d] From nephelometric data of V9, 10 (Marov *et al.*, 1978) and Pioneer (Ragent and Blamont, 1980).

[e] Ragent and Blamont (1980).

[f] If we suppose the spherical shape refraction index is equal to 1.33–0.001i (Ragent and Blamont, 1980). However it is probable that particles of mode 3 are nonspherical and for the refractive index it is possible in this case to give only some broad interval of values from 1.3 to 2.0.

[g] Bimodal distribution which is near to the same in the D layer.

[h] There are strong discrepancies in the data concerning the presence of particles here (see text).

Measurements of scattered solar radiation intensity in the deep layers of the Venusian atmosphere were carried out from 1972 (V8, Avduevsky *et al.*, 1974). Such investigations were executed at first by means of spectral equipment on V11, V12 (Moroz *et al.*, 1979a, b, 1980; Ekonomov *et al.*, 1979). A summary of photometric experiments in situ is given in Table XIV.

4.2. Physical properties of particulate content

According to the properties of particulate content the atmosphere of Venus may be divided in three main parts: the atmosphere under the clouds (the region F), the clouds (in which three layers can be subdivided – B, C, and D) and the haze above the clouds E. The layers B and F are divided by the transitional zone A. The physical characteristics of these layers are represented in Tables XIV–XVI and in Figure 16. Measurements in situ have not been carried out directly during crossing of the upper boundary of clouds, but it is possible to suppose that it is located in some kilometers only from the layer where scientific equipment was switched on (for different probes it is usually 62–66 km). Some of the evidence is the strong fluctuation of the

TABLE XV

Models of particles in the Venus clouds: parameters of size distribution[a]

Mode	Size distribution	Parameter values in the different layers				
		layer	a	b	r_{min}	r_{max}
1′	$n(r) = \text{const}\, r^{(1-3b)/b} \exp(-r/ab)$	E	0.23	0.18	0.1	1.2
		D	—	—	—	—
		C	—	—	—	—
		B	—	—	—	—
		A	—	—	—	—
1	$n(r) = \text{const}\, (0.1/r)^{3.9}$	A	—	—	—	—
		D	—	—	0.1	1.2
		C	—	—	0.1	1.2
		B	—	—	0.1	1.2
		A	—	—	0.1	1.2
2	$n(r) = \text{const}\, (-(r-a)^2/2b^2)$	E	—	—	—	—
		D	1.0	0.74	0.8	2.1
		C	1.3	0.82	0.8	2.1
		B	1.3	0.82	0.8	2.1
		A	—	—	—	—
3	$n(r) = \text{const}\, (1/r) \exp(-b(\ln(r/a))^2)$	E	—	—	—	—
		D	—	—	—	—
		C	2.73	2.73	2.1	30
		B	2.73	2.73	2.1	30
		A	—	—	—	—

[a] Knollenberg and Hunten (1980), Kawabata *et al.* (1980).

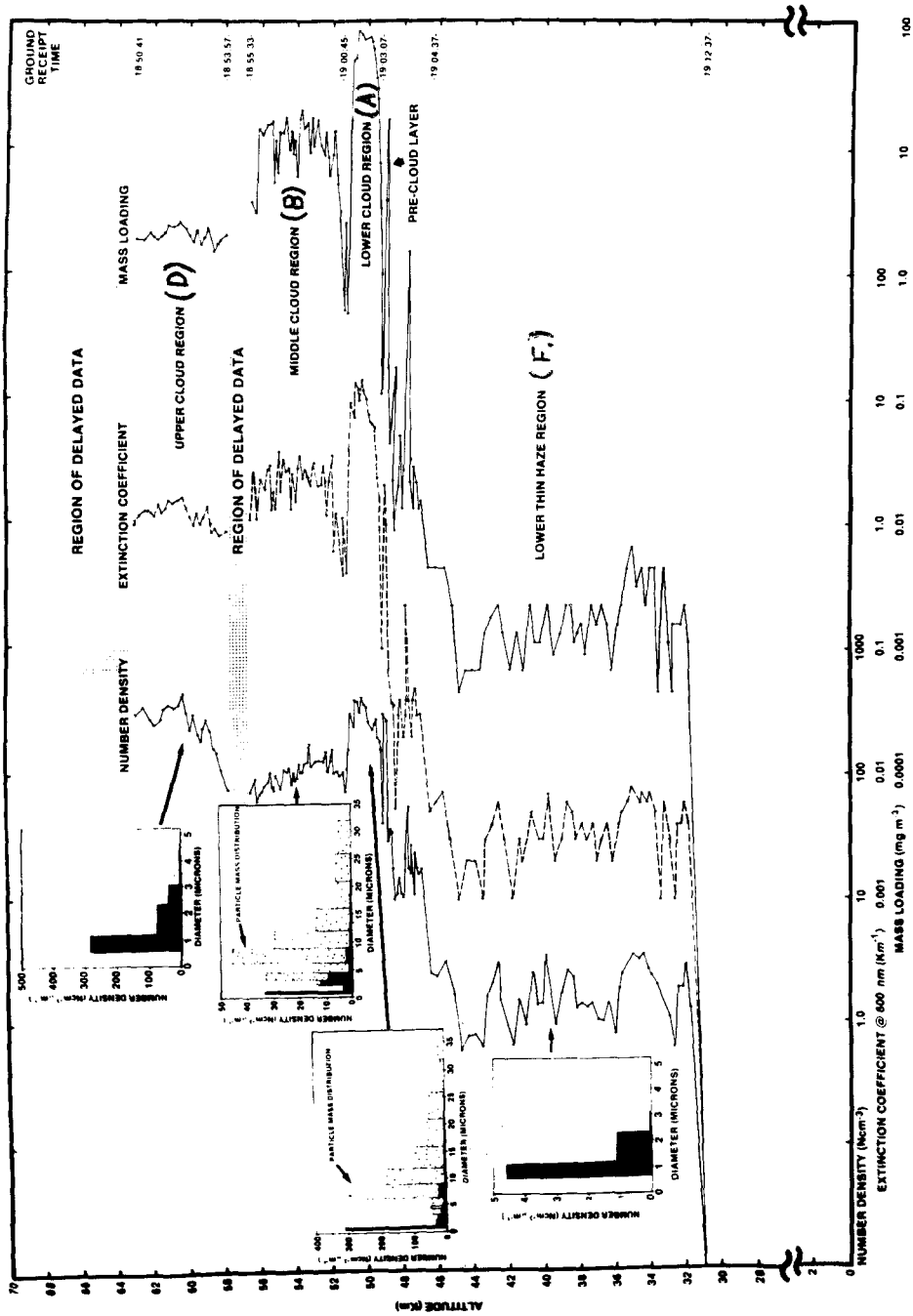

Fig. 16. Aerosol layers' structure in the atmosphere of Venus according to particles size spectrometer data obtained on P-L (Knollenberg and Hunten, 1979a).

TABLE XVI

Optical thickness and mass loading (Knollenberg and Hunten, 1980)

Layer	Optical thickness				Extinction coefficient	Mass loading, g cm^{-2}			
	Mode 1	Mode 2	Mode 3	Sum	10^{-5} cm^{-1}	Mode 1	Mode 2	Mode 3	Sum
Upper cloud layer D	2.15	5.12	0	7.27	0.5	1.1×10^{-4}	9.5×10^{-4}		1.06×10^{-3}
Middle cloud layer C	0.34	3.53	6.2	11.07	1.8	0.2×10^{-4}	4.7×10^{-4}	4×10^{-3}	4.5×10^{-3}
Lower cloud layer B	0.48	1.82	9.9	12.20	4.0	0.2×10^{-4}	3.8×10^{-4}	6×10^{-3}	6.4×10^{-3}
Transition region A	0.06	0.24	0	0.30	0.2	10^{-5}	0.6×10^{-4}	0	6×10^{-5}
Undercloud haze F_1	0.20	0.05	0	0.25	0.016	10^{-5}	1×10^{-5}	0	1×10^{-5}
Sum	3.23	9.76	16.1	31.09		1.5×10^{-4}	1.9×10^{-3}	0.01	1.2×10^{-2}

photometric data observed at these heights (Ragent and Blamont, 1980). An analogous phenomenon was noted on V11, 12.

Ground-based polarimetry shows that the level $\tau = 1$ (for $\lambda = 0.365$ μm) corresponds to a pressure of about 50 mb or a height of 68 km (Hansen and Hovenier, 1974). The analysis of CO_2 bands' equivalent widths gives similar results (V9-0A, V10-0A, Gnedykh *et al.*, 1976). The dependence of equivalent widths W_{CO_2} from the phase angle shows that the upper boundary of clouds is not sharp and that the mean scattering coefficient is about 10^{-5} cm^{-1} near the level of 65–70 km and then decreases smoothly in the region E.

W_{CO_2} variations in time in the interval from 0.8 to 1.6 μm were observed including 4-daily (Barker and Perry, 1975; Taranova, 1977; Cochren *et al.*, 1977) and latitude variations also (Moroz, 1971; Taranova, 1977). W_{CO_2} distribution on the disc in the middle latitudes for the bands at 2 μm is very smooth (V9-0A, V10-0A, Gnedykh *et al.*, 1976). Considering these last data the position of the upper boundary of the clouds remains constant in the daytime with an accuracy of about 1 km on the horizontal scales more than 20 km.

Infrared brightness temperature at $\lambda = 11$ μm is according to different measurements from 217° (Kunde *et al.*, 1977) to 240° (Taylor *et al.*, 1979a, b) for radiation along the normal. For the mean model (Table X) it corresponds to heights from 77 to 66 km for the level $\tau = 1$. The first value seems to be too large if we take into account that the extinction coefficient at 11 mkm is less than in the visible and near UV-region (Lacis, 1975).

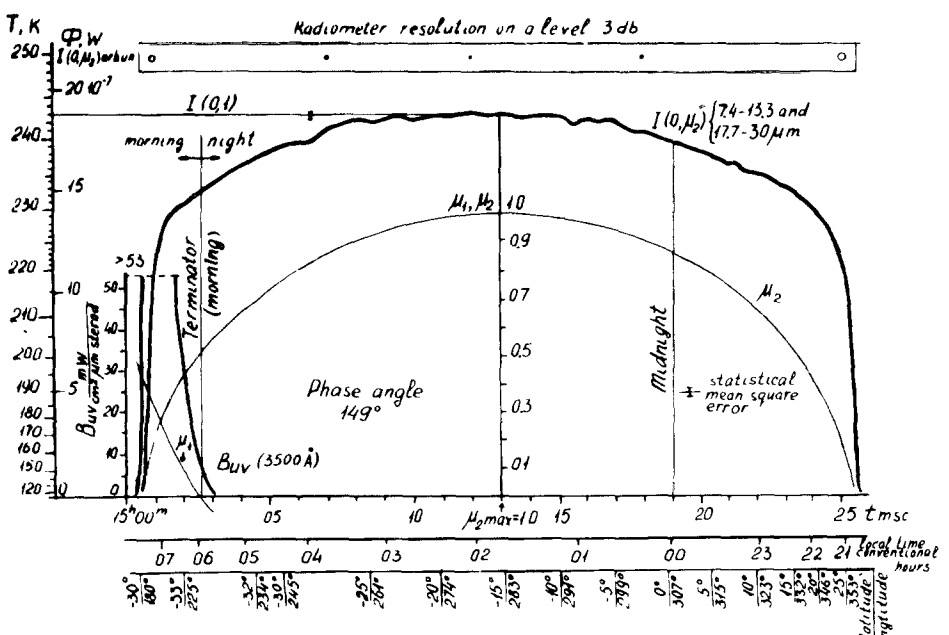

Fig. 17a.

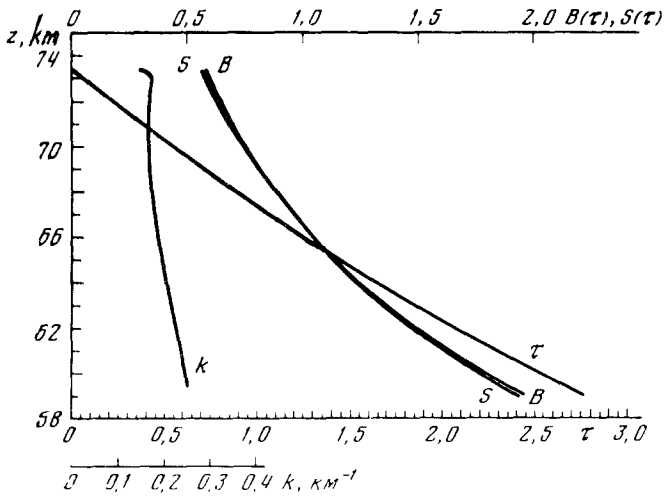

Fig. 17b.

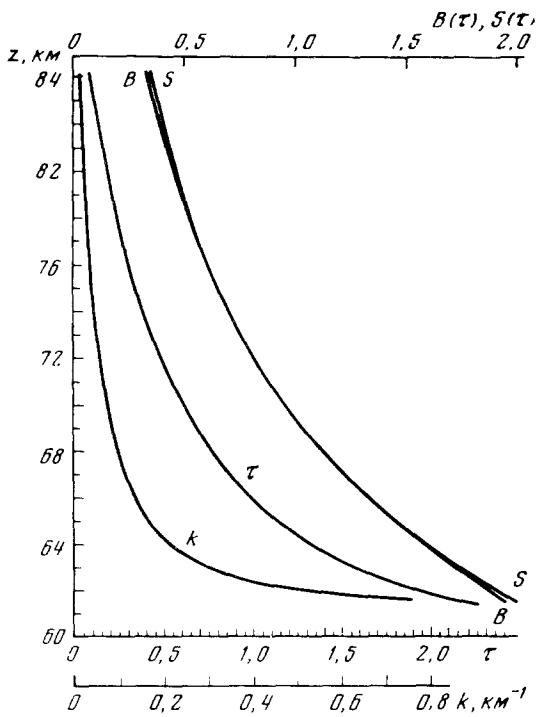

Fig. 17c.

Fig. 17a–c. Brightness temperature of Venus in the low latitudes according to the measurements on V9, V10 (Ksanfomality, 1979c).

(a) The sample of brightness temperature T_B profile, obtained on V9 (December 19, 1975). The scales below – Moscow time, local solar time, latitude and longitude, μ_1 – zenith angle distance of the Sun cosine, μ_2 – angle of emission cosine. The circles above – space resolution.

(b) Profiles of optical depth and extinction coefficient according to the same measurements (night limb).

(c) The same in the evening zone (V10, October 10, 1975).

Some measurements (Pettit, 1961; Westphal *et al.*, 1965; V9-O, V10-O: Ksanfomality *et al.*, 1976a, 1977, 1980) show that brightness temperatures at night are sometimes higher than in the day time. The possible explanation is that the effective boundary of the cloud layer comes down at night. However, radiometric experiment on P-O (F. W. Taylor *et al.*, 1979a, b, 1980) didn't confirm this result. On the other hand, in the observations of Diner and Westphal (1979), the highest brightness temperatures take place near the terminators. Variations in some degree are considered here and its isn't impossible that these contradictions are caused by the real changes in the cloud layer with a characteristic time of some months or even years.

At the middle latitudes the brightness infrared temperature distribution is relatively smooth (Figure 17a). At the high latitudes of the north hemisphere the picture seems to be another (Figure 18). At latitudes of about 70° there is a cold 'collar' and near the pole the temperature increases again and two maximums are observed which form a relatively warm polar 'dipole'. The temperature difference between the 'dipole' and the 'collar' is 30 K and at maximums of the dipole $T_B \simeq 250$–255 K (Taylor *et al.*, 1979b, c, 1980). It is possible that in the dipole region the upper boundary of clouds is some kilometers lower (or the upper layer is more thin) than on the equator. This effect probably can explain the increasing of CO_2 bands'

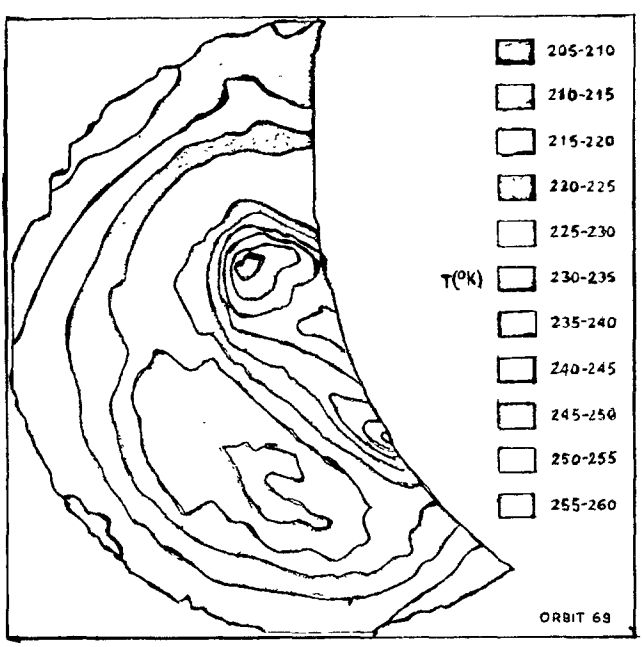

Fig. 18. Brightness temperature isotherms according to the measurements on P-O, orbit No. 69 (Taylor *et al.*, 1980). In the centre – North pole, the edges correspond to the latitude 50°. Two typical details are seen – the bright polar 'dipole' and the dark 'collar' at a latitude about 70°. Such a structure of the radiation field is typical for the northern hemisphere according to the data obtained on P-O.

equivalent widths at high latitudes which were observed from the Earth earlier (Moroz, 1971; Taranova, 1977).

According to V9-O and V10-O data (Ksanfomality, 1979c, 1980) the structure of the upper part of the clouds in the day time (or at least in the second half of a day) differs essentially from the night one. At night the layer D apparently has a sharp upper boundary and in the day time it turns smoothly into the haze above the clouds (the region E). The layer D was investigated both in situ and by remote sensing. The haze above the clouds was investigated only by remote sensing. The main sources of experimental data are photographs obtained by M10 (O'Leary, 1975), photometric (Ksanfomality, 1976b; Ksanfomality and Petrova, 1978; Petrova, 1979) and spectrophotometric (Krasnopolsky, 1979) measurements on V9-O and V10-O, and photometric ones on P-O (Travis *et al.*, 1979a; Kawabata *et al.*, 1980). Data about physical characteristics of the particles in the region E are represented in Figure 19 and in Table XIV. Here the aerosol height scale is

$$H_a \simeq 2.5 \pm 0.5 \text{ km} . \tag{4.1}$$

Particles of submicron size predominate in this region. Optical depth of the haze above the clouds in the polar regions is more than in the equator regions (Travis *et al.*, 1979a).

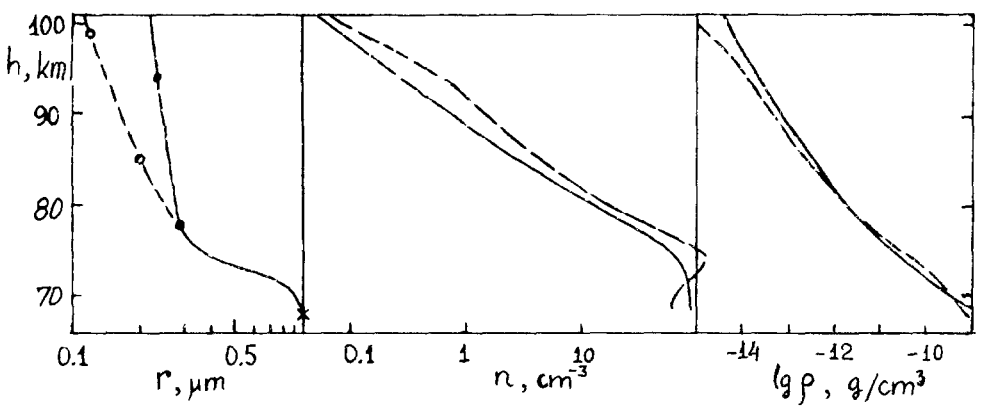

Fig. 19. Altitude dependence on mean radius of particles r, concentration n and mass density ρ of the haze above the clouds (V9, 10, Krasnopolsky, 1976).

In the transitional zone between the regions E and D layered structures with a thickness $\simeq 1$ km were observed (Murray *et al.*, 1974, O'Leary, 1975). The layered structure presents also in the lower transitional region – the zone A (Figure 16). In the Venusian clouds there are particles of three modes whose proportions are different in the different layers. Type 1 – small spherical particles 0.1–1.2 μm (radius) with concentration increasing as power low in the direction of small sizes (Table XV). It is possible that these particles are the same as in the layer E, though for reasons of caution the latter are distinguished in Table XV as a separate mode.

The particles of mode 2 are spherical too but with some more radii, from 0.8 to 2.1 μm. Their refraction index is 1.44–1.46; probable composition – water solution H_2SO_4 (see the next section). Mode 3 – large particles (radius 2–30 μm). Their refraction index is 1.33–0.001·i if we suppose a spherical shape, but most probably it is unregular and in this case it is possible only to indicate very wide limits $1.3 < m_1 < 2$. Apparently the particles of mode 3 are solid (crystals). They compose by mass about 80% of all the particles of the cloud layer and bring in its optical depth about 60% (see Table XVII).

Particles of modes 1 and 2 present at all the heights inside the clouds (the layers B, C, and D), and lower in the layers A (and may be F_1) also. Particles of type 3 present only in layers B and C. During the interpretation of groundbased observations – polarimetric (Hansen and Hovenier, 1974) and photometric (Sobolev, 1968) – the estimations of the middle diameter about 1 μm was obtained. They possibly correspond to type 2. Particles of type 2 contribute to the full optical depth of the layer D by about 70% (see Table XVI). There is a coincidence of the refraction coefficient values in the measurements in situ and groundbased ones (compare data in Tables XI and XIV), but groundbased observations lead to much narrower size distribution.

The presence of several modes of particles – ('multimodal distribution') means that there are particles of different nature in the clouds – with a different phase state or at least with a different mechanism of growth.

The typical values of the concentration in layers B, C, and D are 10^2–10^3 cm^{-3} and scattering coefficients are of the order of 10^{-5} cm^{-1}. In comparison with earth standards the Venusian clouds have very low optical density – the meteorological distance of visibility changes here from several hundreds of meters to some kilometers.

Nephelometric measurements carried out on all of the four Pioneer probes had shown that A and B regions' structure may be different in different points of the planet. For example, the region B was expressed clearly in the nephelometric profile on P-L and almost absent in the profile on P-D (Figure 20). Photometric profiles obtained on V11 and V12 (Figure 21) show a maximal optical density at heights corresponding to the B-region (Moroz *et al.*, 1979). Photometry (Ekonomov *et al.*, 1978) and nephelometry (Marov *et al.*, 1978) on V9 and 10 demonstrate the structure of clouds closer to that obtained on the P-D.

Data on aerosols in the region F_2 – from 30 km to the surface – are contradictory. Nephelometric observations on V9, 10, and 11 (Marov *et al.*, 1978, 1979) have shown the presence of aerosol structures with an optical depth up to 1 and even more in the region F_2. Nephelometric experiments on Pioneer (all of the four probes) haven't discovered aerosols here. It is possible that this difference is connected with the local solar time since measurements on V9, 10, and 11 were carried out near noon and on Pioneer probes – at night and in the morning.

Full optical depth of Venusian clouds according to different estimations (Marov *et al.*, 1976, 1978; Moroz *et al.*, 1976a, 1976b; Ekonomov *et al.*, 1978, 1979;

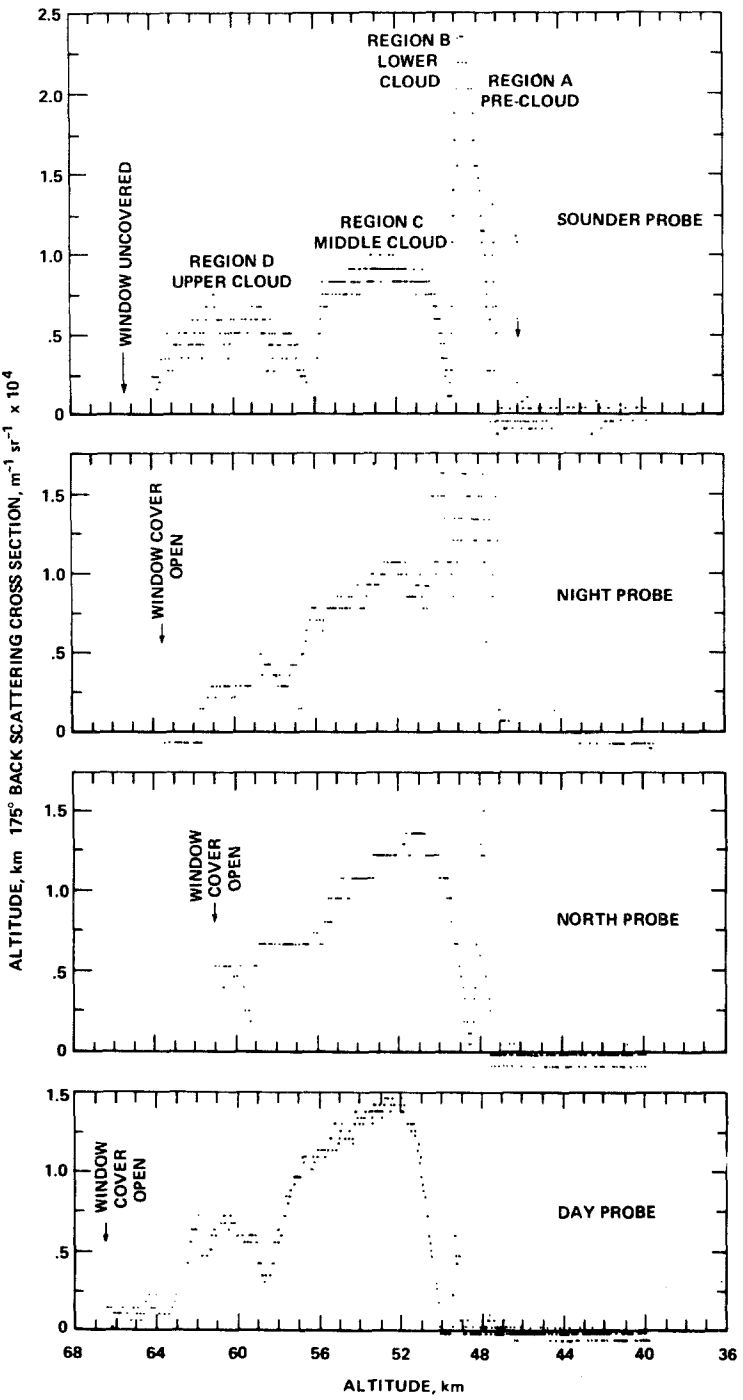

Fig. 20. Nephelometric profiles of Venusian cloudy layer obtained on the Pioneer probes (Ragent and Blamont, 1980).

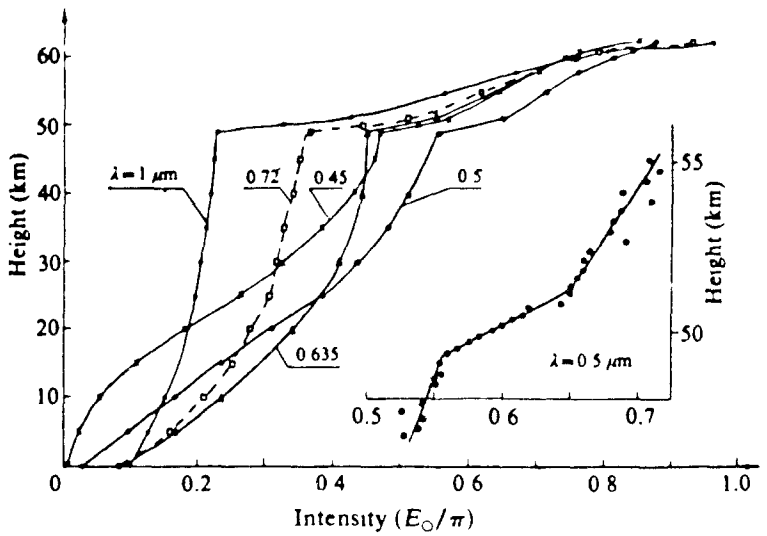

Fig. 21. Photometric profiles obtained on V11: brightness in zenith for five wavelengths (Moroz *et al.*, 1980). Figures by the curves – wavelengths. Along the absciss axis – relative brightness; along the ordinate axis – height.

Knollenberg and Hunten, 1979a, b, 1980; Tomasko *et al.*, 1979a, b; Ragent and Blamont, 1979, 1980; Blamont and Ragent, 1979) is

$$25 < \tau_0 < 35 . \tag{4.2}$$

Curves in Figure 21 show that visible radiation flux on the low boundary of clouds contains about 50% of its value out of the atmosphere. Direct solar radiation is attenuated by the clouds by the factor e^{τ} and its contribution to the flux is insignificantly small when $\tau \gg 1$. The flux measured when $\tau \gg 1$ is created by the multiple scattered photons (number of scatterings $\geqslant \tau$).

Two physical parameters have an influence on the intensity of radiation in the optical thick scattering medium: single scattering albedo $\bar{a}$ and the shape of the phase function. The effect of the phase function is roughly described by the factor g of the unisotropy. This value changes within the limits from 0 (for isotropic scattering) to 0.8–0.9 for very stretched out phase functions. Large dielectric particles have a phase function of the last type. The value

$$x = 2\pi r/\lambda \tag{4.3}$$

is usually in use as the size criterion. When $x > 1$ the limits of g are usually $0.6 < g < 0.9$. In the atmosphere of Venus for the particles of mode 1 the condition $x > 1$ takes place when $\lambda > 1$ μm; for particles of modes 2 and 3 always. From the analysis of the phase curve of stellar magnitude for Venus Sobolev (1944, 1968) found

$$g = 0.7; \qquad a = 0.995 \tag{4.4}$$

for $\lambda = 0.55$ μm.

So far as we speak about ground-based observations these estimations may be concerned with the layer D. The analysis of photometric measurements inside the cloud layer (V9, V10, V11, V12, P-L, see, for example, Moroz *et al.*, 1976, 1978) gives

$$0.99 < a < 1.00 \tag{4.5}$$

for the region 0.6–1.0 μm (out of the absorption CO_2 and H_2O bands). When $\tau \simeq 30$ and the a value is so close to 1, clouds pass radiation almost as well as in the case of conservative scattering when the exact equality $a = 1$ takes place.

Wavelength dependence of the albedo of Venus (Figure 2) contains some information on the chemical nature of the particles in the clouds of Venus (at any rate in their upper part). On the curve of Figure 2 two regions with low albedo can be clearly distinguished ($0.32 < \lambda < 0.5$ μm and $\lambda > 2$ μm). Apparently, absorption is caused by the condensed phase in these regions. Based on such information, attempts at quantitative determination of the absorbing properties of the particle matter was carried out (Moroz, 1971b, Yanovitskij, 1972). Table XVII represents the results of the same type of computations done specially for this survey including all the data which is in use at present. Corresponding explanations are given in the notes to the Table.

For the transition from the Bond albedo A_B to the albedo of single scattering, Sobolev's (Sobolev, 1972) and Yanovitskij's (Yanovitskij, 1972) formulas in the works cited above were used. Their application is limited by the conditions of the half-infinite homogeneous atmosphere and the small absorption ($1 - a \ll 1$). We note that such limitations are absent for the brightness coefficient R in the two streams approximation which differs slightly from A_B about which it is not difficult to be convinced. For the semi-infinite homogeneous atmosphere

$$R = \frac{\sqrt{1-ga} - \sqrt{1-a}}{\sqrt{1-ga} + \sqrt{1-a}}. \tag{4.6}$$

Comparison of the R value calculated using formula (4.6) and A_B, computed using the considerably more complex formula of Yanovitskij, permits us to find the simple connection between R and A_B:

$$1 - A_B = K(1 - R) \tag{4.7}$$

where K – the coefficient being constant within the limits ±2%. When $g = 0.7$ the coefficient $K = 1.127$.

In Table XVII by means of formulae (4.6, 4.7) $a(\lambda)$ is calculated and then $m_2(\lambda)$ and $k(\lambda)$.

From the data of Table XVII we see that strong absorption in the clouds takes place in the region $3 < \lambda < 4$ μm. Investigations of the center-edge effect in the thermal radiation of the planet show that $a(\lambda)$ is essentially less than 1 and at longer waves at least to 40 mkm (see, for example, Ksanfomality, 1980). Apparently, the

TABLE XVII

Bond albedo, single scattering albedo and refractive index (real and imaginary part) in diapason 0.32–3.8 μm

λ, μm	$C(\lambda)$	$A_B(\lambda)$	$g(\lambda)$[a]	$a(\lambda)$	Refractive index[c]		Absorption coefficient $k=4\pi m_2/\lambda$, cm^{-1}	m_2 for 75% H_2SO_4[d]
					m_1	m_2		
0.32	0.43	0.40	0.77	0.966	1.46	8×10^{-4}	3×10^{2}	$<2\times10^{-8}$
0.34	0.54	0.49	0.77	0.979	1.46	5×10^{-4}	2×10^{2}	$<2\times10^{-8}$
0.36	0.54	0.49	0.77	0.979	1.46[b]	5×10^{-4}	2×10^{2}	$<2\times10^{-8}$
0.38	0.57	0.51	0.76	0.980	1.46	5×10^{-4}	2×10^{2}	$<2\times10^{-8}$
0.40	0.67	0.59	0.76	0.988	1.45	3×10^{-4}	1×10^{2}	$<2\times10^{-8}$
0.42	0.80	0.69	0.75	0.994	1.44	1.5×10^{-4}	50	$<2\times10^{-8}$
0.44	0.88	0.75	0.75	0.996	1.44	10^{-4}	30	$<2\times10^{-8}$
0.46	0.91	0.77	0.75	0.997	1.44	10^{-4}	30	$<2\times10^{-8}$
0.48	0.95	0.80	0.74	$\geq$0.998	1.44	$\leq10^{-4}$	<25	$<2\times10^{-8}$
0.50	0.97	0.81	0.74	$\geq$0.998	1.44	$\leq10^{-4}$	<25	$<2\times10^{-8}$
0.55	0.99	0.83	0.74	$\geq$0.998	1.44[b]	$\leq10^{-4}$	<23	$<2\times10^{-8}$
0.60	1.00	0.83	0.72	$\geq$0.998	1.44	$\leq10^{-4}$	<20	$<2\times10^{-8}$
0.80	1.00	0.83	0.70	$\geq$0.998	1.43	$\leq10^{-4}$	<16	9×10^{-8}
1.00	1.00	0.83	0.69	$\geq$0.998	1.43[b]	$\leq10^{-4}$	<12	1.5×10^{-6}
1.20	1.00	0.83	0.70	$\geq$0.998	1.42	$\leq10^{-4}$	<10	5×10^{-6}
1.50	0.95	0.80	0.72	0.997	1.40	$\sim10^{-4}$	10	1×10^{-4}
1.75	0.90	0.76	0.75	0.996	1.39	6×10^{-4}	40	4×10^{-4}
2.20	0.79	0.68	0.80	0.994	1.38	1×10^{-3}	60	2×10^{-3}
2.40	0.71	0.62	0.81	0.992	1.36	1.3×10^{-3}	70	2×10^{-3}
2.85	0.080	0.078	0.80	0.844	1.29	8×10^{-2}	3500	6×10^{-2}
3.00	0.055	0.054	0.79	0.813	1.28	1×10^{-1}	4200	9×10^{-2}
3.20	0.035	0.034	0.78	0.780	1.28	1.2×10^{-1}	4700	1.3×10^{-1}
3.40	0.040	0.039	0.77	0.779	1.36	1.2×10^{-1}	4400	1.6×10^{-1}
3.60	0.055	0.054	0.76	0.792	1.39	1.2×10^{-1}	4200	1.4×10^{-1}
3.80	0.065	0.063	0.75	0.796	1.40	1.1×10^{-1}	3600	1.3×10^{-1}

[a] Factor of anisotropy g is calculated for polydisperse distribution in the D layer.

[b] Hansen and Hovenier (1974). The values m_1 for other wavelengths are interpolated or extrapolated on the basis of the hypothesis that particles of the upper cloud layer are composed of 75% water solution of H_2SO_4.

[c] Imaginary part of the refractive index is calculated for polydisperse distribution in the D layer. For $1-a \ll 1$, fixed m_1 and given size distribution there is approximately proportional dependence $m_2 \propto (1-a)$. Factors of efficiency of the scattering, extinction and light pressure which were necessary to find a and g and were calculated on the base of Mie theory were taken from the Tables Zelmanovich and Shifrin (1968).

[d] Palmer and Williams (1975).

particles of the cloud layer are the most important absorbing agent having influence on the thermal radiation transfer in the diapason of heights from 48 to 70 km.

In the visible and near infrared (0.5–1.0 μm) region the photometric structure of the planetary disk is very homogeneous – details may be seen very rarely except for the regular darkening to the edge. However, in the near ultraviolet region ($\lambda <$ <0.45 μm) the Venusian disk looks quite different (Figure 22). The details are seen

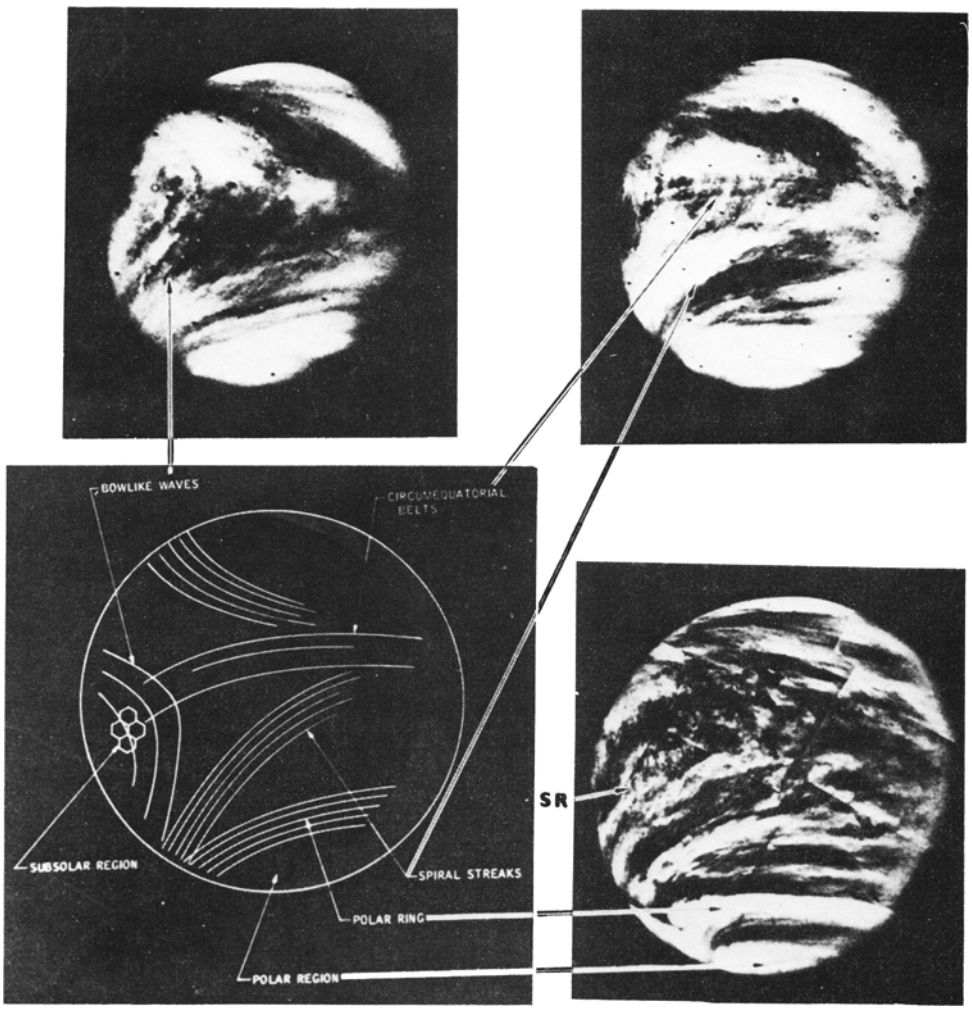

Fig. 22. Main details of the structure of UV-image of Venus according to the TV imaging on M10.

with the scales from some thousand kilometers (they are distinguished clearly on the photographs, obtained from the Earth – Ross, 1928; Boyer and Camichel, 1961; Dollfus, 1961b; Boyer and Guerin, 1969; Dollfus, 1975) and to 10 km from spacecraft (M10: Murray *et al.*, 1974; Hapke, 1976; Limae and Suomi, 1976; V9: Ksanfomality and Selivanov, 1978; Selivanov *et al.*, 1978; P-O: Travis *et al.*, 1979a, b). The life time of large (>1000 km) details reaches to many days, smaller ones ($\simeq 100$ km) usually exist for not more than a day. The contrast of UV-details' dependence on wavelength is represented in Figure 23: contrast reaches 30–40% at wavelength 0.30–0.35 μm and practically fully disappears at $\lambda > 0.50$ μm.

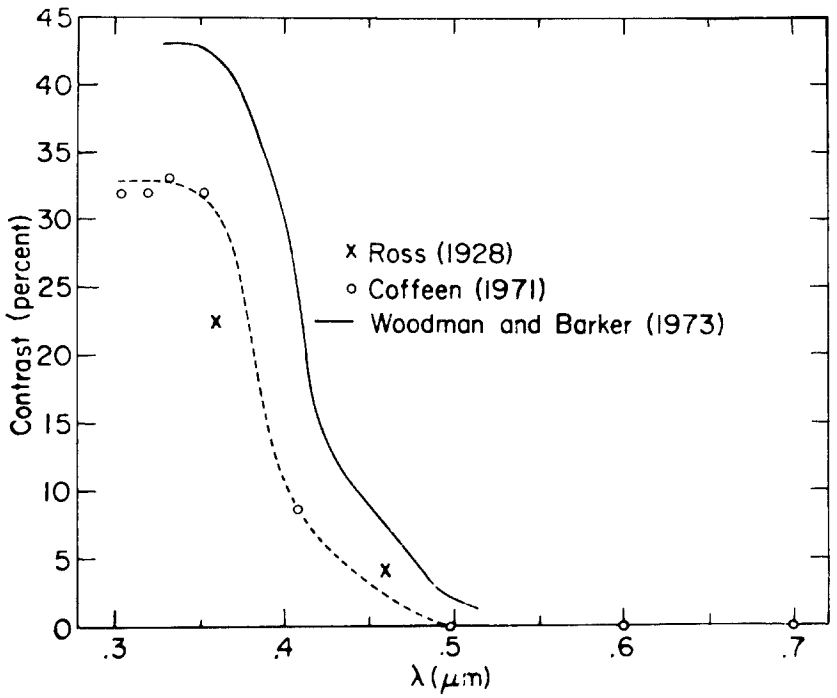

Fig. 23. The wavelength dependence of dark and bright details contrast (on the disk of Venus) (Travis, 1975).

4.3. The problem of chemical composition (experimental data)

In the past a great number of hypotheses concerning the chemical composition of cloud layer particles was proposed. First of all it was necessary to understand if the cloud layer consists of mineral dust or of condensates. It is possible to give three objections against dust: (1) the high transparency of the particles in the region 0.6–2.0 μm, (2) the great height of the clouds, (3) the sharp boundary above and below – a strong sign of the influence of temperature on the processes of particle creation. Mineral particles may dominate in clouds E and F (above and under the clouds) and serve as condensation nuclei in the clouds themselves but the main content of the cloud particles is without any doubt condensate.

The cloud layer temperature is too high for condensation of the main component – CO_2. Apparently also, CO_2 doesn't condense at great heights. The next possible candidate is H_2O. However neither reflective spectrum, nor refractive coefficient nor modern data on H_2O quantity in the gas state agree with the water content hypothesis (Moroz, 1971).

Many other assumptions were proposed: polymerized carbon suboxide C_3O_2 (Kuiper, 1962), hydrocarbons (Hoyle, 1965), ammonium chloride NH_4Cl (Lewis, 1968), mercury chloride Hg_2Cl_2 (Lewis, 1969), hydrated ferrum chloride $FeCl_2$ $2H_2O$ (Kuiper, 1969), hydrochloric acid HCl (Lewis, 1971), elementary mercury

(Potter, 1972), sulfuric acid H_2SO_4 (Sill, 1972, Young, 1973), hydrobromic acid HBr (Sill, 1975), elemental sulfur (Hapke and Nelson, 1975).

Many of these hypothesis were rejected because of the unsuitable refractive coefficient and absorption spectrum. This concerns C_3O_2, carbon hydrates, Hg, Hg_2Cl_2, Cl_2, and HCl. Recently the most popular hypothesis is sulfuric acid. Sulfuric acid water solution with nearly 75%-concentration permits us to explain the following properties of the layer D (particles of types 1 and 2): (1) refractive index (real part m_1), (2) absorption coefficient (or equivalently, imaginary part of refractive index m_2) in the region 0.6–4 μm (see Table XVII), (3) low pressure of H_2O vapor, (4) small discontinuity in the temperature curve near 0 °C, discovered on the Pioneer probes (it corresponds to the phase transition crystal liquid not only for H_2O but for H_2SO_4 water solution also). However sulfuric acid water solution is transparent in blue and near ultraviolet regions. Addition of some other substance (in the form of an admixture to H_2SO_4 in the same particles or of the particles with another content) is necessary to explain absorption in the region 0.32–0.5 μm. Among substances mentioned above $FeCl_2\,2H_2O$, HBr, elementary sulfur may serve as such a colouring admixture. Young (1977) considered the model of Venusian clouds, consisting of small ($\geqslant 1$ μm) H_2SO_4 particles and large ($\simeq 10$ μm) sulfur particles. According to Young's model the large particles are located deeper on average but the depth of the upper boundary of this layer may change in time and from one point to another. In this model Young tried to explain ultraviolet contrasts quantitatively. One would think that particles of type 3 may fully correspond to Young's population of large particles, consisting of elementary sulfur. However there are a few new results which are in contradiction with such a possibility.

The first of them – direct measurements of the particle content on V12 (Surkov *et al.*, 1979). X-ray fluorescent analysis of the particles sample collected in the cloud layer gave the following results:

(1) The most abundant component is chlorine.

(2) Mercury doesn't present in the quantities more than 10^{-11} g cm^{-3}.

(3) The content of sulfur is not more than 10% of the chlorine content.

Quantitative estimations of chlorine and sulfur must be defined more precisely, but it is possible to tell definitely that the chlorine content is by mass close to the full mass density of the clouds.

The other fact which doesn't agree with the assumption that the particles of type 3 consist of sulfur are optical measurements in situ. Joint analysis of albedo curve at wavelength near 0.35 μm, nephelometric data, particle spectrometer data and wideband photometry on the Pioneer probes show that the optical properties of sulfur and particles of type 3 don't coincide (Pollack *et al.*, 1979, 1980).

A third objection may be put forward on the basis of the estimations of gaseous sulfur amount according to spectrophotometric data obtained on V11. It is sufficiently small (see Section 2) and according to these estimations the condensation level is located at a height of about 56 km. But this argument is not strong because such an estimation supposes a constant mixing ratio for gaseous sulfur between 30

and 56 km. We shall see in Section 7 that the situation may be different from this.

Particles of mode 3 are apparently not composed of sulfur. Taking into account that in the particles of H_2SO_4 water solution the sulfur content is less than $\frac{1}{3}$ and particles of types 1 and 2 comprise less than $\frac{1}{2}$ by mass (Table XII), it is probably possible to remain with the hypothesis of sulfuric acid content for particles of types 1 and 2. In Section 7.4 we shall again consider the question about the chemical composition of the Venusian clouds.

The analysis of Pioneer probes and ground-based data carried out by Pollack *et al.* (1980) led to the following conclusions concerning the nature of UV-absorption and UV-contrasts:

(1) there are two different absorbents:

– in the region $\lambda < 0.32$ μm the absorbing gas SO_2,

– in the region $\lambda > 0.32$ μm the unknown absorbent apparently in a condensed phase (see Figure 24).

(2) Some different physical mechanisms lead to the appearance of contrasts:

(a) change of optical depth of the haze above the clouds – this mechanism is responsible mainly for the constrasts between the polar and the equatorial regions;

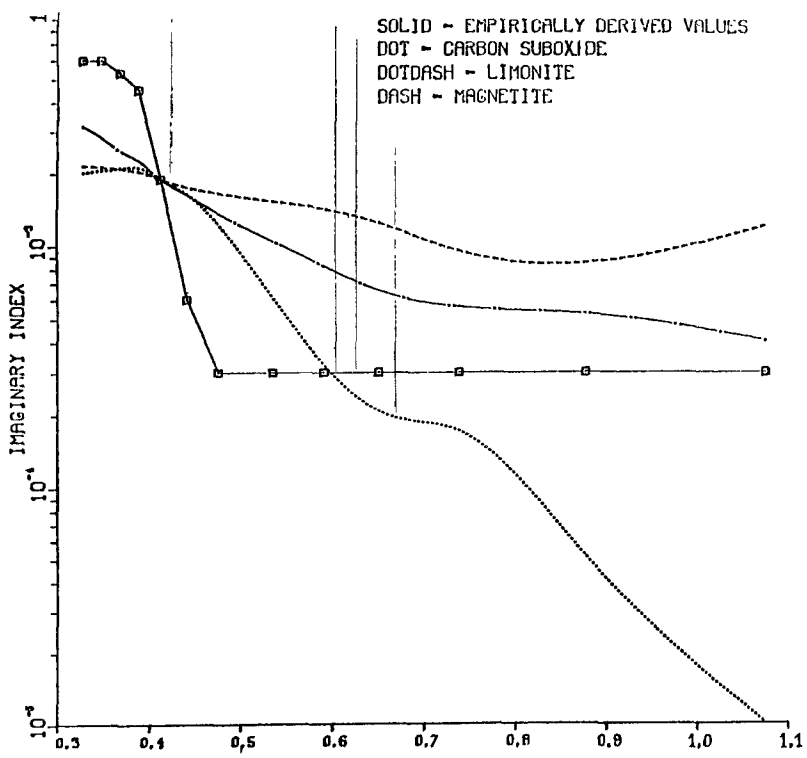

Fig. 24. Imaginary part of the refraction coefficient m_2 for the particles of type 1 according to the data by Pollack *et al.* (1980). The solid curve was inferred from the optical measurements on Pioneer probes and spectral reflectance data.

(b) change of the absorption coefficient of the unknown absorbent because of temperature variations, mixing or chemical processes – this mechanism acts in the equatorial regions.

The atmospheric motions can have an influence on two aspects: by means of local temperature variations and local variations of mixing.

It is possible to see that the problem of the chemical consistency of the clouds has not found a satisfactory solution in the meanwhile. Further experimental investigations in situ are necessary, particularly by direct methods (the analysis of collected material samples). Also it is necessary to study the variations of cloud layer characteristics in space and in time. The most effective for the problems of this aspect would be the measurements from a balloon flying in the atmosphere of Venus.

4.4. Thunderstorm phenomena

On the probes V11 and 12 special equipment named 'Groza' ('Thunderstorm') was installed for the search of lowfrequency electromagnetic radiation pulses which must be radiated by thunderstorm charges if they are present in the atmosphere of Venus (Ksanfomality *et al.*, 1979a; Ksanfomality, 1979, 1980). Before this experiment there was no experimental data on such phenomena on Venus. The measurements were carried out in four diapasons – 10, 18, 36, and 80 kc s^{-1}. On both probes during parachute descent in all these diapasons groups of pulses were discovered whose character was like terrestrial thunderstorm radiation. Insofar as the height of the lower boundary of the clouds above the surface is large ($\simeq 50$ km), discharges between the clouds and the surface are not probable. Apparently, the pulses are caused by discharges between separate condensations of cloudy masses.

Lately some other evidence on thunderstorm activity on Venus has been published. In the plasma wave experiment on P-O pulse radiation of 100 c s^{-1} was registered, but observed only at the lowest points of the orbit. It is proposed that the radiation sources are also thunderstorm charges (W. W. L. Taylor *et al.*, 1979a, b; Scarf *et al.*, 1980). Krasnopolsky (1980) published an analysis of the case when the optical spectrometer on V9-O above the night side of the planet had registered a group of light flashes which is probably connected with thunderstorms also.

According to the estimations of Ksanfomality and Krasnopolsky thunderstorm activity on Venus may be more than on the Earth. Thunderstorm charges may play a role in the chemistry of small constituents of the cloudy layer of Venus (Section 7).

5. Thermal Regime. Greenhouse Effect

All the main facts concerning vertical and horizontal temperature distribution in the atmosphere of Venus have been described above. In this and partly in the next section we shall consider the physical events which are responsible for the thermal regime of the Venusian atmosphere and experiments concerning their investigation directly. We shall consider in this Section 5.1 the balance between solar and outgoing

planetary thermal radiation, then Section 5.2 the results of measurements of solar and thermal radiation streams on descent probes. Section 5.3 hypotheses about the physical processes supporting the high temperatures of the surface.

5.1. Solar and planetary thermal radiation balance

The average effective temperature of the planet T_e and its integral Bond albedo A_I are connected by the equation of balance

$$4\sigma\bar{T}_e^4 = E_0(1-A_I)+q\,, \tag{5.1}$$

where $E = 2600\ \mathrm{W\,m^{-2}}$ is the solar constant of the orbit of Venus, $\sigma = 5.67\times$ $\times 10^{-8}\ \mathrm{W\,m^{-2}\ degree^{-4}}$ is the Stefan–Boltzman constant, q is the flux of internal heat which is usually neglected in the case of the planets of the Earth's group ($q = 0.06\ \mathrm{W\,m^{-2}}$ for the Earth).

Determination of the exact value of $\bar{T}_e$ is a difficult problem, because it is necessary to take into consideration the angle diagram of radiation, latitude and longitude distribution and deviations from the Plank function also. On the basis of the infrared measurements on V9-O and V10-O, Ksanfomality (1977) found that $A_I = 0.79^{+0.02}_{-0.01}$, if it is determined by means of infrared radiation flux using the Equation (5.1). Hence his measurements give $\bar{T}_e = 222^{+2}_{-6}$ K. Taylor *et al.* (1980) on the base of the measurements on P-O obtained a higher value of $\bar{T}_e = 228 \pm 5$ K, corresponding value $A_I = 0.76^{+0.02}_{-0.03}$, and it coincides within the limits of error with the value obtained using the reflecting radiation spectrum (0.74 ± 0.02) – see Section 1). For further consideration we shall use self-conformed values

$$A_I = 0.75 \pm 0.03$$
$$\bar{T}_e = 231 \pm 7\ \mathrm{K}\,. \tag{5.2}$$

Corresponding mean value of the outgoing flux is

$$\bar{F}_0 = \sigma\bar{T}_e^4 = 162 \pm 20\ \mathrm{W\,m^{-2}}\,. \tag{5.3}$$

It is clear from the data represented in Section 3, that temperature profiles of the atmosphere lower than 70 km are close enough at night and in the day time, on the equator and in the high latitudes. Differences of 10–20° appear only higher than 50 km. Accordingly there are no large local differences in the effective temperature T_e. The small value of the daily effects in the low atmosphere may be explained by the large thermal inertia of the atmosphere. In fact the relative amplitude of daily temperature fluctuations in the order of the value can be determined by the equation

$$\frac{\Delta T_d}{T_0} \simeq \frac{F_0 P_i}{2Mc_p T_s} = 10^{-3}\,. \tag{5.4}$$

Here M is the mass of the atmospheric column with a unit area section, P_i is the solar day duration (117 d), T_s is the temperature of the surface, c_p is the heat capacity by constant pressure.

The temperature difference between the equator and the pole ΔT_φ depends on how the heat is transported by atmospheric circulation from the equator to the pole. Golitsyn (1970) has shown that

$$\Delta T_\varphi = \left(\frac{\tau}{2}\right)^{1/2} \left(\frac{\lambda_1}{k\alpha}\right)^{1/4} \frac{F_0^{9/16}}{\sigma^{1/16} c_p^{3/4}} \left(\frac{R}{M}\right)^{1/2} \simeq 2\,\mathrm{K}\,. \tag{5.5}$$

Here $k \simeq 0.1$ is the coefficient of the 'atmospheric heat machine', $\lambda_1 = 1$ for slowly rotating planets, R is the radius of the planet, $\alpha = T_s/T_e$.

The estimations (5.4) and (5.5) correspond to the deep layers of the atmosphere (the lowest layer with thickness about one height scale), but they control the thermal regime even in higher layers till the effective level $\tau \simeq 1$ where the planetary thermal radiation passes away to space.

5.2. The results of measurements of solar and thermal radiation fluxes on the descent probes

In 1972 on V8 solar radiation fluxes in the deep layers of the Venusian atmosphere up to the surface were first measured (Avduevsky *et al.*, 1973). Then analogous measurements were repeated with a more perfect method. The list of corresponding experiments is represented in Table XIII. Integrated over all the spectrum and averaged by the angles, the flux of the scattered solar radiation near the surface according to the measurements on V9 and 10 (Avduevsky *et al.*, 1976c) and on V11 (Ekonomov *et al.*, 1979; Moroz *et al.*, 1980) is about 3% from the solar constant on the orbit of Venus or when averaged over all the surface

$$F_s \simeq 20\ \mathrm{W\,m^{-2}}\,. \tag{5.6}$$

Close results were obtained using measurements on P-L (Tomasko *et al.*, 1979). So a rather significant flux of 10–15% from F_0 reaches the surface. Here it is absorbed almost completely (the albedo of the surface is about 0.1, Golovin, 1980) and reemitted in the infrared. Narrow band photometric profiles are shown in Figure 21. Photometric profiles obtained by Yomasko *et al.* (1979) in wide bands in situ (0.4–1.0 and 0.4–1.8 μm) are represented in Figure 25. During in situ measurements the value of net flux

$$N_s(z) = F_s{\downarrow}(z) - F_s{\uparrow}(z) \tag{5.7}$$

which is the difference of the fluxes of the scattered radiation from above and from below is of special interest. An analogous value may be introduced for thermal fluxes

$$N_p(z) = F_p{\uparrow}(z) - F_p{\downarrow}(z)\,. \tag{5.8}$$

In the limit when $\tau \ll 0$

$$F_0 = N_p(\infty)\,. \tag{5.9}$$

The altitude profile of the full net flux $N = N_s + N_p$ determines the energy influx in

the unit of volume per unit of time:

$$\frac{dq}{dt} = \frac{dN}{dz}. \tag{5.10}$$

Planetary thermal radiation fluxes in the deep layers of atmosphere were measured at first on Pioneer probes. Unfortunately the measurements weren't successful in reaching the surface: on P-L they were interrupted about the level 45 km and on the small probes – about 12 km. The results are represented in Figure 26 and 27. In

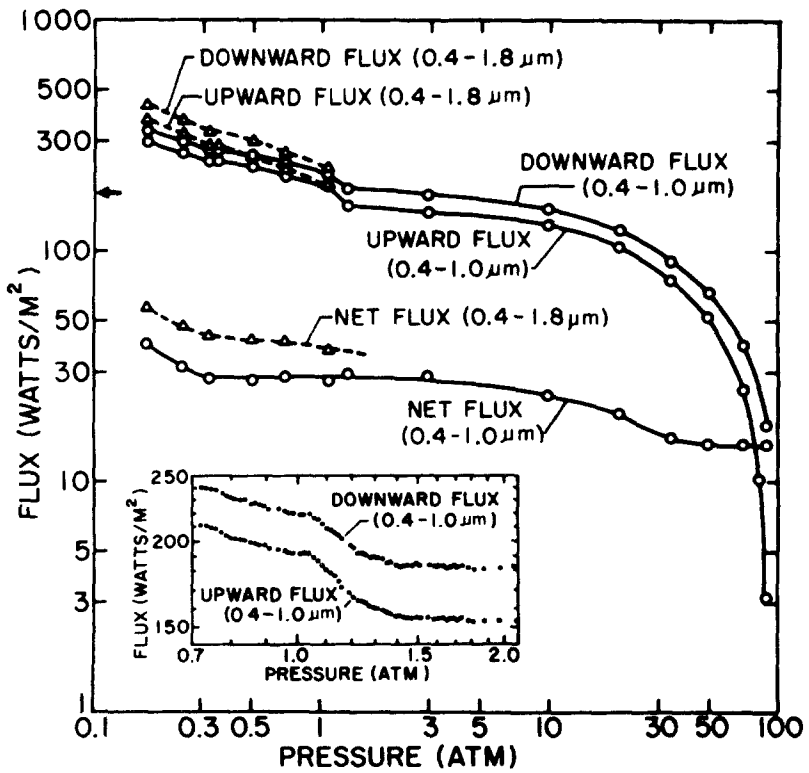

Fig. 25. Results of the measurements of the scattering solar radiation fluxes on P-L (Tomasko *et al.*, 1979). Downward flux, upward flux and net flux are given dependent on the pressure. Flux out of the atmosphere is 820 W m^{-2} for the interval 0.4–1.8 μm and 600 W m^{-2} for 0.4–1.0 μm.

the experiment Boese *et al.* (1979) on the P-L the value N_p was measured in the diapason from 3 to 100 μm. In the experiment Suomi *et al.* (1979, 1980) on three small probes full net flux N (in the diapason from 0.2 to 50 μm) was measured. For P-Ni and P-No $N = N_p$, for P-D one scattered solar radiation is added. Flux data analysis leads to the following qualitative conclusions:

(1) There is significant solar and thermal radiation absorption at heights of about 60 km ($P < 0.25$ atm.); most probably it is connected with the presence of absorbing

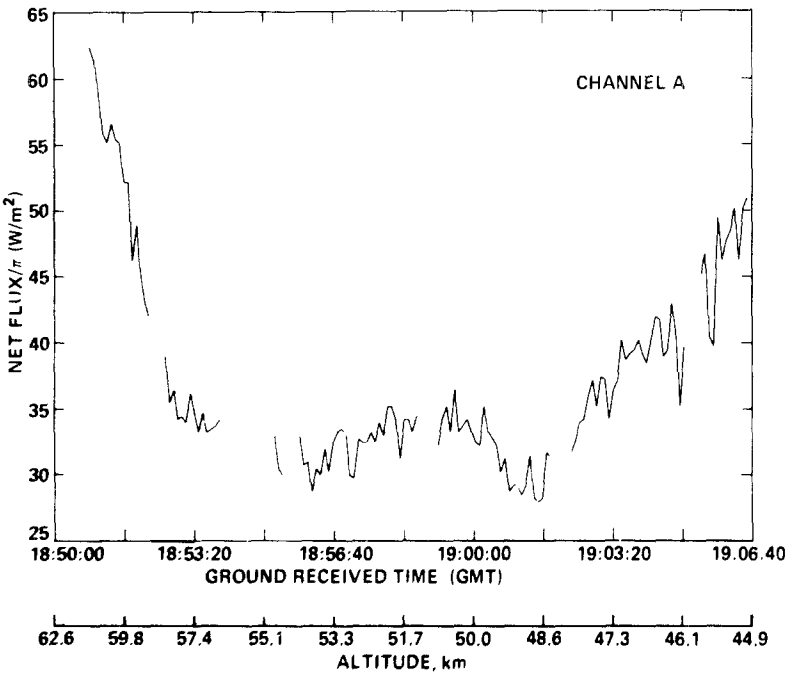

Fig. 26. Net flux N_p of the thermal planetary radiation in the 3–100 μm diapason from P-L measurements (Boese *et al.*, 1979).

particles of small size (not discovered by nephelometer or particle size spectrometer);

(2) Solar radiation at a height of 50–60 km is weakened very little. In this part of the cloudy layer thermal radiation is weakened strongly.

(3) In the diapason from 50 to 20 km solar radiation decreases gradually, net flux N_p for thermal radiation is here on the average more than in the cloudy layer at heights of 50–60 km (there, convective heat transfer is added), however the character of the profile $N_p(z)$ is complex. Variation in $N_p(z)$ may be connected both with dynamical phenomena and with local absorption effects.

(4) From 20 km to the surface derivative $|dN_s/dz|$ increases more and more quickly. The reason for this phenomenon is clear from the spectral measurements on V11: the presence of some atmospheric gases absorption (Figure 9). As it is possible to notice, N_p values on the height of 12–20 km obtained in the Suomi experiment (Figure 27) essentially exceed the N_s values measured by Tomasko (Figure 26).

(5) Below 55 km the radiation fluxes N_p are less than the outgoing flux F_0 by several times. The evidence is that either the convective transfer role is significant or the essential part of the planetary thermal radiation is generated high above the surface. Probably both assumptions are true.

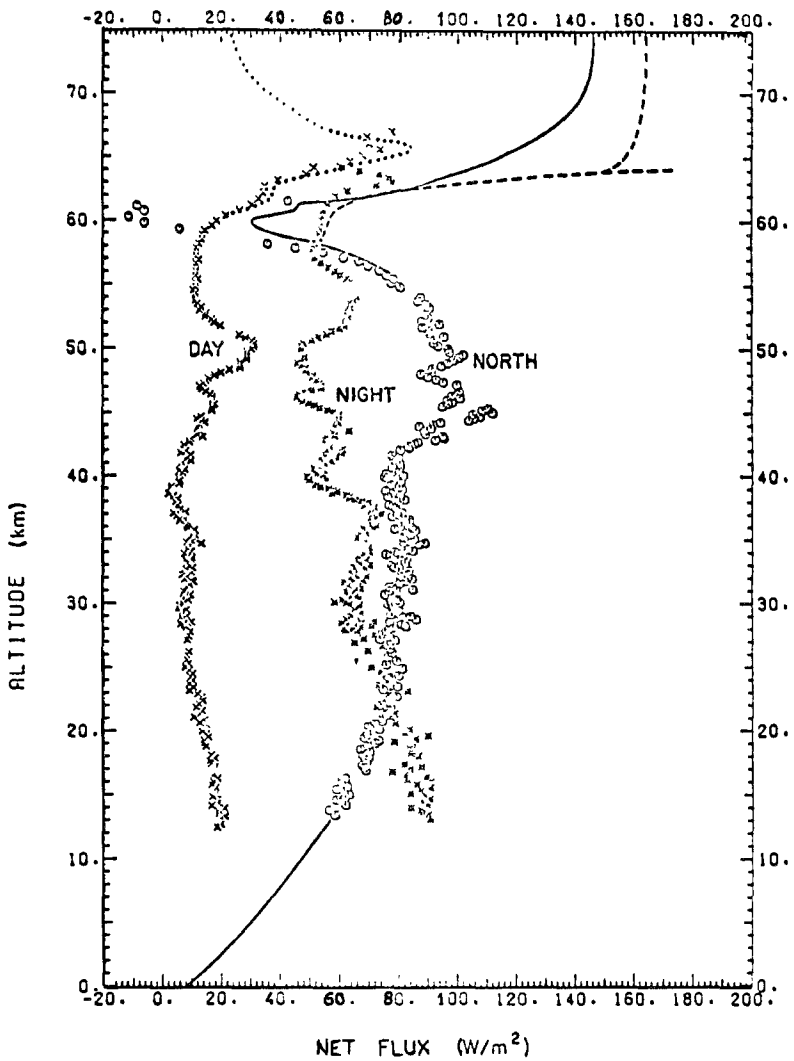

Fig. 27. Net flux $N = N_p + N_s$ in the 0.2–50 μm diapason from measurements on the small Pioneer probes (Suomi *et al.*, 1980).

5.3. The Problem of the Mechanism Responsible for the High Temperatures in the Deep Layers of the Atmosphere

5.3.1. *The Greenhouse Effect*

Four hypotheses proposing different sources of energy have been suggested to explain the high temperature of the surface and deep layers of atmosphere.

(1) The greenhouse effect.
(2) Heating by general circulation.
(3) Heating by intrinsic thermal source.
(4) The Eolospheric hypothesis.

The latter hypothesis (Opik, 1961) suggests that clouds consist of mineral dust and fill in all the atmosphere from the surface to the upper cloud boundary. This doesn't correspond to reality, and the eolospheric hypothesis may be immediately excluded from the analysis in accordance with modern data. We shall consider the other three.

5.3.2. *The Greenhouse Effect*

The source of energy is solar radiation which is absorbed partly on the surface and partly in the atmosphere. This energy is transformed into planetary thermal radiation with flux directed upward and creating a temperature gradient. This gradient value depends on the opacity of the atmosphere for the thermal infrared radiation. Heat is transported upward by the radiative transfer, if the static stability parameter

$$S = \frac{dT}{dz} + \frac{g}{c_p} > 0 ; \tag{5.11}$$

if $S < 0$, convective transfer is added. Here the value $g/c_p = (dT/dz)_{ad}$ is the adiabatic gradient. If the parameter S is negative its absolute value is very small. In other words, the real gradient must not be more than $(dT/dz)_{ad}$ by the module.

The value of the heating of the surface on account of the greenhouse effect may be described by the parameter $\alpha = T_s/T_0$. On the Earth $T_s = 287$, $T_0 = 250$ K and $\alpha = 1.16$. On Venus $\alpha = 3.2$ and 20 years ago it was necessary to have some courage to propose the greenhouse effect for the explanation of such strong heating (Sagan, 1960, 1962). For the presence of the greenhouse effect in the atmosphere two conditions must exist: (1) atmospheric transparency (even though partly) for solar radiation, (2) strong absorption of thermal planetary radiation in the atmosphere. From a qualitative point of view both these conditions exist. Scattered solar radiation runs through to the surface. Atmospheric gases (CO_2, H_2O, SO_2) and cloudy layer particles absorb infrared planetary radiation. However it is necessary to consider the question quantitatively.

We shall carry out this analysis within the limits of a 'grey' atmosphere model. Thermal radiation flux at radiative transfer in Eddington's approximation is

$$N_p = \frac{16}{3} \frac{\sigma}{\bar{k}} T^3 \frac{dT}{dz} \tag{5.12}$$

where $\bar{k}$ is the 'grey' absorption coefficient. If convection takes plasce convective flux adds to the radiative flux. By free convection according to mixing length theory the convective heat flux is:

$$N_k \simeq -\rho c_p v H S , \tag{5.13}$$

where H is the scale of height, v is the characteristic speed

$$v = \left(\frac{R}{c_p} \frac{N_k}{\rho} \right)^{1/3} , \tag{5.14}$$

TABLE XVIII

Mean absorption coefficients of thermal radiation in the Venusian atmosphere

z (km)	T (K)	dT/dz (K km^{-1})	c_p [a] (j g^{-1} deg^{-1})	$\left\|\frac{dT}{dz}\right\|_{ad} = \frac{g}{c_p}$ (K km^{-1})	s (K km^{-1})	ρ (g cm^{-3})	N_p [b] (W m^{-2})	$\bar{k}_m$ (cm^{-1})	(CO_2+H_2O), k_R, cm^{-1} [c]		
									$f_{H_2O}=0$	10^{-4}	10^{-3}
0	735	7.6	1.17	7.6	0	6.5×10^{-2}	(20)	(4.5×10^{-4})	3.0×10^{-4}	1.2×10^{-3}	2.6×10^{-3}
10	658	8.0	1.10	8.0	0	3.7×10^{-2}	(30)	(2.2×10^{-4})	4.5×10^{-5}	4.3×10^{-4}	8.8×10^{-4}
20	576	8.0	1.07	8.0	0.2	2.0×10^{-2}	40	1.1×10^{-4}	9.0×10^{-6}	2.0×10^{-4}	3.7×10^{-4}
30	492	8.0	1.01	8.7	0.7	1.0×10^{-2}	50	5.8×10^{-5}	7.6×10^{-7}	5.2×10^{-5}	1.2×10^{-4}
40	413	6.5	0.99	8.8	2.3	4.3×10^{-3}	50	2.7×10^{-5}	1.9×10^{-8}	1.6×10^{-5}	3.6×10^{-5}
50	347	9.9	0.88	9.9	0	1.5×10^{-3}	30[d]	4.1×10^{-5} [d]	9.3×10^{-9}	2.3×10^{-6}	5.4×10^{-6}
55	299	9.5	0.83	10.5	1.0	8.7×10^{-4}	30[d]	2.5×10^{-5} [d]	6.6×10^{-9}	1.3×10^{-6}	3.0×10^{-6}

[a] c_p is given for a mixture of 97% CO_2 and 3% N_2 taking into account T, P-dependence from the Rables, Vukalowitch and Altunin (1965).

[b] Net flux N_p was evaluated approximately from the data presented in Figures 26 and 27 for altitudes 20–55 km. For fluxes at 0 and 10 km, a balance between solar and heat radiation was proposed.

[c] f_{H_2O} is the mixing ratio of H_2O. Rosseland's mean absorption coefficients K_R are given on the base Galtsev and Safraj calculations (1980).

[d] Evaluations are based on the P-L measurements of N_p (Boese *et al.*, 1979). Measurements on the small probes gave two times less fluxes N_p and the value of k_m must also be two times less. These variations possibly reflect the real local differences in the cloud structure.

where R is the gas constant. If we take the measured values of dT/dz (from Table X) and the planetary thermal radiation fluxes it is possible to find the vertical distribution $\bar{k}(z)$ in the atmosphere of Venus (Table XVIII). By integrating $\bar{k}(z)$ by the height we obtain the total optical depth for thermal radiation:

$$\tau = \int_0^\infty \bar{k}(z)\,dz = 700\,. \tag{5.15}$$

This is the measured value, which doesn't depend on the correctness of the greenhouse hypothesis. Statical stability parameter S and atmospheric gases absorption coefficient are represented in Table XVIII. The latter are calculated by means of a Rosseland mean for pure CO_2 and for CO_2 with small H_2O amounts admixture. We ought to take into account the absorption of SO_2 in the region 6–10 μm also, but it is possible to expect that the results will change very little.

Static stability S is close to 0 at heights from 0 to 20 km. This is the region where convective transfer adds to radiative transfer. Direct measurements of thermal radiation are absent here, represented values of N_p must be considered as maximum and value of $\bar{k}_m$ as minimum. Nevertheless it is clear that the addition of H_2O with a mixing ratio of $10^{-5} < f_{H_2O} < 10^{-4}$ may fully provide the required value of $\bar{k}_m$. At the heights 30 and 40 km only radiative transfer takes place ($S > 0$), here it is necessary to have f_{H_2O} about 10^{-4} and 3×10^{-4} accordingly. Increasing of f_{H_2O} to the level 10^{-3} would lead to convection instability. So the temperature profile measured on P-L conforms more closely with the H_2O profile obtained on V11 than with the results of chromatographic measurements, carried out on P-L (see Section 2) immediately.

At 50 km height $S = 0$ again and opacity k_m increases simultaneously. CO_2 and H_2O don't provide it even when $f_{H_2O} = 10^{-3}$ (one order of value more is necessary). Apparently here opacity is provided by the cloudy layer particles. If we compare $\bar{k}_m$ with extinction coefficients in the visible spectral region (Table XVII, layers B, C) it is possible to see that they coincide almost fully. Large particles (type 3) give the main contribution. We ought to note that aerosol density in the layer B is not constant and radiative flux variations are probably connected with this circumstance (compare Figure 26 and 27).

If the greenhouse hypothesis is correct, on the average (over all the planetary surface and over time) the identity must take place:

$$\bar{N}(z) = \bar{N}_s(z) + \bar{N}_p(z) + \bar{N}_k(z) \equiv 0\,. \tag{5.16}$$

The $\bar{N}_k(z)$ component may be estimated only very approximately though in the stable zone between 30 and 50 km it may be neglected. However there is another difficulty: the measurements of the fluxes $\bar{N}_s(z)$ are carried out only at separate points, and extrapolation to other points (and other solar times) requires definite assumptions. It would be possible to propose that the sum $\bar{N}_p(z) + \bar{N}_k(z)$ ($= N_p$ in the stable zone) remains approximately constant over all the planet, but the experiment by Suomi

et al. (1979, 1980) has shown that there are significant (some tens percent) variations in $N_p(z)$.

In connection with it Suomi *et al.* (1980) even express doubt about the correctness of the greenhouse effect hypothesis. It is difficult to agree with such doubts because with reasonable models of $N_s(z)$ horizontal distribution, the balance (5.16) is present for the stable zone (30–50 km) within the limits of error and it is difficult to expect more. On the whole the greenhouse effect conception is in quite satisfactory agreement with solar and planetary thermal flux measurements, and with the data on the gaseous content of the atmosphere and the characteristics of the clouds.

An unusual peculiarity of Venus is the presence of not one but two unstable zones in the low atmosphere. Seiff *et al.* (1979b) according to the measurements on Pioneer probes give very large values of S for these zones – to $-1\ \mathrm{K\,km^{-1}}$. It is difficult to believe in the reality of these values. In fact with $v = 1\ \mathrm{m\,s^{-1}}$ (see Section 6) and $N_k = 10^2\ \mathrm{W\,m^{-2}}$ the formula (5.8) gives

$$S \simeq 2 \times 10^{-5}\ \mathrm{K\,km^{-1}}\,. \tag{5.17}$$

More exact convective theory may lead to other values of S but at any rate they don't reach the values cited in the above mentioned article. Large superadiabatic gradients may exist only in the narrow (some meters) atmospheric layer near the surface, where convective transfer isn't effective.

We shall note that the circumstance that the most part of solar energy is absorbed at a significant height above the surface isn't in contradiction with the greenhouse hypothesis. It is important that the part which reaches the surface as we have seen is sufficient for the support of the temperature profile measured in the troposphere of Venus.

Detailed calculations of thermal fluxes in the Venusian atmosphere taking into account the deflexion from the 'grey' model were carried out by Shari (1975, 1976). Useful information on the method of greenhouse effect calculation may be found in the articles by Sagan (1962, 1969), Ostriker (1963), Wattson (1968), Ginzburg and Fejgel'son (1969), Strelkov and Kukharskaja (1969), Pollack and Ohring (1973), Moroz and Mukhin (1977).

5.3.3. *Heating by General Circulation*

Analyzed by Goody and Robinson (1966) and Robinson (1970). The basic assumption is that atmospheric motions would be able to maintain high temperatures by themselves owing to adiabatic compression of atmospheric volumes falling down. Here the main idea is to release the theory from the condition of partial transparency of the atmosphere for solar radiation which it is now clear actually exists. There is another objection also. Mechanical mixing may create an adiabatic gradient; however in the case of atmospheric circulation we are dealing with a thermal source of energy and require transport of heat from a colder body to a warmer one and this is forbidden by the second law of thermodynamics.

5.3.4. *The Hypothesis of Intrinsic Planetary Heat*

(Kuzmin, 1964; Hansen and Matzushima, 1967). So far as the balance between solar radiation influx and outgoing radiation takes place within the limits of the error of measurement (see Section 5.2.) we may speak only about 10–15% of the value F_0, i.e., about the flux 20 W m^{-2} being approximately equal to solar radiation flux near the surface. However for an intrinsic heat source it is too much – it is 300 times more than on the Earth. Taking into account that different rocks have approximately the same heat conductivity it would mean that the temperature gradient in the crust of Venus is in the order of 300 times more than on the Earth and the temperature difference reaches 10^4 K within the limits of several kilometers. So the fact itself of the solid surface presence on Venus makes us reject inner heat as a possible source of the atmosphere heating (Moroz, 1971b; Morrison, 1976).

6. Dynamics

Atmospheric motions smooth the temperature differences caused by the latitudes' differences in solar influx. On the Earth the structure of the general circulation is complicated by the presence of oceans and by the inhomogeneity of the cloud cover. These factors are absent on Venus and this is the reason for hoping that model calculation of the Venusian general circulation may be a simpler problem. Absence of seazones provide additional simplification. Here we shall review experimental data about winds (6.1.), turbulency, convection and waves (6.2.), hypotheses proposed for explanation of the superrotation (6.3.), the problem of general circulation (6.4.). There are a few reviews especially devoted to the dynamics of the Venusian atmosphere: by Stone (1975) and by Schubert *et al.* (1977, 1980).

6.1. Experimental data about winds

Winds in the atmosphere of Venus were investigated by ground-based observations and by space missions. The following methods were used:

(1) measurement of movements of the details on the UV-photographs ($\lambda \simeq \simeq 3500$ Å) of the planet;

(2) measurements of the Doppler shifts of the spectral lines on the edges of the planetary disk;

(3) measurements of the Doppler shifts of the radio-frequency signal from descent probe;

(4) determination of motion of the descent probe by means of VLBI;

(5) direct measurements of the wind velocities after the landing;

(6) reconstruction of the velocity field on the base of temperature and pressure data.

We shall discuss below results obtained by means of these methods. We shall use conventional meteorological designations of zonal, meridional and vertical components of wind – u, v, w respectively.

6.1.1. *Displacements of the UV-details*

The first observations were made in the twenties (Ross, 1928), and many attempts to define the rotation period were made on the base of UV-pictures. However, reliable results were obtained much later (Boyer et Camichel, 1961). A period of rotation $P_{UV} \simeq 4^d$ was found, much less than the rotation period of the solid planetary body, deduced from radar (243^d – see Table I). The natural explanation is presence of a strong zonal wind at the altitude of UV details (approximately 65–68 km). The velocity is equal to

$$u = 2\pi R/P_{UV} \simeq 100 \text{ m s}^{-1} . \tag{6.1}$$

The wind direction is the same as the direction of planetary rotation (clockwise if looking from the North Pole, that is Easterly). This zonal circulation with a high velocity (much exceeding the velocity of planetary rotation) was given the name 'superrotation'. The summary of UV-measurements of wind velocity is given in Table XIX. The UV pictures of Venus were obtained not only from the Earth but also from the fly-by probe M10 and orbiters (V9, P-O). These provided strong improvements of the spatial resolution – from 500 km to nearly 10 km. Studies of

TABLE XIX

Wind velocities: measurements of the movements of UV details – ground-based and on M10

Reference	Zonal wind ($m s^{-1}$)[a]	Period (day)	Meridianal wind, v_m ($m s^{-1}$)	Remarks
Boyer and Camichel (1961)	−110	~4	—	[b]
Boyer and Camichel (1965)	−100 ± 10	4–5	—	[b]
Smith (1967)	−90 ± 20	3–5	—	[b]
Nikander and Boyer (1970)	−110 ± 10	4.0 ± 0.5	—	[b]
Scott and Rese (1972)	−107 ± 20	4.2 ± 0.8	—	[b]
Coldwell (1972)	−100	4.5	—	[b]
Boyer (1973)	−83	5, 4	—	[b] morning
	−122	3, 7		afternoon
Murray *et al.* (1974)	−100	4.5	to 10	[c]
Dollfus (1975)	−110	4	—	[b]
Sidi (1976)	−81.6 ± 1.0	5.3		[c] morning
	−126.4 ± 7.2	3.5		evening
			1.8 ± 1.3	North hemisphere
			4.1 ± 2.5	South hemisphere

$\bar{u} = 104 \pm 11$.

[a] Sign '−' means that the direction of the zonal wind is the same as that of planetary rotation (reverse).
[b] Ground-based observation, equatorial regions.
[c] M10, zonal velocity in middle altitude are larger. Meridianal velocities are poleward and are related to the latitudes from 30 to 50°.

M10 TV-pictures lead to the following conclusions:

(1) Angle velocity is rising with latitude to $\varphi \simeq 50°$. Momentum per mass unit is approximately constant inside the latitude's band $-50 < \varphi < +50°$. For latitudes $|\varphi| > 50°$ angle velocity decreases with the approach to the pole (Murray *et al.*, 1974; Suomi, 1974, see Figure 28).

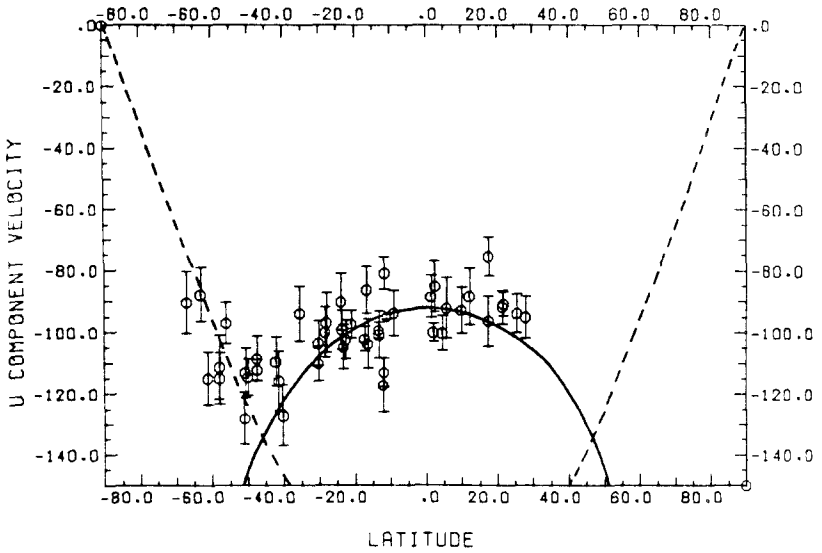

Fig. 28. Latitude profile of zonal wind from analysis of UV images obtained on M10. Continuous line corresponds to the constant angle momentum; dashed line – to the constant angle velocity (Suomi *et al.*, 1974).

(2) Meridional velocity $v \simeq 5$ m s^{-1} is observed between latitudes 30 and 50°. The meridional winds are poleward. In the equatorial regions $v \simeq 0$ (Murray *et al.*, 1974; Suomi, 1974).

(3) There are longitude variations of zonal wind velocity (Sidi, 1976), which are partially correlated with the local solar time (in the morning time velocity is less, in the afternoon more – see Table XIX).

(4) Spatial distribution of UV-contrasts has a complicated structure (Figures 22 and 29) with the scales from a few thousands kilometers to the limit of resolution. The largest and most prominent details are shown in Figure 22: a subsolar region with cell structure, bow waves, equatorial bands, spiral streaks and so on (Murray *et al.*, 1974; Dollfus, 1974; Belton *et al.*, 1976a, b). The dark horizontal Y-detail is visible even on ground-based photographs.

6.1.2. *Doppler Shift of the Absorption Lines*

Most measurements of Doppler shifts of CO_2 and Fraunhofer lines on the limbs confirmed the large value of zonal velocity (Table XX). These observations were provided by means of ground-based telescopes and spectral instruments with the

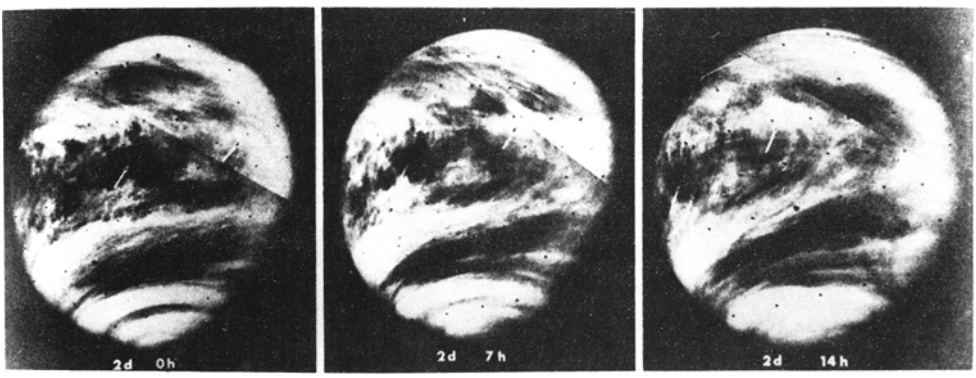

Fig. 29. The set of composed images which were obtained by M10 with the time interval 7^h. Large lifetime of big UV details is demonstrated. Two of these are shown by the arrows, one detail is dark and one is light (Murray, 1974).

TABLE XX

Wind velocity: ground-based observations of the line Doppler shifts

Reference	Zonal wind ($m\,s^{-1}$)	Period (day)	Meridianal wind ($m\,s^{-1}$)	Remarks
Guinot (1965)	-108 ± 18	4.1 ± 0.7	—	[a]
Guinot and Feissel (1968)	-103 ± 10	4.3 ± 0.4	—	[a]
Traub and Carleton (1975)	-83 ± 10	5.4 ± 0.6	<30	[b]
Young (1975)	$+10 \pm 33$	45	—	[c]
Betz *et al.* (1977)	<10	>45	—	[d]
Betz *et al.* (1977)	-90 ± 7	$4{\cdot}9 \pm 0.4$	—	[e]
Traub and Carleton (1979)	-85 ± 10	$5.2 \pm 0{\cdot}6$	—	[f]
Young *et al.* (1979)	$+26 \pm 36$	18^d	—	[g]
	$+27 \pm 16$			
Serkovski *et al.* (1979)				[h]

[a] Fraunhofer lines in the region 5500–5700 Å.

[b] CO_2 lines near 8708 Å and Fraunhofer near 6717 Å. Mean equatorial velocity before noon ($73\ m\,s^{-1}$) is less than afternoon ($111\ m\,s^{-1}$).

[c] On the basis of the spectrograms of Richardson (1956).

[d] Heterodyne spectroscopy velocity was determined from the measurements of emission nuclei of rotational lines of band $C_2^{12}O^{16}$ 9.6 μm. Velocity is related to the altitude near 115 km.

[e] The same for lines of $C^{13}O_2^{16}$, velocity is related to the altitude near 75 km.

[f] CO_2 lines near 8708 Å. Some periodical variations were marked (amplitude $40 \pm 14\ m\,s^{-1}$, period $4.3^d \pm 0.2^d$).

[g] Spectral region 6300 A (Fraunhofer lines), the two numbers are related to different sets of observations.

[h] Fraunhofer lines in the region λ 4260 Å.

ultimate high resolving power (Fabry–Perot interferometers, heterodyn spectrometers). There are some contradictions in the results, connected probably with the very small value of the shifts (comparable with the linewidths). Some observers didn't find measurable shifts at all (Young *et al.*, 1979). Such discrepancies gave Young (1975) the possibility of doubting the reality of the velocities which were found from movements of UV-details. He supposed that visible displacements reflect some propagation of the phase of wave movements and have no connection with the flux of the substance. It was difficult to agree with such a point of view because wind profiles found from descent probe missions were in good agreement (by some extrapolation up) with the UV-data (Kerzhanovich and Marov, 1977; Ainsworth and Herman, 1977). We shall see below that wave movements are important by the formation of the dark UV-details; however the zonal flux of substance with a velocity $\simeq 100$ m s^{-1} is real at the same time.

6.1.3. *Measurements by Means of Descent Probes*

Horizontal velocity gives some contribution in the radial velocity of a descent probe if the local vertical doesn't coincide with the line connecting the probe and the ground-based antenna. It is possible to deduce the projection of the horizontal velocity on the line of view if the vertical velocity of descent is known. This leads to

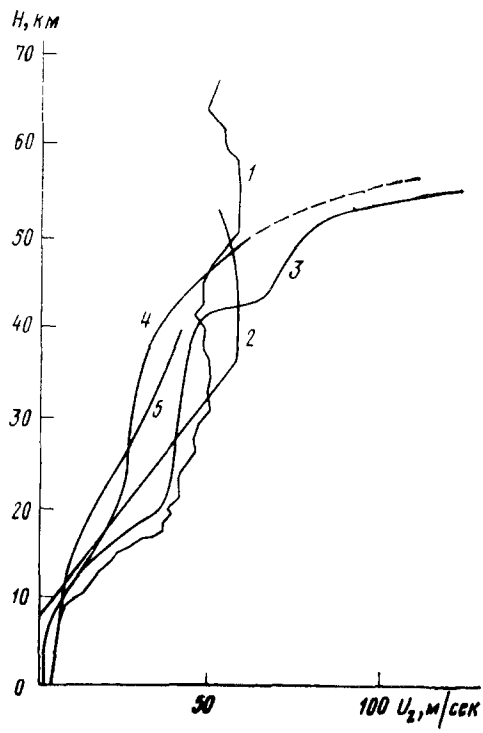

Fig. 30. Altitude profile of zonal wind $u(z)$ from Doppler measurements. 1-V12; 2-V9, 10; 3-V8; 4-P-D; 5-P-Ni (Kerzhanovich *et al.*, 1979).

TABLE XXI

Wind velocities: measurements with the descent probes

Altitude (km)	Doppler velocities, v_z (m s^{-1})[g]									VLBI Pioneer data, v_z and v_m (m s^{-1})[f,g]						Mean[h] value $\bar{v}_z$
	V4 [a]	V6 [a,b]	V7 [b]	V8 [a,b]	V9 [c]	V10 [c]	V12 [d]	P-D [e]	P-Ni	P-D		P-Ni		P-N		
										v_z	v_m	v_z	v_m	v_z	v_m	
60	—	—	—	—	55	50	53	70	75	80	0	80	−2	—	—	6±12
55	—	—	—	—	55	50	58	47	45	60	+2	60	+2	80	+5	56±10
50	75	—	50	80	55	50	50	60	55	60	+2	52	+6	70	+6	59±10
45	70	—	20	67	57	52	47	47	40	50	+3	50	−2	60	+0.5	51±13
40	40	—	10	45	58	55	47	42	27	37	−2	35	−5	40	0	40±12
30	40	—	15	40	40	40	47	—	—	30	+1	30	+1	26	+1	34±9
20	—	—	15	32	25	25	37	—	—	22	0	22	0	15	0	24±7
10	—	—	—	5	5	2	10	—	—	3	0	3	0	3	0	3±3
0	—	—	—	0	0	0	2	—	—	0	0	0	0	0	0	~0

[a] Kerzhanovich *et al.* (1969, 1971, 1972).
[b] Kerzhanovich and Marov (1974, 1977), Andreev *et al.* (1974).
[c] Antsibor *et al.* (1976).
[d] Kerzhanovich *et al.* (1979).
[e] Seiff *et al.* (1980).
[f] Counselman *et al.* (1979a, b, 1980).
[g] Zonal wind direction is eastward (clockwise if looking from the North Pole). Sign for meridianal wind '+' for equatorward, '−' for poleward.
[h] Mean square error. Values of P-D and P-Ni are taken from VLBI.

the evaluation of zonal wind if we suppose that $u \gg v, w$. This idea of the determination of the $u(z)$ profile was proposed by Kerzhanovich *et al.* (1969) and was used successfully on many Venera probes (beginning with V4) and Pioneer probes also. Results are presented in Table XXI and partially in Figure 30.

Very long base interferometry (VLBI) is known as a strong method for investigation of fine spatial structure of distant sources in radioastronomy. This method was also used for observations of movements of Pioneer sondes in the Venus atmosphere (Counselman *et al.*, 1979a, b, 1980) and leads to profiles of zonal and meridional wind in the locations of descent (Figure 31a, b) which are independent of any additional hypothesis about the relation u/v.

The conclusion about $u(z)$, $v(z)$ profiles are the following:

(1) Zonal winds velocity is maximal (50–80 m s^{-1}) at altitudes of 50–60 km (where the measurements are beginning). Direction is westward (the same as for the movements of the UV details).

(2) Meridional velocity is a few m s^{-1} at the same altitudes. Direction is equatorward (opposite to the meridional movements of UV details).

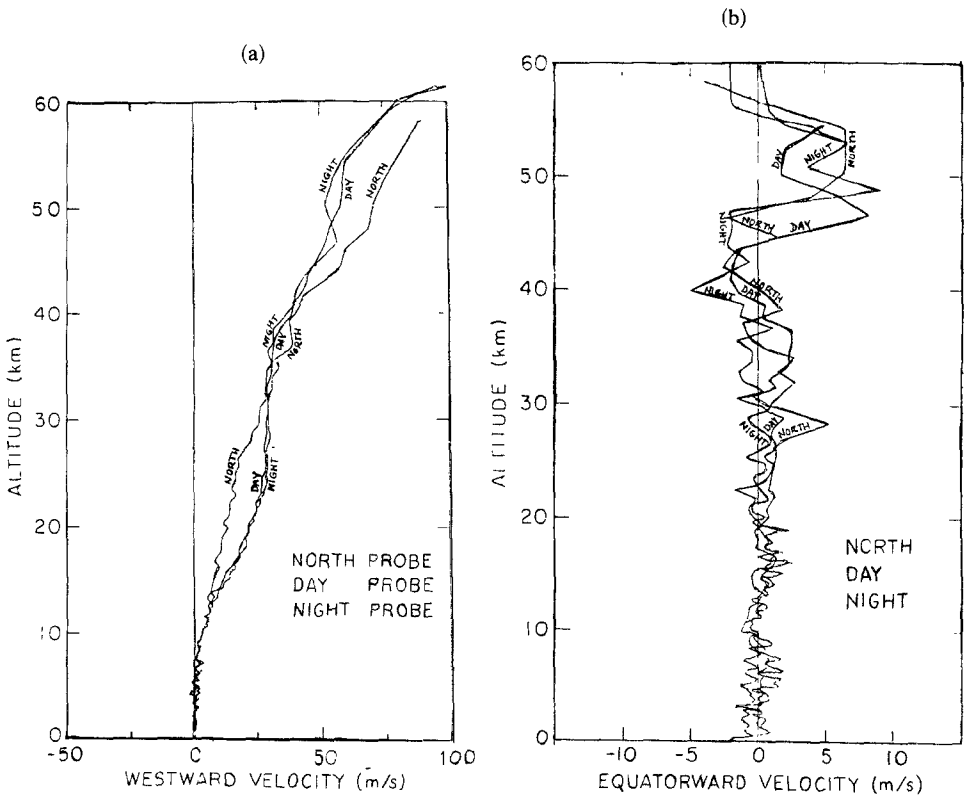

Fig. 31. (a) Altitude profile of the zonal wind $u(z)$ from VLBI measurements of movements of Pioneer probes. (b) Meridional winds from the same source (Counselman, 1980).

(3) Velocities decrease smoothly with the decrease of altitude: zonal wind is 30–40 m s^{-1} at 30 km, between 15 and 30 m s^{-1} at 20 km but near the surface is too low for measurements by these methods (their sensitivity is about 1 m s^{-1}).

The vertical velocity component w can be evaluated by comparison of the real velocity of the probe (if it is measured by VLBI) and calculated on the base of the T, P-model. The other possibility for the evaluation of w is by comparison of the independent determination of derivative dz/dt for the probe by means of aerodynamical drag equation and hydrostatics, if T and P are measured as a function of time. Both these methods give an upper limit of vertical wind of 1–2 m s^{-1} (see Kuzmin and Marov, 1974).

Measurements near the surface after landing were provided in the frame of the V9 and 10 mission (Avduevsky *et al.*, 1976b). Average velocity measured on V9 was 0.5 m s^{-1}, duration of measurements set was 49 min. On V10 duration was much less (1.5 min), and average velocity was about 1 m s^{-1}. Conventional meteorological rotoanemometer was used for these experiments. Measurements were made at a height of about 1 m above the surface.

6.1.4. *Reconstruction of the Velocity Field on the Base of T, P Data*

Hydrodynamic equations give relations connecting wind velocities and thermodynamical parameters of the atmosphere and provide the possibility of making such calculations. Substantive simplifications are possible in some cases. Leovy (1973) supposed that some upper layers of the Venusian atmosphere (60–70 km) are in a state of cyclonic motion. There are low pressure regions near the poles and atmospherical masses move to them along some spiral trajectories. Zonal wind velocity u is defined by the balance of the three forces: pressure gradients, centrifugal and Coriolis:

$$\rho \frac{u^2}{R} \operatorname{tg} \varphi = -2u\omega \sin \varphi + \frac{1}{R} \frac{dP}{d\varphi}, \tag{6.2}$$

where ρ is density, φ is latitude, R is the radius of the planet, ω is its angle velocity, P is pressure. It is possible to omit the geostrophycal term $2u\omega \sin \varphi$ in the case of Venus (see Section 6.4.). Such state of motion is named 'cyclostrophycal balance'. Values of $u(z)$ deduced from pressure measurements on the P-D and P-No zondes by means of cyclostrophycal approximation are in good agreement with the VLBI results (Seiff *et al.*, 1980). This gives strong confirmation of the idea of cyclostrophycal balance in the atmosphere of Venus.

Chub and Yakovlev (1980) used Equation (6.2) to deduce wind profiles from the altitude profiles of P, T, measured by numerous radiooccultations on the V9 and 10. A zonal velocity near to 100 m s^{-1} was found for altitudes 60–70 km. Taylor *et al.* (1979b, 1980, see also Elson, 1979) used a more detailed balance equation. They found not only zonal but also meridional circulation (Figure 32). Data presented in

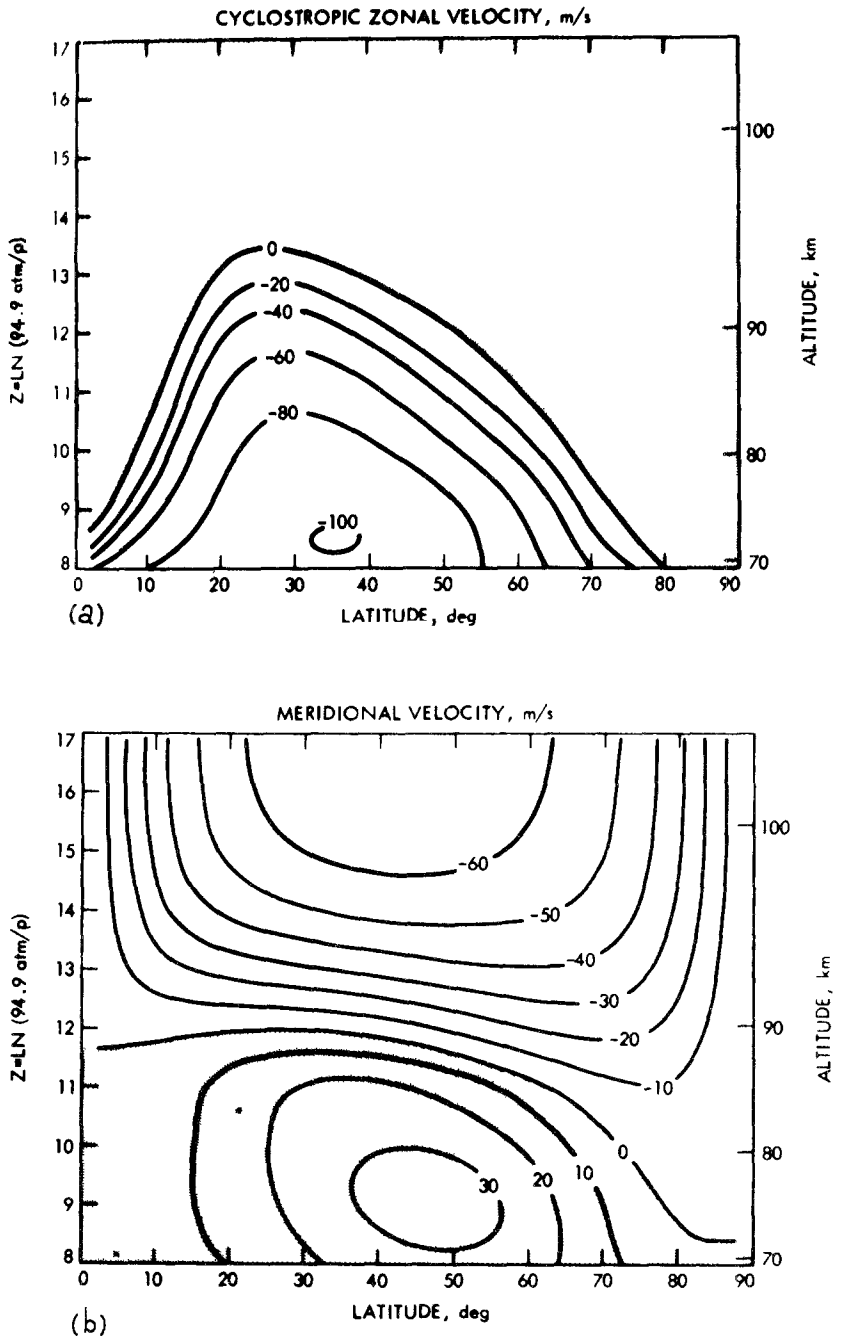

Fig. 32. Zonal (a) and meridional (b) winds from the P-O thermal sounding data (Elson, 1979).

Figure 32 show that superrotation effect decreases above 70 km but meridional velocity rises to 60 m s^{-1} at altitudes near 100 km. However results are very sensitive to the conditions on the low boundary. If the value $u = 100$ m s^{-1} is taken as a boundary condition at the level 70 km, superrotation fully disappears at 100 km, but if $u = 120$ m s^{-1} on 70 km, zonal wind on 100 km is strong enough – about 50 m s^{-1}. There is some experimental evidence of low zonal wind at high altitudes: heterodyne spectrometry CO_2 of lines near 10 μm give no superrotation at 90 km (Betz *et al.*, 1977, see Table XXI).

6.1.5. *Empirical Conclusions Concerning General Circulation*

Two modes of the general circulation of planetary atmosphere are known well enough: symmetrical (Hadley regime) and wave (Rossby regime). In the symmetrical regime there is regular motion from equator to pole on the high altitudes and from pole to equator on the low altitudes. This is a direct Hadley cell which provides transport of the heat from equator (where solar insolation is maximal) to the pole.

In the second regime wave processes (cyclones and anticyclones) arose which provided more effective horizontal heat transfer. The meaning of the wave regime in horizontal heat transfer is the same as convection in vertical.

Atmospheric circulation smooths latitude temperature gradient $dT/d\varphi$ but is itself dependent on $dT/d\varphi$. For the fast rotating planet there is some critical value of the differential thermal influx ΔO_c and the corresponding latitude gradient $(dT/d\varphi)_c$. If the differential influx is less than ΔO_c the symmetrical regime is stable and in the opposite case there is stability for the wave regime (Mintz, 1961). If rotation is slow (Rossby number $R_0 \gg 1$, see Section 6.4.) the symmetrical regime is dominating for all ΔO.

It was mentioned above that meridional wind is equatorward at heights of 50–60 km (VLBI) and poleward at 65 km (UV details). Such movements correspond to the direct Hadley cell. Meridional circulation of the same type as demonstrated by Figure 32 and the higher temperature of the polar stratosphere than equatorial (Figure 12) both are some evidence for the Hadley regime (Schubert *et al.*, 1980). The general picture is complicated by strong zonal motion (superrotation) and by some wave processes.

This description supposes the base of the Hadley cell to be at 45–50 km approximately. Between 30 and 50 km high static stability was observed (see Section 3.3) and this means that the direct cell does not penetrate here. Schubert *et al.* (1980) suppose that in the layer between the surface and altitudes of 20 km the second Hadley cell is possible, but data about wind velocities are too scarce here.

6.2. Turbulency, Convection, Waves

The small static stability ($S \simeq 0$) between 0 and 20 km can be explained not only by a 'lower' Hadley cell but also by local convection. The source of energy in both cases is the solar flux which has penetrated to the surface and the lower part of the atmosphere.

Information about the turbulent motions on different scales were obtained from the observations of three types:

(1) analysis of the fluctuation of the Doppler shift of frequency of the signal transmitted by the descent probe,

(2) analysis of the fluctuations of power by radio occultations and also by detection of the descent probe signal,

(3) analysis of UV images of the planet.

The first two methods make it possible to study the altitude structure of turbulence with the spatial scales from tens of meters to a few kilometers. The third method gives information about large scale turbulence (wave structure of the general circulation).

Measurements of the first type immediately provide radial velocity pulsations. Such pulsation with an amplitude of 2–3 m s^{-1} were found on V11 and 12 in the clouds for a maximal spatial scale of 600–800 m (Kerzhanovich *et al.*, 1979).

Analysis of power fluctuations also leads to the conclusion that turbulent motions have a maximal intensity between 50 and 60 km (radio occultations V9 and 10, Timofeeva *et al.*, 1978, 1980). In this case fluctuations of the refractive index are measured and its structural function is calculated:

$$|m(a_1) - m(a_2)|^2 = C_m^2 a^{2/3}, \tag{6.4}$$

where $m(a_1)$ and $m(a_2)$ are refractive indexes as in the points determined by vectors a_1 and a_2, a – distance between these points. The final result of the calculations is the structural constant C_m. It is supposed that fluctuations of m correspond to fluctuations of ρ, and the latter depend on temperature fluctuations. There is a structural constant C_T which describes temperature fluctuations ($\Delta T \simeq C_T r^{1/2}$). The typical deduced value of $C_m = 2 \times 10^{-8}$ $cm^{-1/3}$ in the altitude region 50–60 km (Timofeeva *et al.*, 1978). A value of $C_T \simeq 2 \times 10^{-2}$ K $cm^{-1/2}$ was obtained from M10 radiooccultations (Woo, 1975). It corresponds to the difference ΔT from 1 to 3° on the scale 5 km. From analysis of V4–V8, an evaluation of $C_m \simeq 10^{-7}$ $cm^{-1/3}$ was obtained (Kolosov *et al.*, 1970; Yakovlev *et al.*, 1974). These early results are in contradiction with the Pioneer measurements which gave an upper limit of $C_m \simeq$ $\simeq 4 \times 10^{-8}$ $cm^{-1/3}$ (Woo *et al.*, 1979) and with the above mentioned radio occultation data.

As was mentioned earlier (Section 5) static stability is nearly zero in the altitude region 50–55 km and the presence of strong turbulent motions is natural there. The considerable opacity of the clouds probably leads to the thermal convection. The possible vertical scale of the thermal convection is approximately equal to the scale of height $H = kT/mg \simeq 7$ km, but the horizontal scale is a few tens times more. Such convection cells really are observed among the UV details near the subsolar point (Belton *et al.*, 1976a, b). The same authors analyzed movements of UV details from the point of view of possible identifications with the atmospheric waves. They supposed that displacements of the little scale details (<100 km) are reflected the substance flux, but the largest details (100 km and more) correspond to the waves

superposed on the mean zonal wind. For example, the Y-detail moves as a whole without distortion although the angle velocities of small details are twice more at a latitude of 50° than on the equator (see Section 6.1). Belton *et al.* (1976b) argued that the Y-detail is the planetary wave with the wave number 1 and period 4.2^{d}. 'Bow waves' can be real waves created by the flowing of zonal flux around the solar point region. Equatorial bands are interpreted as internal gravitational waves.

6.3. Hypotheses concerning the mechanism of superrotation

The most natural way to search for the nature of the superrotation is full enough numerical simulation of Venusian atmospheric dynamics. The first step on this path was made (see Section 6.4.) but the whole set of hypotheses to explain superrotation was proposed earlier and independently from the problem of full numerical simulation of the general circulation. Five different mechanisms were proposed, all of them are reviewed by Stone (1975). Here we shall give only a very short presentation of these proposals.

(1) Moving flame mechanism. Schubert and Whitehead (1969) described a laboratory experiment which as they thought simulated the Venusian superrotation. A Bunsen burner was moved under a toroidal pan containing mercury. The mercury began to move also though some times faster but in the opposite direction. The supposed reason was the formation of the inclined isotherms and inclined convective cells. Motion of the liquid in the direction opposite to the moving flame is correlated with the stream up movements and there is some transfer of momentum from convection cells to the regular flux. The situation on Venus is not so simple because both direct and opposite regular flux is possible dependent on the vertical distribution of solar energy influx. This mechanism was analyzed later by Young and Schubert (1973) more carefully, but the real meaning of such a process on Venus is not yet clear.

(2) Thompson's (1970) mechanism also used the idea of inclined convective cells, but the inclination in this version arose from the horizontal wind shear (Figure 33). As a result some stable horizontal flow arises. A detailed numerical simulation of this possible process was made by Vasin and Marov (1977).

(3) Atmospheric tides (Gold and Soter, 1971). Solar tides influenced by the second harmonic connected with the semidiuznal thermal wave can in principle accelerate the atmosphere and lead to observed zonal motions. The sign and value of the resulting zonal wind depend on amplitude and phase of the tide and on the effective kinematic viscosity of the atmosphere. None of these quantities is known and the possibility of such an explanation is difficult to prove.

(4) Internal gravitational waves. It was shown (Lindzen, 1973; Fels and Lindzen, 1975) that internal gravitational waves generated by the daily variations of the solar thermal influx can amplify the reverse movements in the layer of maximal influx. However a beginning velocity $\simeq 25$ m s^{-1}, created by other mechanisms, is necessary to provide a superrotation of 100 m s^{-1}.

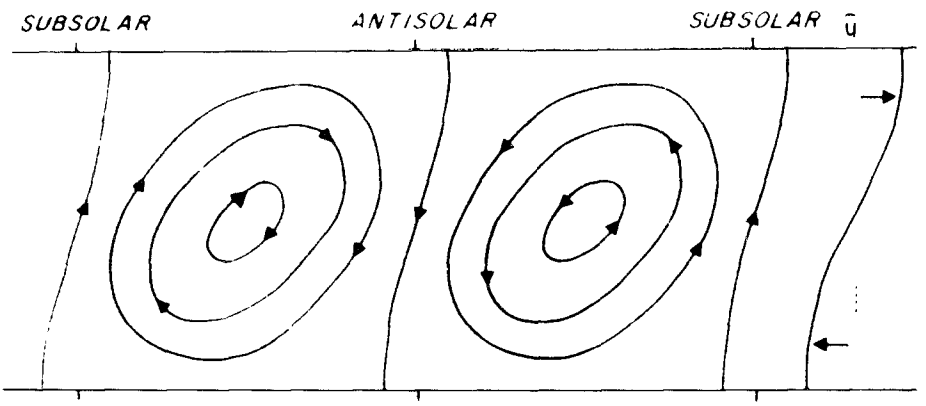

Fig. 33. Schematic presentation of lines of flow in the inclined convective cells which show the possibility of generation of some regular zonal flow (on upper level) with the direction opposite to that of the visible moving of the Sun.

(5) Momentum transport from below upwards by the meridional Hadley cell. Cyclostrophical balance is supported in this process (see Section 6). Gierash (1975) showed that a very large horizontal eddy viscosity ($\gg 10^7$ cm^2 s^{-1}) is necessary for this mechanism.

6.4. The problem of general circulation

It is possible to predict some properties of the general circulation in the planetary atmosphere by means of a simple analysis of the time scales of the different atmospherical processes. Golitsyn (1970a, b, 1973) developed on the resembling basis the similarity approach to general circulation. This approach provides many important semiquantitative estimations. More difficult but more precise is numerical simulation.

6.4.1. *Characteristic Time Scales and Some Results of the Similarity Approach*

Three times are most important for evaluation of general circulation.

(1) Duration of the solar day

$$\tau_{\text{day}} \simeq 10^7 \text{ s} . \tag{6.5}$$

(2) Relaxation time τ_{rad} of the temperature disturbances. If defined for the spatial scale order of H (scale of height)

$$\tau_{\text{rad}} \simeq \tau_{\text{sol}} = \frac{\frac{C_p}{C_v} P(z) H(z)}{\left(\frac{C_p}{C_v}\right) - 1) \sigma T_e^4} . \tag{6.6}$$

where τ_{sol} is the time which is necessary to remove heat energy from the atmosphere above altitude z by the radiation if we switch out the solar insolation. τ_{rad} is changed from 10^9 s near the surface to 10^5 s at an altitude of 60 km.

(3) Characteristic time of dynamical processes

$$\tau_{\text{dyn}} = R/v_s \simeq 10^5 \text{ s}, \tag{6.7}$$

where R is the radius of the planet, v_s is the velocity of sound.

The relations of the time scales give information about the relative importance of the different processes. Let's discuss these relations:

$$\delta = \tau_{\text{rad}}/\tau_{\text{day}},$$

$$\gamma = \tau_{\text{dyn}}/\tau_{\text{day}} = R_0/v\,\tau_{\text{day}},$$

$$\varepsilon = \tau_{\text{dyn}}/\tau_{\text{rad}}.$$

Daily effects are small if $\delta \gg 1$ but if $\delta < 1$ or $\delta \simeq 1$ they are important. Coriolis forces are substantive if $\gamma \gg 1$, but if $\gamma \ll 1$ it is possible to neglect it ($\gamma \simeq 1/R_0$, where $R_0 = v/2\omega \sin\varphi\, R$ is a Rossby number, ω – angle velocity, φ – latitude). There is a local radiative equilibrium and a large latitude gradient $\partial T/\partial\varphi$ if $\varepsilon \gg 1$, in the opposite case $\partial T/\partial\varphi \to 0$.

In Figure 34 the dependences δ, γ, ε on the altitude in the atmosphere of Venus are presented. The conclusions are evident: (1) Coriolis forces are small enough, the atmosphere of Venus is nongeostrophic; (2) daily effects are small lower than 60 km and are substantive above 60 km (in good enough accordance with the experimental data – see Section 3); (3) the latitude temperature gradient must be small even at 60 km above the surface and practically absent on the surface.

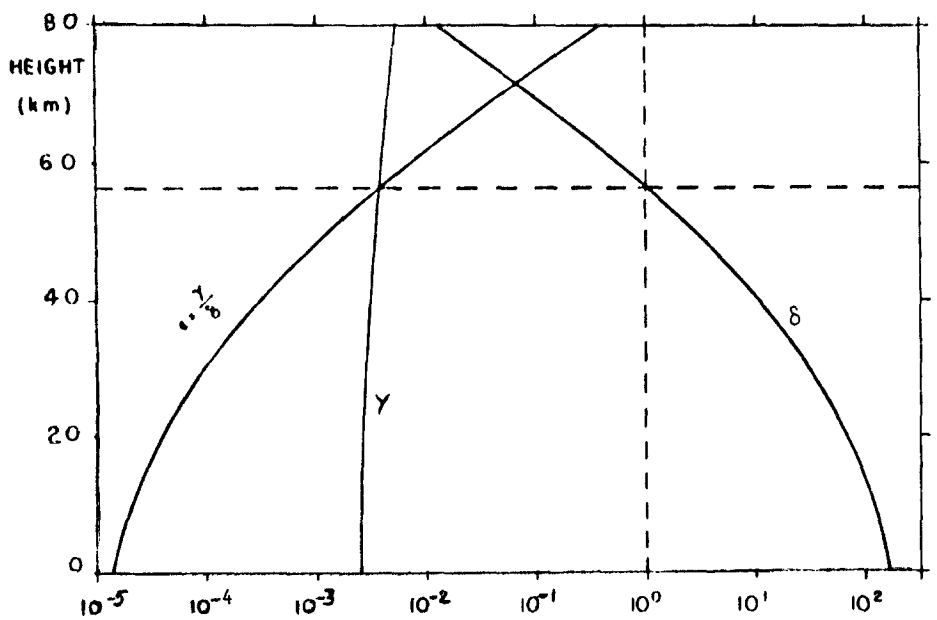

Fig. 34. Relations of the time scales γ, δ, ε as function of altitude (Stone, 1975).

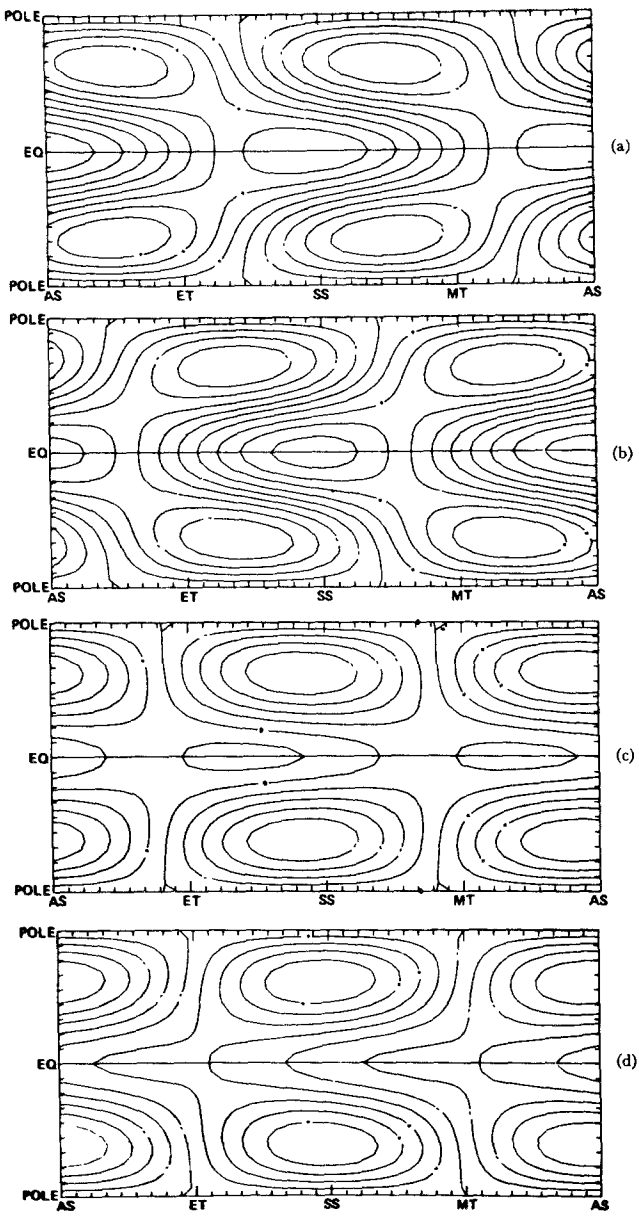

Fig. 35. Some results of the numerical simulation of the Venus atmosphere general circulation (Young and Pollack, 1977): field of vertical velocity w (a) and of the potential temperature (b) at a height of 56 km. Isolines for w are given through the intervals $|w|_{max}/5$, where $|w|_{max} = 0.83$ cm s^{-1}, interval for isotherms are equal $|\Delta T|_{max}/5$, where $|\Delta T|_{max} = 3.6$ K. (c) and (d) are the same through 5 days (respectively $|w|_{max} = 0.57$ cm s^{-1}, $|\Delta T|_{max} = 3.9$ K). The shape of the isolines is nearly similar to the Y-detail observed on UV photographs of Venus.

The estimation of the temperature difference between pole and equator, based on the Golitsyn approach, was discussed in Section 5 (see formula 5.5). The estimated difference was only about 2°. The same approach gives an estimation of wind velocities in the low atmosphere

$$v \simeq \left(\frac{\pi}{2}\right)^{1/2} \left(\frac{k}{\lambda_1}\right)^{1/4} \frac{\sigma^{1/16} F_0^{9/16}}{c_p^{1/4}} \left(\frac{R}{M}\right)^{1/2} \simeq 1 \text{ m s}^{-1} \tag{6.8}$$

in fine coincidence with the measurements on V9 and 10 (see Section 6.4).

6.4.2. *Results of Numerical Simulations*

Many attempts at numerical simulations of the Venus atmosphere modelled as two dimensional (Goody and Robinson, 1966; Stone, 1968; Sasamory, 1971; Kalnai de Rivas, 1973, 1975), later as three-dimensional (Burangulov *et al.*, 1974; Pollack and Young, 1975) had limited success because they didn't provide for super-rotation. The first and only published model in which superrotation was 'observed' belongs to Young and Pollack (1977). It gave an altitude wind profile in good enough agreement with the measurements, approximately right values for the meridional velocities and even the formation of the Y-detail by planetary waves (wave number 1 – see Figure 35). In the frame of this model superrotation arises from momentum transfer provided by meridional circulation and large scale eddies.

7. Chemical Processes in the Atmosphere

The structure and evolution of the atmosphere are influenced by some chemical processes. Among these processes there are (7.1.) interaction between the atmosphere and rocks, (7.2.) thermochemical reactions between gaseous components, (7.3.) photochemical processes, (7.4.) chemistry of the clouds. Theoretical consideration in the field of atmospherical chemistry must explain the observed atmospheric composition and its change with altitude. Such investigations gave some interesting results and we shall review them here.

7.1. Interaction between the atmosphere and rocks

Urey (1952) was the first who indicated the important process which has a strong influence on CO_2 abundance in the planetary atmosphere. These are the reactions between carbonates and quartz with silicates and carbonic dioxide, for example

$$\underset{\text{calcite}}{CaCo_3} + \underset{\text{quartz}}{SiO_2} \rightleftarrows \underset{\text{vollastonite}}{CaSiO_3} + CO_2 \,. \tag{7.1}$$

At high temperatures the process goes from left to right; and CO_2 in large amounts appears to be in the atmosphere. In Figure 36 the dependence of CO_2 pressure on temperature in the case of equilibrium is represented by Urey (sometimes the term 'vollastonite equilibrium' is in use). At 750 K a pressure of about 100 atm. is provided by Urey with the reaction (7.1) equilibrium and its application to Venus

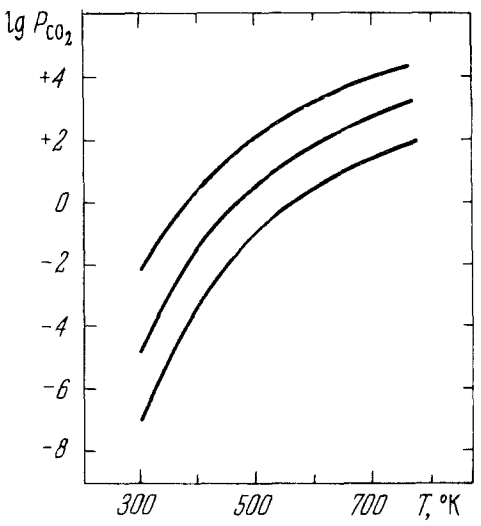

Fig. 36. Dependence pressure of CO_2 on the temperature by the Urey equilibrium. The middle curve corresponds to the reaction (7.1), upper curve to the similar reaction with participation of $FeCO_3$, lower – with $MgCO_3$.

was considered independently in a few papers (Adamchik and Draper, 1963; Lewis, 1968, 1970; Vinogradov and Volkov, 1971). The time scale of the equilibrium setting at temperatures of 700–800 K is only several hundreds years (Mueller and Kriegelbaugh, 1973). Later a great amount of possible reactions between minerals and the gaseous phase were considered (Mueller, 1963, 1964, 1968; Lewis, 1968, 1971). For example, it is supposed that the abundance of HCl and HF in the lower atmosphere is controlled by the reactions

$$\underset{\text{gallite}}{2NaCl} + \underset{\text{anorthite}}{CaAl_2Si_2O_2} + \underset{\text{quartz}}{SiO_2} + H_2O \rightleftarrows \underset{\text{nephelite}}{2NaAlSiO_4} + \underset{\text{vollastonite}}{CaSiO_3} + 2HCl\,; \qquad (7.2)$$

$$\underset{\text{fluorite}}{CaF_2} + \underset{\text{quartz}}{SiO_2} + H_2O \rightleftarrows \underset{\text{vollastonite}}{CaSiO_3} + 2HF\,; \qquad (7.3)$$

and other processes of a similar type. There is a simple relation between H_2O and HCl partial pressure

$$p_{HCl} = K(p_{H_2O})^{1/2} \qquad (7.4)$$

where $K \simeq 3 \times 10^{-4}$ at $T = 750$ K (Mueller, 1968). At the abundance $f_{H_2O} = 2 \times 10^{-5}$ near the surface (see Table V) and a pressure of 90 atm., formula (7.4) gives $f_{HCl} = 1.5 \times 10^{-7}$. According to spectroscopic ground-based data $f_{HCl} = 4 \times 10^{-7}$ and this is good enough agreement. A similar relation takes place for HF but in this case the discrepancy is more (almost by an order).

There are some 'buffer' reactions for hydrated rocks, for example

$$\underset{\text{enstatite}}{Ca_2Mg_5Si_8O_{22}(OH)_2} \rightleftarrows 3\underset{\text{enstatite}}{MgSiO_3} + 2\underset{\text{diopside}}{CaMgSi_2O_6} + + \underset{\text{quartz}}{SiO_2} + H_2O\,. \quad (7.5)$$

According to calculations of the thermodynamical equilibrium between rocks and the atmosphere carried out by Khodakovsky *et al.* (1978, 1979), in hydrated rocks on Venus an amount of water equivalent to 10% of the terrestrial hydrosphere may be present. Even more amounts of water according to the evaluations of the same authors might be spent on Fe^{2+} oxidation by means of the reaction

$$2FeO + H_2O \rightleftarrows Fe_2O_3 + H_2 \quad (7.6)$$

with the consequent dissipation of hydrogen.

Mueller (1965) and then Lewis (1968, 1970) discussed the equilibrium of sulfur components in gaseous and solid phases. According to Lewis (1970) the mixing ratios of COS, SO_2, and H_2S must be 5×10^{-5}, 3×10^{-7} and 5×10^{-6} respectively, i.e., the main form is COS, and SO_2 was expected only in very little amounts. However the gas chromatographs on V12 and P-L showed that it is exactly SO_2 which appears to be the most abundant sulfuric compound in the lower atmosphere of Venus. It is possible that photochemical processes in the lower layers of the atmosphere provide the shift to SO_2 (see Section 7.3).

All the calculations of the rocks–atmosphere equilibrium lead to very small amounts of free oxygen (mixture ratio is 10^{-25}). Lewis and Kreimendahl (1980) reconsidered later the problem of the atmosphere–rocks equilibrium with the account of chemical measurements on P-L, V11, and V12, however they didn't explain the difference of the observed ratios of COS, SO_2, H_2S from the predicted ones of the old Lewis model.

7.2. Thermochemical reactions between gaseous components

Mueller (1963, 1964) proposed that it is possible to distinguish three zones in the atmosphere of Venus: (1) the lower one, where only thermochemical reactions take place, (2) the middle one, where thermochemical reactions rates are small and the content is defined by thermochemical equilibrium in the lower zone, (3) the upper one (above the clouds and in the upper part of the cloud layer, where photochemical processes dominate. Analogous stratification was supposed in the works by Florensky *et al.* (1976, 1978) but they didn't suppose a 'frozen' equilibrium in the intermediate zone. It is clear now that the models of such a type may not reflect the real situation, because visible radiation penetrates to the surface and photochemical processes can disturb the thermodynamical equilibrium even in the lower zone. Nevertheless calculations of the thermochemical equilibrium of the gaseous components are of interest because their results, in comparison with the measured data, permits us to reveal which deflections from the equilibrium take place.

Thermochemical equilibrium calculations carried out by Florensky *et al.* (1976, 1978) were made on the assumption that it is determined by the local

thermodynamical characteristics of the atmosphere at each given level. This hypothesis is realistic in the case where the time scale of the equilibrium setting is less than the effective time of mixing

$$\tau_e < \tau_m = H^2 K^{-1} 10^7 \text{ s} ; \tag{7.7}$$

here H – scale of height, K – eddy diffusion coefficient (10^5 cm^{-2} s^{-1} in the lower zone with an accuracy to one order). Krasnopolsky and Parshev (1979) have shown that condition (7.7) is not carried out if we consider only reactions in the gaseous phase. Nevertheless they supposed that the average content of the lower atmosphere corresponds to thermochemical equilibrium near the surface. This point of view was based on the circumstance that the reactions with rocks must play the role of catalytic ones and reduce τ_e significantly but they have no influence on the equilibrium ratios of gases abundances. Some results of the calculation of the lower Venusian atmosphere content on the base of the thermochemical equilibrium hypothesis are represented in Table XXII. There are evaluations here which were obtained by two groups of authors (Krasnopolsky and Parshev, 1979; Khodakovsky *et al.*, 1979) on the basis of V11, V12, and P-L data.

TABLE XXII

Composition of the low atmosphere derived thermodynamic equilibrium calculations

Gas	Mixing ratio	
	Krasnopolsky and Parshev (1979)	Khodakovsky *et al.* (1979)
CO_2	0.96[(a)]	0.97[(a)]
CO	1.5×10^{-5}	1.4×10^{-5} [(a)]
H_2O	3×10^{-5} [(a)]	2×10^{-5} [(a)]
SO_2	1.5×10^{-4} [(a)]	1.3×10^{-4} [(a)]
SO_3	—	1×10^{-30}
H_2S	5×10^{-8}	1.35×10^{-10}
COS	2×10^{-5}	1×10^{-5}
O_2	—	1.7×10^{-23}
S_2	1×10^{-7} [(a)]	1×10^{-7}
H_2	3×10^{-5}	3×10^{-9}

[(a)] Mixing ratio was taken from measurements. Difference between the two columns (and with Table V) are explained by the use of different references or some corrections in the data.

Mainly the components of H, O, C, S including CO_2, CO, O_2, SO_2, SO_3, S_2, COS, CS_2, H_2O, H_2, and H_2S were considered. It is sufficient to set n components including n types of atoms to determine the mixing ratio of all the rest if the system is closed. The results of the calculations are in agreement with the measurements if we take, for example, CO_2, SO_2, S_2, and H_2O abundances as the initial ones. Then CO

amount and upper limits for COS and H_2O agree with the measurements. Oxygen is practically absent ($f_{O_2} \simeq 10^{-22}$). If, on the contrary, the group CO_2, SO_2, H_2O, O_2 are taken as the basis and $f_{O_2} = 4 \times 10^{-6}$ is accepted in accordance with the primary communication by Oyama (Oyama, 1979a – see Section 2), CO and S_2 disappear practically entirely. Apparently this second possibility ceased to be actual in the connection with the reconsideration of chromatographic results obtained on P-L.

7.3. Photochemical processes

Absorption of the solar ultraviolet radiation $\lambda < 1700$ Å provide photolysis of carbon dioxide

$$CO_2 + h\nu \rightarrow CO + O\,. \tag{7.8}$$

The reaction of recombination takes place with the third molecule participation

$$CO + O + M \rightarrow CO_2 + M\,; \tag{7.9}$$

and molecular oxygen is formed in a similar process simultaneously

$$O + O + M \rightarrow O_2 + M\,. \tag{7.10}$$

The reactions (7.9) and (7.10) are effective only at relatively low heights, because they require triple collisions. In the result the CO_2 dissociation level calculated according to this scheme appears to be at a height of about 110 km. The reaction rate of (7.10) is four orders more than that of (7.9) and molecular oxygen must be accumulated in the atmosphere. Both conclusions contradict the facts, because really the CO_2 dissociation level was observed much higher (about 160 km, see Section 8.1); and the amount of molecular oxygen in the atmosphere above the clouds is much less than CO. It is clear therefore that the other processes removing photolysis products more effectively act in the atmosphere. One of the schemes (Donahue, 1968, 1971) proposed HO_2 formation from the oxygen molecules

$$H + O_2 + M \rightarrow HO_2 + M \tag{7.11}$$

with the following reaction

$$HO_2 + CO \rightarrow CO_2 + OH\,. \tag{7.12}$$

The reaction (7.12) appeared to be too slow. Other continuation is more effective (McElroy *et al.*, 1973)

$$HO_2 + O \rightarrow OH + O_2\,; \tag{7.13}$$

$$CO + OH \rightarrow CO_2 + H\,. \tag{7.14}$$

Prinn (1971) payed attention to the role of chlorine and sulfuric compounds. Photodissociation of HCl appeared to be the more important source of hydrogen in the atmosphere of Venus than H_2O. Besides it is the source of chlorine which may

be a catalyst itself at CO oxidation:

$$\begin{aligned} &Cl+O_2+M \rightarrow ClO_2+M\,; \\ &ClO_2+CO \rightarrow CO_2+ClO\,; \\ &ClO_2+Cl \rightarrow 2ClO\,; \\ &ClO+CO \rightarrow CO_2+Cl\,. \end{aligned} \tag{7.15}$$

McElroy *et al.* (1973) were the first who considered the photochemical model with the participation of both hydrogen and chlorine. One of the interesting conclusions of this work is the idea of the formation of water in the reaction

$$OH+HO_2 \rightarrow H_2O+O_2 \tag{7.16}$$

in the amount approximately equal to CO amount. We shall notice that such equality really takes place within the limits of the accuracy of measurement (see Section 2).

In the results of the next stage of photochemical calculations (Sze and McElroy, 1975) 47 reactions are included. The most developed model (Krasnopolsky and Parshev, 1980) already takes into consideration 102 reactions. The cycles of hydrogen, chlorine and sulfur are considered jointly. It is essential that this model takes into account data on the chemical composition of the Venusian atmosphere, obtained on V11, 12 and P-L. The main new fact from the point of view of photochemistry is that SO_2 and not COS is the most abundant compound containing sulfur. Photolysis of SO_2 gives three times more O atoms as compared with CO_2 because of the greater longwave length limit of photodissociation (2280 Å). Krasnopolsky and Parshev introduced into consideration some new reactions including chlorine–carbonile

$$COCl+O_2 \rightarrow CO_2+ClO \tag{7.17}$$

which appeared to give 60% fall in the molecules of CO_2 in the sum of different recombination processes. In the frame of a single model the vertical profiles of concentration for large amounts of compounds including H_2SO_4 (one of the components of the cloud layer) are obtained in this work. The profiles for some of the most important components are presented in Figure 37.

We must notice that the chemical calculations mentioned above don't take into account reactions with nitrogen participation. Electric discharges may play a significant role in the chemistry of the small constituents, in particular they may lead to the formation of nitrogen compounds (Watson *et al.*, 1979).

All the published models suppose that the lower boundary of the photochemical processes zone is located in the diapason from 50 to approximately 60 km.

Prinn (1979) noticed that photochemical processes may be practically essential to the surface for gaseous sulfur molecules and some other sulfuric compounds. For example, photodissociation

$$S_n+h\nu \rightarrow S_{n-1}+S \tag{7.18}$$

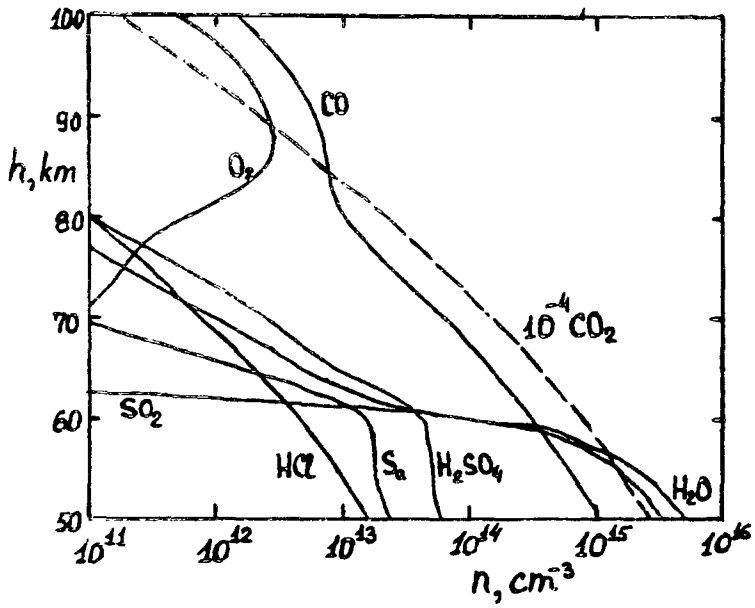

Fig. 37. Altitude dependence of the number density of CO, O_2, H_2O, SO_2, HCl, H_2SO_4, and S_a according to the model of Krasnopolsky and Parshev (1980). S_a – sulfur in the condensed phase, H_2SO_4 also, the rest of the constituents are in the gas phase.

which gives free atoms of sulfur may, in principle, lead to COS destruction in the reaction

$$COS + S \rightarrow CO + S_2 .$$

In the meanwhile photochemistry of the lower atmosphere has not been considered quantitatively because of the deficiency in the data of reaction rates.

7.4. Chemistry of clouds and H_2O vertical profile

The experimental data on chemical composition of the clouds were presented in Section 5. They are rather contradictory but nevertheless there are some grounds to suppose that modes 1 and 2 consist of concentrated sulfuric acid. H_2O and SO_3 molecules are necessary for its formation. The first of them is present undoubtedly, the second one may arise in an SO_2 oxidation process.

Prinn (1973, 1975) proceeding from the idea about COS as the most abundant sulfuric compound in the atmosphere of Venus proposed that SO_2 arises in the result of COS photolysis. Now it is clear that the main component of the lower atmosphere containing sulfur is SO_2 itself, and the problem became simpler. The role of photochemistry is the providing of free oxygen (or, for example H_2O) influx for sulfur dioxide oxidation. The simplest version is the oxygen formation in the result of photolysis of the SO_2 molecule itself.

Krasnopolsky and Parshev (1980) have shown that H_2SO_4 formation in the clouds may be explained by the chain of reactions:

$$\begin{aligned} &SO_2 + h\nu \rightarrow SO + O\,; \\ &SO_2 + O + CO_2 \rightarrow SO_3 + CO_2\,; \\ &SO_3 + H_2O \rightarrow H_2SO_4\,; \\ &SO + SO \rightarrow SO_2 + S\,. \end{aligned} \tag{7.19}$$

Molecules of gaseous sulfur arise at that time also

$$\begin{aligned} &S + S \rightarrow S_2\,; \\ &S_{n-1} + S \rightarrow S_n\,; \end{aligned} \tag{7.20}$$

(till $n = 8$) which then condenses. Sulfuric acid forms as concentrated water solution. Quantitative calculation appears to be sensible to H_2O abundance in the base of the cloudy layer (50 km). At $f_{H_2O} = 2 \times 10^{-4}$ at 50 km the best agreement with experimental data is obtained – such data as H_2SO_4 water solution concentration (at an average of about 85%), H_2O abundance in the upper part of the cloudy layer, H_2O molecules flux to the upper atmosphere. At the same time $f_{H_2O} = 2 \times 10^{-4}$ at 50 km is in good agreement with the data of spectrophotometers on V11 and 12.

Krasnopolsky and Parshev gave arguments in favor of the view that mode 3 (large particles) in the layer C must consist of sulfuric acid as in mode 2, but they assume that in the lower layer this mode may have another content.

The experiment with X-ray fluorescent analysis on V12 (Surkov *et al.*, 1979) didn't show the presence of sulfur in the clouds of Venus but chlorine was found instead of sulfur. It is natural to propose that at least mode 3 consists of the chlorine compounds, however the question of their identification remains unsolved. Hydrochloric acid is dropped because in the condensated phase it exists only in the presence of sufficiently large amounts of H_2O – it is necessary to have $f_{H_2O} \simeq 0.01$ in the gaseous phase. The mixture of H_2SO_4 and HCl particles is unstable, because H_2SO_4 condensate dries the atmosphere and HCl turns into the gaseous phase. The high speeds of horizontal transport and convection make the separate existence of H_2SO_4 and HCl cloudy masses practically impossible.

For an explanation of the yellowish color of Venus, among different versions ferrum chloride ($FeCl_2\,2H_2O$, see Section 5.3) was suggested, but it was considered only as a small admixture. As a possible component of the clouds aluminum chloride Al_2Cl_6 was suggested also (Krasnopolsky and Parshev, 1979). Later the same authors put forward the hypothesis that it forms mode 3 of the lower layer (Krasnopolsky and Parshev, 1980). However the difficulty is that according to the results of X-ray fluorescent analysis chlorine must be the most abundant component of the particles at all heights (lower <60 km) and it remains completely incomprehensible. Watson *et al.* (1979) suggested such molecules as $NOHSO_4$ as a possible constituent of the large particles (mode 3). Its formation takes place with the

participation of nitrogen dioxide NO_2 which may arise in the electrical discharges.

A separate discussion is necessary for the H_2O vertical profile in the atmosphere of Venus (see Figure 10 and Section 2.4). The decrease of the mixing ratio in the interval of 50–70 km is explained well enough if H_2SO_4 particles present in the clouds (it is sufficient, for example, to have mode 2 particles composed of sulfuric acid). Saturated vapor H_2O pressure above sulfuric acid water solution depends strongly on the temperature and concentration of the solution. At a concentration equal to 90% and at a height of 50 km the mixing ratio of water vapor $f_{H_2O} = 2 \times 10^{-4}$ and at a height of 65 km – $f_{H_2O} = 3 \times 10^{-7}$. Lower than 50 km the liquid phase disappears and this is in approximate agreement with the observable location of cloudy layer C's lower boundary (the mean layer of the height 50.5–56.5 km, see Table XV). At a concentration equal to 85% sulfuric acid solution can't exist already at the height of 50 km; at the height of 65 km $f_{H_2O} \simeq 2 \times 10^{-6}$, and at a concentration equal to 75%, this value increases to 4×10^{-5}. Thus very small f_{H_2O} values given by ground-based spectroscopy are explained by the presence of H_2SO_4 particles in the clouds.

It is more difficult to explain f_{H_2O} decrease in the interval between the clouds and the surface. For this purpose it is necessary to have some H_2O source above 50 km and sink on the surface or in the low atmosphere. The source can be chemical (for example reactions 7.11 and 7.16 if hydrogen is provided by HCl), or physical – local discharge of water by volcanoes or hydrothermal systems in some surface location. The possible sinking on the surface may be provided by reactions similar to 7.2, 7.3, and 7.5.

8. Upper Atmosphere

Experimental data about the structure of the upper atmosphere of Venus was given almost only by the measurements on the space probes. To the subject of this section belong (8.1.) in situ studies, (8.2.) radio occultation data concerning ionosphere structure, (8.3.) emission spectroscopy data, (8.4.) solar wind interaction. We shall review experimental results and later (in Section 8.5) theoretical models.

8.1. In situ studies

The first attempt of in situ measurements in the Venusian ionosphere was made on V4 (Gringauz *et al.*, 1978). But the main bulk of data was provided by means of a set of instruments on P-B and P-O. Owing to low periapsis (about 150 km) conditions for the in situ studies was very favorable on the orbiter. Two mass-spectrometers were installed on board of every probe – for neutral composition measurements (BNMS and ONMS) and ion composition (BIMS and OIMS). The first letters of the abbreviations stand for 'bus' and 'orbiter' respectively. Five other instruments for upper atmosphere in situ measurements were used on board of the orbiter: retarding potential analyzer (RPA), instrument for measurements of electron concentration and temperature (OETP), magnetometer, plasma wave analyzer

and solar wind ion and electron energy spectra analyzer. Observations of the orbital evolution caused by the aerodynamical drag provided full mass density data on the altitudes near periapsis.

Concentrations of CO_2, CO, N_2, O, N, and He were measured by the ONMS (Niemann *et al.*, 1979a, b, 1980) at altitudes above 150 km. Daily variations of concentrations were studied in detail. In Figure 38 vertical concentrations of profiles in the near-equatorial atmosphere are presented for 0^h and 12^h of local solar time.

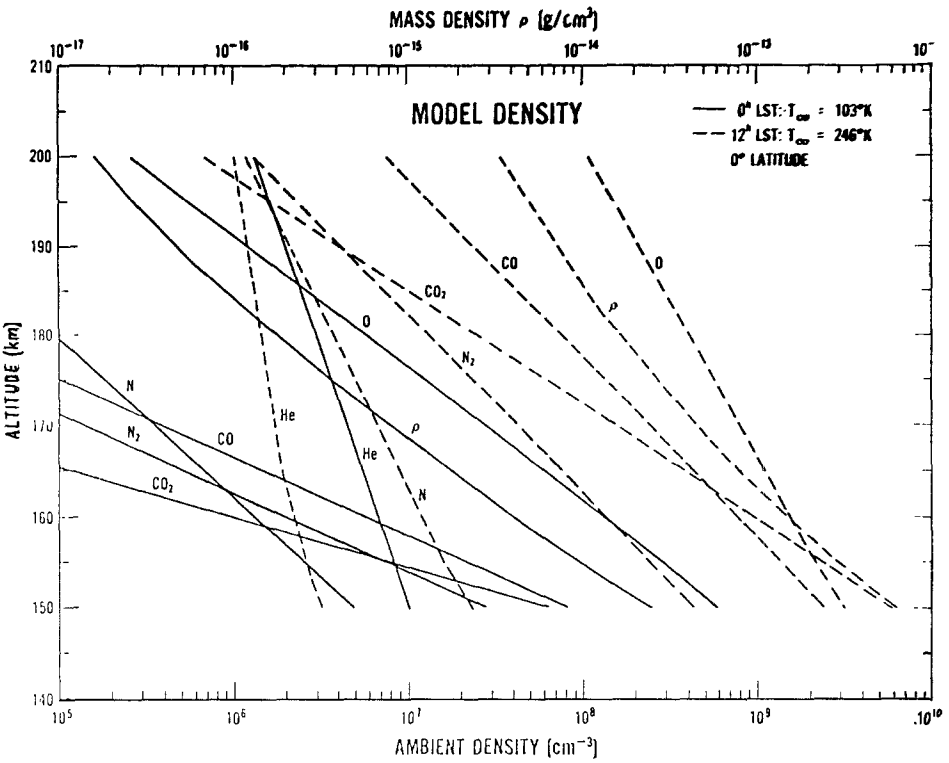

Fig. 38. Altitude dependence of the number density of CO_2, CO, N_2, N, O, He from the ONMS data for 0^h and 12^h of local solar time on the equator (Niemann *et al.*, 1980). Full mass density profile is presented here also (upper scale).

BNMS (von Zahn *et al.*, 1979a, b, 1980) gave only one profile (latitude 38°, local time 8^h30^m, solar zenith angle 61°) but to the essentially less minimal altitude −127 km.

Results of both experiments are in good accordance. The most important conclusions are the following.

(1) The level of the CO_2 dissociation (above which concentrations of CO and O are more than CO_2) is at an altitude of approximately 155–160 km (both experiments).

(2) Above 200 km at night (corresponding altitude is more in the day time) the main component of the atmosphere is helium (both experiments). We shall see

in the next section that above 700 km hydrogen becomes the most abundant constituent.

(3) The altitude of homopause

$$z_h = 140 \text{ km} \tag{8.1}$$

for N_2, a little lower, 134 km approximately for He (BNMS – morning terminator).

(4) The altitude of exobase

$$z_e \simeq 190 \text{ km} \tag{8.2}$$

for O; It is between 185 and 200 km for all measured components (BNMS).

(5) Day time exospheric neutral temperature

$$T_n \simeq 250 \text{ K}, \tag{8.3}$$

but night temperature is much less,

$$T_n \simeq 100 \text{ K}. \tag{8.4}$$

There is the cryosphere instead of the thermosphere at night on Venus (ONMS). Such a situation is extraordinary, for example on the Earth it has never been observed.

(6) There are strong daily variations of density above 150 km (ONMS). Full mass density at an altitude of 150 is less by an order of value at night than in the day time. At 200 km, variation of density is 10^3 times approximately. Large daily variations of full density were independently deduced by drag analysis (Keating *et al.*, 1979a, b; Shapiro, 1979b).

Number densities of CO_2, CO, O, N_2, and N are maximal in the day time. Variations of the number density are opposite in sign – there is maximum at night, hydrogen concentration also (OIMS, Brinton *et al.*, 1980).

Measured day temperatures of the upper atmosphere are in satisfactory accordance with the early published models (Dickinson and Ridley, 1977) but there is no real explanation for the low night temperature. We shall return to this problem in the Section 8.4. Large daily pressure variations in the upper atmosphere must lead to the strong winds (a few hundreds m s^{-1}) which support mass flow through the terminator.

Experiments BIMS and OIMS (Taylor *et al.*, 1979a, b, c, 1980) provided a measurement of the concentration of 11 ions: O^+, O_2^+, NO^+, CO_2^+, C^+, N^+, H^+, He^+, $^{18}O^+$, O^{2+} and mass 28 (CO^+ and N_2^+; photochemistry considerations show that the quantity of CO^+ is probably more). In Figure 39 the vertical profile obtained on the bus is shown. The main ionospheric layer is composed of O_2^+, the peak is at an altitude of 150 km, the number density of ions here is $\simeq 10^6$ cm^{-3}. The second peak is at an altitude $\simeq$200 km and O^+ is the dominating ion there. At night the same ions are dominated (Figure 40) but the peak number density is nearly 10 times less. Fluctuations of the measured number densities (for given altitude and local time) are maximal at night. Probably at night turbulent motions are strongest.

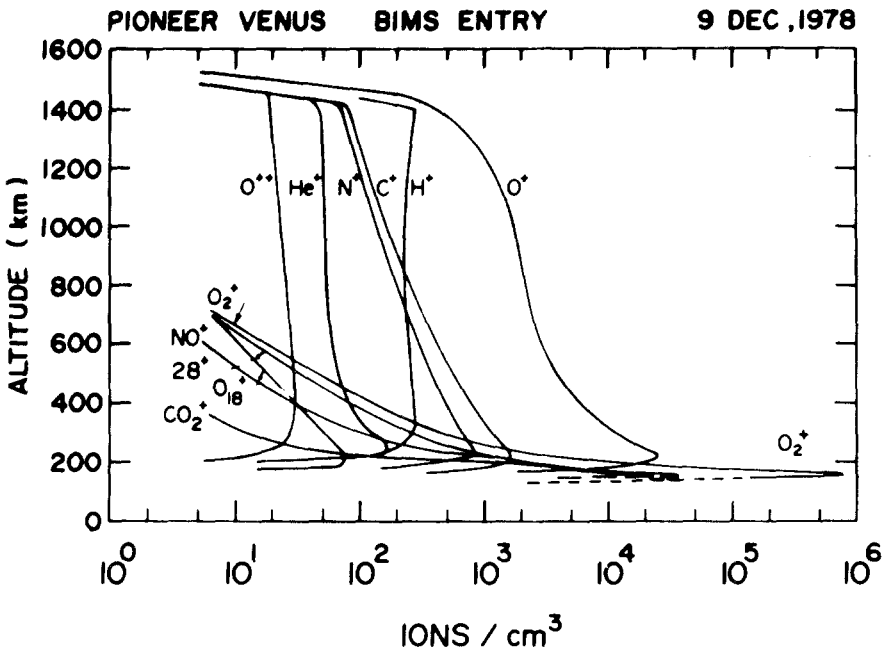

Fig. 39. Ion composition of the upper atmosphere from the BIMS data (zenith solar angle $z_0 = 61°$, latitude 38°; Taylor *et al.*, 1979a).

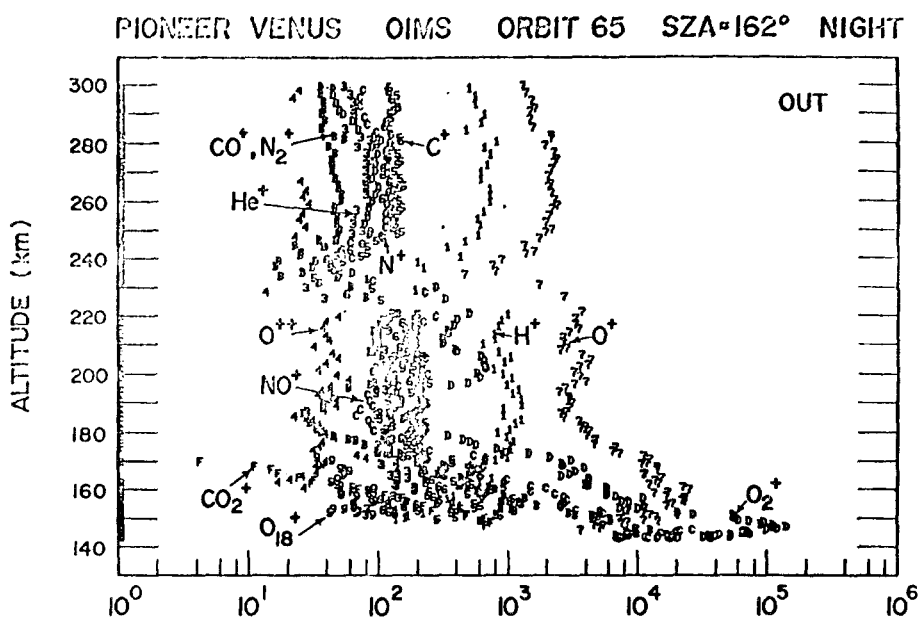

Fig. 40. Ion composition of the upper atmosphere at night ($z_0 = 162°$, OIMS; Taylor *et al.*, 1980).

There are large variations (in space and time) in ion number density above 200 km. Ionospheric convection generated by solar wind interaction is probably the reason for these variations. Even the height of the ionopause is changed within very large limits – from a few hundreds to a few thousands km. These changes are probably caused by the solar wind pressure variations.

The pattern of altitude distributions of the main ions (O_2^+, O^+, CO^+) obtained by the mass-spectrometer is independently confirmed by RPA experiment (Knudsen *et al.*, 1979a, b). This experiment and also OETP (Brace *et al.*, 1979a, b) demonstrated strong time variations of n_e and T_e. There are large differences from one orbit to another and along the same orbit. Typical values of T_i and T_e are 2000° and 4000° respectively.

8.2. Radiooccultations

The first profiles of n_e in the Venusian atmosphere were measured by radiooccultation of M5 (Kliore *et al.*, 1967). Frequencies 49.8 and 423.3 Mc s^{-1} were used. The general properties of the planetary ionosphere – the position of the main peak, the differences between the day and night ionosphere – were defined in this first experiment. On M10 the experiment was repeated on frequencies 2.3 and 8.4 Gc s^{-1} (S and X bands, Fjeldbo *et al.*, 1975). It was possible to observe only two profiles (one day and one night) by means of both of these two fly-by probes. Many more occultation measurements were provided by orbiters V9-O, V10-O and P-O. In Soviet experiments frequencies 940 Mc s^{-1} and 3.75 Gc s^{-1} and on Pioneer S and X bands were used. Simultaneous measurements on two frequencies are very effective for studies of the ionosphere because its refractive index depends on the frequency.

The results of V9-O, V10-O, were published for 22 radiooccultations (Aleksandrov *et al.*, 1976a, b; Yakovlev *et al.*, 1976). In Figure 41 some of the n_e profiles deduced from these experiments are shown. The day profiles are stable in general beside positions of the ionopause. The main maximum is at a height of nearly 150 km; there are also some secondary maxima at 200 and 125 km approximately. The night ionosphere is much more variable. For 13 cases out of 19, a double structure of the ionospheric peak was observed; sometimes more than 2 maxima are present. Double structure of the night peak was observed on M10. However 36 profiles registered on P-O (Kliore *et al.*, 1979b) have no double structure as a rule. P-O measurements show a very stable altitude of the night peak (142.2 ± 4.1 km, very near to the peak in the day time near terminator) but the other properties of the profile are variable. The typical value of n_e is 3×10^4 cm^{-3} at the night peak. Measurements in the polar region by $85 < z_0 < 92°$ gave $n_e \simeq 10^5$ cm^{-3} (Kliore *et al.*, 1979a).

In general, outline profiles n_e obtained by radio occultations are in good accordance with in situ measurements described in previous section. An important advantage of radio occultations is the possibility of studying the ionosphere to its lower boundary.

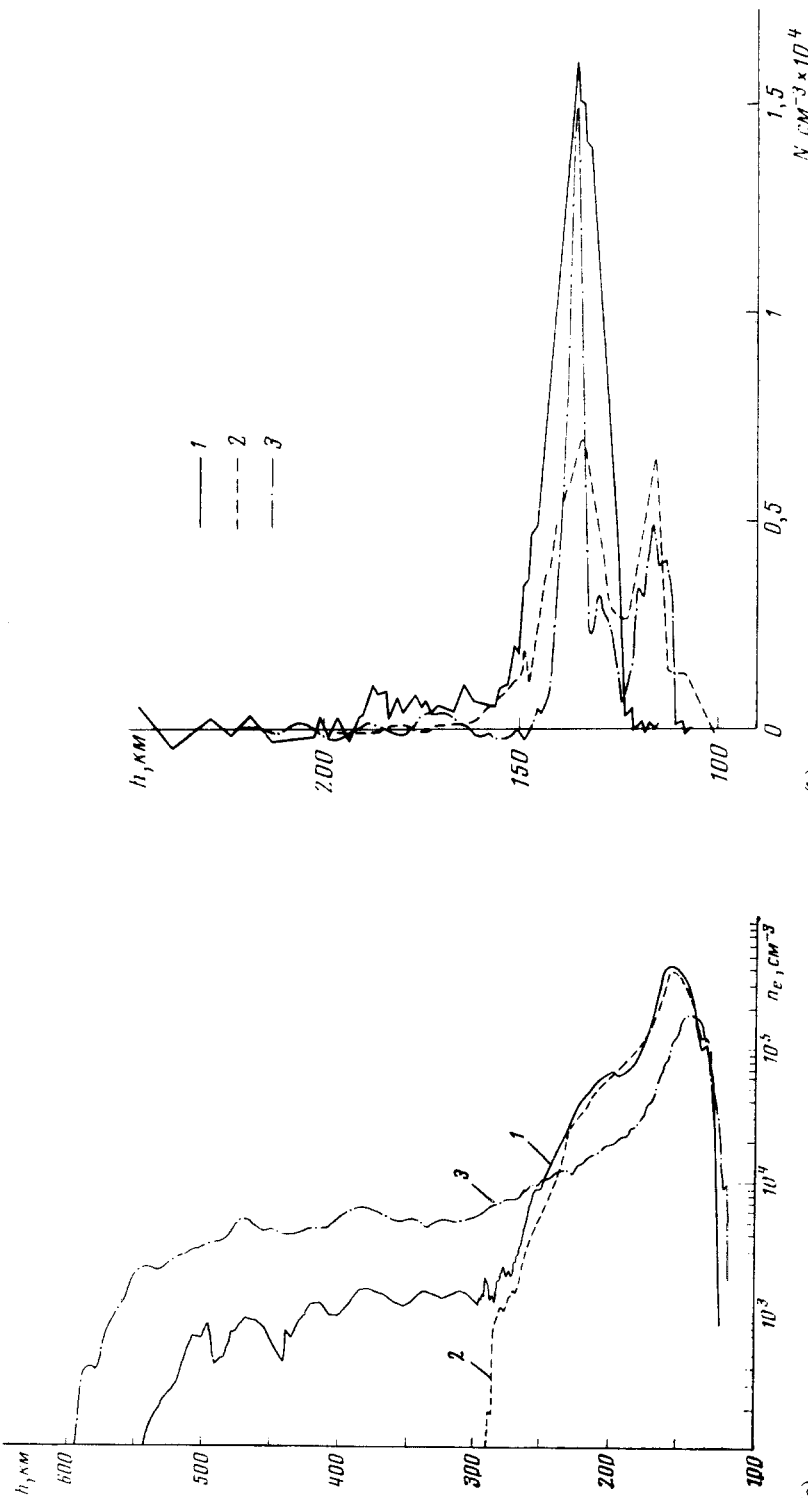

Fig. 41. Examples of the profiles of the electron number density in the Venusian atmosphere from radio occultations on V9, 10 (Aleksandrov *et al.*, 1976a, b). (a) day (1 – November 2, 1975, $z_0 = 14°$; 2 – October 20, 1975, $z_0 = 46°$; 3 – November 23, 1975, $z_0 = 85°$), (b) night (1 – October 28, 1975, $z_0 = 150°$; 2 – November 2, 1975, $z_0 = 144°$; 3 – November 4, 1975, $z_0 = 146°$).

8.3. Emission spectroscopy

Resonance scattering and chemical processes created optical emission in the upper atmosphere. Analysis of the emission spectrum of the upper atmosphere can be an important source of information about this part of the atmosphere.

The strongest resonance emission (≃100 kR near limb) is Lα 1216 Å. This is a strong solar chromospheric line which is scattered resonantly by neutral hydrogen atoms in the upper atmosphere. A similar emission was studied in more detail in the Earth's upper atmosphere. The earliest measurements on Venus (V4, Kurt *et al.*, 1968; M5, Barth *et al.*, 1968a, b) demonstrated the presence of Lα emission there also. Venusian Lα emission was observed to an altitude about 7000 km and shows that Venus (the same as Earth and Mars) has an extended hydrogen corona. This is the most external part of the planetary atmosphere.

Lα measurements were repeated on V6 (Belyaev *et al.*, 1970), M10 (Broadfoot *et al.*, 1974), V9-O, V10-O (Bertaux *et al.*, 1976, 1978). V11-F and V12-F (Kurt *et al.*, 1979). Measured intensities can be explained at a first approximation by the exospheric model with a concentration

$$n(H) \simeq 2 \times 10^4 \text{ cm}^{-3} \tag{8.5}$$

on exobase and a temperature from 325 to 600 K. The last number is substantially more than was given by in situ measurements – 250° by day and 100° at night. The altitude n_H profile deduced from V9 and V10 measurements is in Table XXIII. There $n(\text{H}) > n(\text{He})$ at an altitude more than 700 km and hydrogen becomes the main atmospherical constituent.

TABLE XXIII

Number density of the neutral hydrogen from the exospheric model, based on V9, 10 data (Bertaux *et al.* 1978)

Altitude (km)	$n(H)$ (cm^{-3})	Altitude (km)	$n(H)$ (cm^{-3})
250	1.5×10^4	1800	1.3×10^3
350	1.2×10^4	2500	5.7×10^2
500	9.3×10^3	3500	2.1×10^2
750	6.0×10^3	5000	6.8×10^1
1000	4.0×10^3	7000	2.1×10^1
1300	2.5×10^3		

Approximations by the models with a single temperature for all heights are not satisfactory. It is possible to explain the disagreement between the observed and the calculated profiles by the change of molecular weight (D/H relation) or the presence of some high-temperature component of H at an altitude above 3000 km. The choice between these two possibilities was made by the experiments on V9-O and V10-O, which provided, beside convenient intensities, also Doppler width measurements and an evaluation of the D/H relation (Lα – photometer with the deuterium and

hydrogen cells). The second explanation proved to be right: there are a few percents of hydrogen atoms with a temperature of a few thousand degrees. Probably such hot atoms arise in the charge-exchange processes between atmospherically neutral hydrogen and solar winds protons. The upper limit of D/H was defined as $\simeq 0.01$. Measurements of some other resonance lines were provided by experiment on M10, P-O and V11-F, V12-F (He 584 Å, O II 304 Å, Ar 869 Å *et al.*).

There were attempts to observe the visible spectrum of Venus' nightglow by means of ground-based telescopes (Kozyrev, 1954; Newkirk, 1959; Owen, 1962), but such observations are very difficult because light from the day part of the planetary disk gives to strong a background. Results are negative or nonrepresentative.

However in the near infrared recently some upper atmospheric emission was discovered which is so strong that it is observable even on the illuminated part of the Venusian disk if spectral resolution is high enough. This is the O_2 band λ 1.27 μm (Connes *et al.*, 1979). Intensity of this emission is 3.4×10^6 R at day time and 4.3×10^6 *R* at night. This emission arises at the altitudes between 80–100 km. Rotational temperature 185 ± 15 K is in good accordance with the other estimations of T for these altitudes. One of the possible excitation processes is trial collision

$$O + O + CO_2 \rightarrow O_2^* + CO_2 + 5\,\text{eV}. \tag{8.6}$$

Krasnopolsky (1980) supposed that some reactions with the participation of ClO are more effective and can better provide the approximate coincidence of the day and night intensities.

Night emission in the visible part of the spectrum (4000–7000 Å) is also defined by O_2 bands – there is here a Herzberg II band system $c^1\Sigma_u^- \cdots X^3\Sigma_g^-$ (Figure 42). These bands were discovered in 1975 by means of the highly sensitive scanning spectrometers installed aboard orbiters V9-O and V10-O (Krasnopolsky *et al.*, 1976). Identification was made by Lawrence *et al.* (1977). These bands are absent in the Earth's atmosphere but can be simulated in the laboratory when O_2 is added to CO_2 as a small trace. In the Venusian spectrum the vertical intensity of these bands is a few kR. The probable excitation process is trial collision. Localization altitude is 80–100 km.

By means of the optical spectrometer on board P-O the other emissive constituent was found – NO (Stewart and Barth, 1979).

Bands of NO were observed in the region 1800–2800 Å. The vertical intensity is 0.5 kR. Possibly the excitation process is a binary recombination of N and O. Maximum of emission is localized on the altitudes between 100 and 120 km.

For visible O_2 (Krasnopolsky and Tomasheva, 1980) and NO bands (Stewart and Barth, 1979) the spatial time distribution of intensity was investigated. Both emissions have a maximal intensity near the equator at $\sim 30°$ from the antisolar point toward the morning terminator. It is supposed that the position of the maximum corresponds to the region of downward flow of the upper atmospherical circulation. Atoms of N and O are born by photodissociation on the day side and transferred to

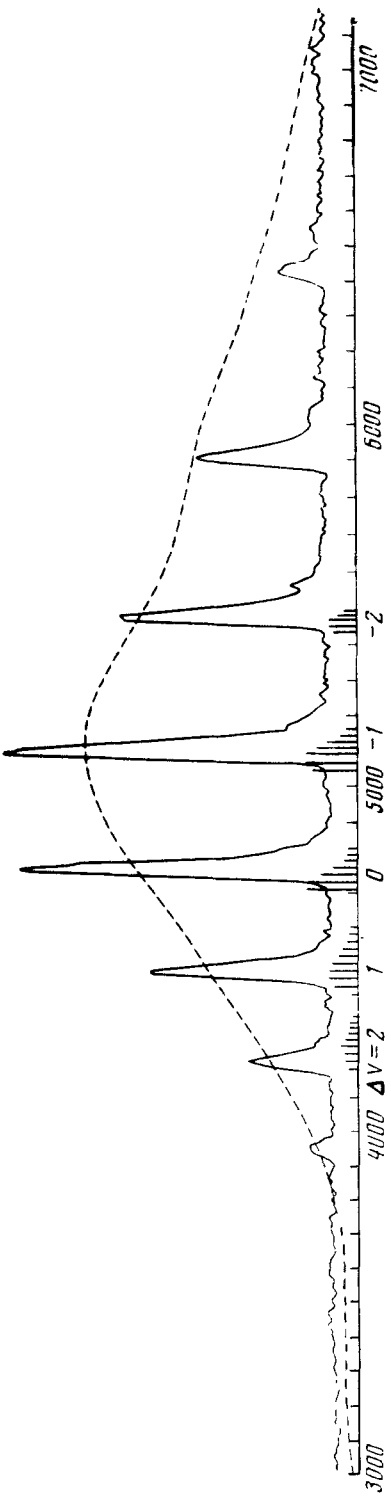

Fig. 42. The spectrum of the Venus nightglow in the interval 4000–7000 Å (Krasnopolsky *et al.*, 1976).

the night side by the winds; there they go down, and emission maximum is a consequence of their concentration rise in the region of downflow.

By means of ground-based heterodyne spectrometry nonthermal emission of the Venusian upper atmosphere near 10 μm was discovered (Johnson *et al.*, 1976). This emission presented by very narrow nuclei inside the normal rotational absorption lines of band $00°1-[10°0-02°0]_I$ $^{12}CO_2^{16}$. The probable excitation mechanism is energy transfer in collisions with CO_2, excited by near infrared solar radiation. Altitude of this emission is ≈120 km.

8.4. Solar wind interaction

The earliest measurements of solar plasma (V4, Gringauz *et al.*, 1968; M5, Bridge *et al.*, 1967; V6, Gringauz *et al.*, 1970; M10, Bridge *et al.*, 1974) and magnetic field near Venus showed that some bow shock is present in the region of interaction of solar wind with the planet. The general pattern was the same as that expected for a planet without a magnetic field. The ionosphere is an obstacle for solar wind in the case of Venus in contrast to the Earth, where the terrestrial magnetic field is such an obstacle. However behind the front of the bow shock, the magnetic field strength rises and formation of an induced magnetosphere takes place. In Figure 43 the positions of the different boundaries (bow wave, rarefaction wave, ionopause) are shown. These positions depend on the parameter H/r_0, where H is the scale of the height, r_0 is the radius of the obstacle. Comparisons with model calculations lead to quantitative estimations of this parameter inside the interval 0.01 to 0.2.

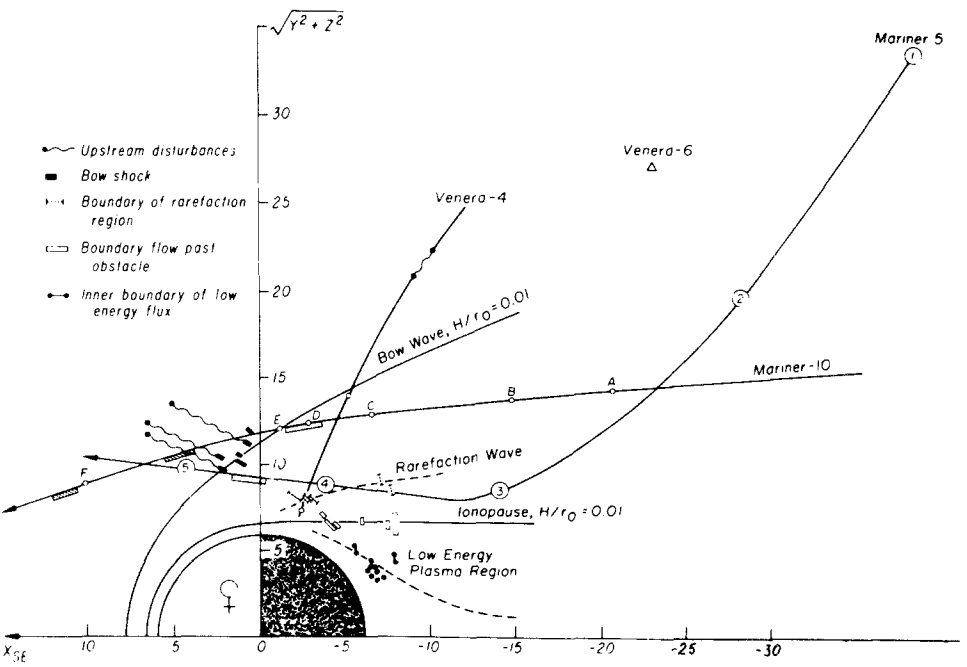

Fig. 43. Solar wind interaction with Venus from the data V9, 10 (Vaisberg *et al.*, 1976).

Measurements of V9-O and V10-O (Vaisberg *et al.*, 1976; Gringauz *et al.*, 1976; Dolginov *et al.*, 1976) confirmed this picture and made it possible to study it in much detail. Some of these details permitted Dolginov *et al.* (1978) to suppose the existence of a small intrinsic magnetic field ($\simeq 10^{-3}$ from the Earth's field). But such argumentation was not very convincing. Dubinin *et al.* (1978) showed by laboratory experiment that all results can be interpreted without the supposed intrinsic magnetic field.

Important new Venusian magnetic field measurements were made on P-O (Russel *et al.*, 1979a, b). Some examples are presented in Figure 44. Magnetic field rises

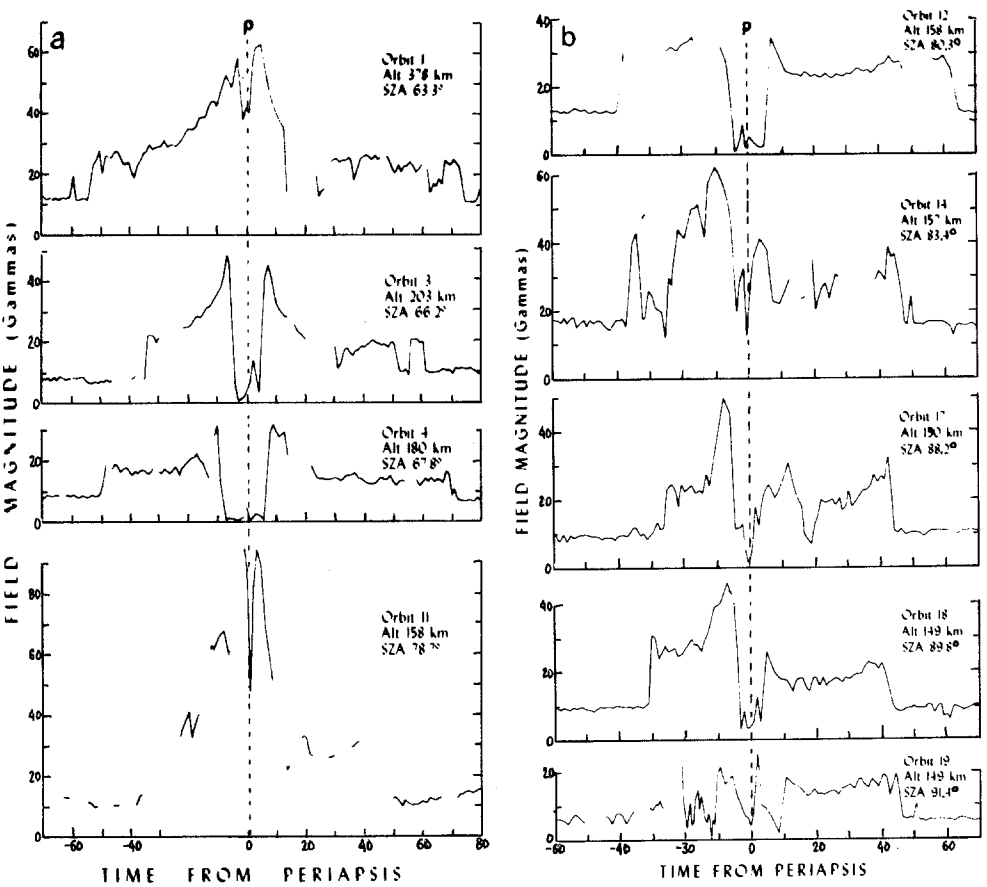

Fig. 44. The average magnetic field strength as a function of time from the periapsis (P-O. Russell *et al.*, 1979a).

suddenly by the intersection of the bow shock from a typical interplanetary value $\simeq 10\gamma$ to 20γ. Then the field rises gradually, with some variations toward periapsis, to 40–80γ, but diminishes suddenly before periapsis by intersection of the ionopause. After passage of the periapsis region the changes follow in the reverse order. Measurements of the magnetic field on the night side of the planet (Russel

et al., 1979b) showed that the intrinsic field (if it exists) is below the sensitivity limits. The relationship of the magnetic moments of Venus and Earth is

$$\mu_{\varphi}/\mu_{\oplus} \leqslant 10^{-4}.$$

The extended region between the ionopause and the bow shock (ionosheath) is occupied by fluxes of ions and electrons, with bulk velocities which are less and concentrations and temperature which are more than in undisturbed solar wind (see Table XXIV).

TABLE XXIV

Typical characteristics of protons in the solar wind and the ionosheath (P-O, orbit No. 6, Wolf *et al.*, 1979)

	Solar wind	Ionosheath
Bulk velocity (km s^{-1})	287	254
Number density (cm^{-3})	33	87
Temperature (K)	207 000	67 000
Azimuth angle	4.2	6.5
Polar angle	0.5	17.0

There is a strong correlation between ionopause altitude and solar wind pressure. When the solar wind is most intensive, velocities inside the ionosheath rise to 750 km and the electronic temperature to 10^6 K. The altitude ionopause in this case is about 400 km near the terminator. For undisturbed conditions the ionopause altitude here is 1500–2000 km.

The typical value of the magnetic field inside the ionosphere is very little – a few γ only, but sometimes impulse bursts of field strength are observed with an amplitude of a few tenths γ and duration of a few seconds. These bursts are interpreted as the effects of intersections of magnetic ropes penetrating the ionosphere (Russel *et al.*, 1979a; Russel and Elfic, 1979).

Electron concentration in the solar wind plasma near Venus corresponds to the intrinsic resonance plasma oscillation frequency near 30 kc s^{-1} approximately. By means of the electric field detector on P-O intensive electromagnetic radiation was observed on this frequency (Scarf *et al.*, 1979; Taylor *et al.*, 1979). Low (a few kc s^{-1}) radiation connected with turbulency was observed by the same instrument inside the ionosheath. Whistler type noises (on frequency 100 c s^{-1}) were observed also. Intensity of the whistler type noises is sharply diminished after intersection of the day ionopause.

8.5. Theoretical Models

8.5.1. *The Neutral Upper Atmosphere*

Structure of the upper atmosphere crucially depends on the energy sources and sinks. Let's remember the processes which are important from this point of view.

The main source of energy in the day time is the solar ultraviolet emission. It leads to the dissociation, ionization and excitation processes. Absorbed energy is partially reradiated in other wavelengths, partially converted into heat. A very effective sink in the atmosphere rich enough in CO_2 is infrared emission in the resonance band 15 μm. Above the level of vibrational relaxation in the mesosphere the volume emissivity is

$$R = n^2 f \eta h\nu \exp(-h\nu/kT) \tag{8.7}$$

where n is the number density, f is the mixing ratio of CO_2, $h\nu$ is the energy of the quantum, η is the deactivation factor. Exponential dependence from $1/T$ leads to the possibility of the compensation of large changes of thermal influx by small temperature variations. As a result CO_2 rich mesosphere is a good enough thermostat and this explains small temperature variations on the altitudes 80–100 km. Detailed analysis of the mesospherical thermal regime on Venus was given by Dickinson (1971, 1973, 1976). His results are in good agreement with the measured temperature.

The infrared sink is most effective immediately above the level of vibrational relaxation ($n \simeq 10^{15}$ cm^{-3}, $z \simeq 100$ km). Vertical optical depth for solar UV (shorter dissociation limit of CO_2) $\tau \simeq 100$ on this altitude. Consequently the most part of solar UV radiation is absorbed much higher than can be reradiated. The source and the sink are separated spatially. Molecular and eddy thermoconductivity provide the transfer of heat down and this leads to the positive temperature gradient dT/dz in some part of the upper atmosphere. As a result the day time upper atmosphere is hot enough. There is a temperature minimum in the mesopause with the strongest infrared cooling. At large enough altitudes the atmosphere becomes optically thin for solar UV and temperature goes to the limit value $T = T_e$ (exospheric temperature) because the sink is absent on the upper boundary.

It is important to note that the solar source of energy is time variable. This source is switched out at night. The upper atmosphere at night is cooled: temperature and scales of height are decreased. One of the consequences is strong horizontal pressure gradients between day and night upper atmosphere and mass transport through the terminators from day side toward night. Every correct model of the upper atmosphere must take into account such dynamical processes. The other time-dependence factor is variation of solar UV with the solar activity phase. It leads to a hotter upper atmosphere in the years of high solar activity.

Some additional sources of upper atmospheric heating may give appreciable contributions to the heat balance, for example dissipation of acoustic or internal gravity waves propagated from down to up (Del Genio *et al.*, 1979).

A few attempts at numerical simulation of the Venusian upper atmosphere with simultaneous analysis of the thermal regime and dynamics were published in the last years (Izakov and Morozov, 1975; Dickinson and Ridley, 1977; Mayr *et al.*, 1978). Calculated day temperatures depend on the EUV heating efficiency ε. Value $\varepsilon \simeq 0.03$ gives good enough coincidence with measured temperatures. Night maxima

of He and H were predicted in one of the above mentioned models (Mayr *et al.*, 1978). Qualitatively this maximum can be explained by the large scale of heights for light gases. As a result a light gas can be greatly enriched in the downward direction.

The altitude of homopause is defined as level for which two diffusion coefficients – molecular and eddy – are equal. By adjustment of the theoretical models to the best coincidence with the measurements of the eddy diffusion coefficient there is some free parameter. Analysis of BNMS results (von Zahn *et al.*, 1979b, 1980) shows that it is possible to describe the eddy diffusion coefficient K by the relation

$$K = 2.2 \times 10^{13}/\sqrt{n}\ \mathrm{cm^2\ s^{-1}} \tag{8.8}$$

for $K < K_{\max} = 5 \times 10^8\ \mathrm{cm^2\ s^{-1}}$; n is number density.

There are no published models which could explain the very low measured night temperatures ($\simeq$100 K). Only some possibilities were shortly discussed (Niemann *et al.*, 1979b, 1980). One of the possible cooling processes is infrared radiation of some unknown molecule. Another mechanism is cooling by eddy heat conduction. Turbulence can lead to net cooling or to net heating of the upper atmosphere independently of the real conditions (Izakov, 1978), but there is no reliable estimations for the case of Venus.

Very high wind velocities ($\simeq$200 m s^{-1}) were predicted for the terminator region of the upper atmosphere. Quantitative description of the general circulation at high altitudes depends on the penetration of superrotation into the upper atmosphere. There are some observational arguments opposed to such penetration (see Section 6.1), but direct data concerning wind above 100 km is absent. The secondary effects, such as daily variations of some constituents (based on mass-spectrometry and optical spectroscopy data), cannot give any convincing criteria.

CO_2 photochemistry has already been reviewed in Section 7.3. The early single-dimension photochemistry models (Liu and Donahue, 1975; Sze and McElroy, 1975) are not in good agreement with the measurements. The model of Dickinson and Ridley (1977) which takes into account the dynamics gives too little O and CO number density. Relatively good agreement was provided by the model of Krasnopolsky and Parshev (1980). This is a single-dimension model but it perhaps provides a more reliable description of the chemical processes and the vertical eddy diffusion profile.

8.5.2. *Ionospheric Models*

In the first years after discovery of the ionospheres of Mars and Venus ion CO_2^+ was considered as dominating. But laboratory study of some ionospheric reaction rates (Fehsenfeld *et al.*, 1970) show that the processes

$$CO_2^+ + O \rightarrow \begin{cases} O_2^+ + CO \\ O^+ + CO_2 \end{cases} \tag{8.9}$$

$$O^+ + CO_2 \rightarrow O_2^+ + CO \tag{8.10}$$

lead to substitution of CO_2^+ for O_2^+ that was confirmed by P-O in situ measurements (see Section 8.1).

Four main ionospheric layers are known in the terrestrial ionosphere. Inside the F_1 layer ($z \simeq 180$ km) the electron number density n_e decreases above the peak owing to decrease of the neutral number density. n_e decreases under the peak owing to the absorption of solar UV radiation. At an altitude of 300 km the F_2 layer is present as a consequence of too low a recombination rate there. Ions and electrons are accumulated in the F_2 peak region in the quantities which provide gradient n_e big enough to support plasma flux down (by ambipolar diffusion) which compensates for the ionization rate. The F_1 and F_2 layers are created by solar UV $\lambda < 900$ Å. Below F_1 there are the E and D layers with peaks at altitudes 110 and 70 km respectively. In the E layer the ionization source is solar UV $\lambda > 900$ Å and the main ion O_2^+. Solar X-rays create ionization in the D layer; the dominating ions there are O_2^+ and NO^+.

One of the most sophisticated models of the Venusian day ionosphere among those published before the Pioneer mission was elaborated by Chen and Nagy (1978). There are references in this paper to the previous model calculations. Time dependent equations of continuity, momentum and energy were analyzed in this work and a combined solution was found. Number densities of CO_2^+, O_2^+, O^+, He^+, H^+ and also T_e and T_i were calculated for the altitudes from 120 to 500 km. This model (as in most previous works) describes the main peak in the Venusian ionosphere as the F_1 layer with dominating ion O_2^+. The altitude of the peak and the dominating ion was given correctly by this model but there are some differences between the calculated and measured profiles. A few reasons are possible, among them the following two: (1) calculations were based on the not exact enough model of neutral composition; (2) photochemical equilibrium is absent above 200 km, where processes of ionospheric convection are dominating.

Naturally some attempts to improve the ionospheric model after the first Pioneer data publications were made (Nagy *et al.*, 1979, 1980; Bauer *et al.*, 1980; Izakov *et al.*, 1981). These new calculations based on the measured profiles of neutral constituents demonstrate good coincidence of calculated and measured profiles for the main ions – O_2^+, O^+, CO_2^+, He^+ below 200 km. For small ionic constituents (C^+, N^+, NO^+, CO^+, N_2^+) there are strong disagreements. The calculations of Izakov *et al.* provided a little better accordance for small constituents perhaps owing to a most full list of photochemical processes (64 reactions). One of the important conclusions of this paper is the large influence of H_2 concentration on the altitude of the upper secondary maximum.

By the photoionization processes superthermal photoelectrons arise and as a consequence T_e and T_i can be much bigger than the temperature of neutral particles. Models of the energy balance of the day ionosphere (Gravens *et al.*, 1979, 1980) show that for an explanation of the relatively high electronic and ionic temperature on Venus it is necessary to suppose that plasma thermoconductivity is suppressed by some horizontal magnetic field ($\approx 10\gamma$). The mean value of magnetic field strength

is lower inside the ionosphere ($\simeq 1\gamma$), but there are fluctuations in the magnetic ropes.

It is necessary to explain the existence of an essential night ionosphere. Two possibilities are discussed: transport of the ionization from the day side (McElroy and Strobel, 1969; Brace *et al.*, 1979b) and local production by the precipitation of electrons and ions (Gravens *et al.*, 1978; Gringauz *et al.*, 1979; Gombosi *et al.*, 1979). Comparison of the profiles calculated for both these processes with those measured is presented in Figure 45. Evidently both calculated profiles fit the measurements well enough above 150 km. For the precipitation source the altitude of the ionospheric peak depends on the electron energy (average energy $\simeq 100$ eV

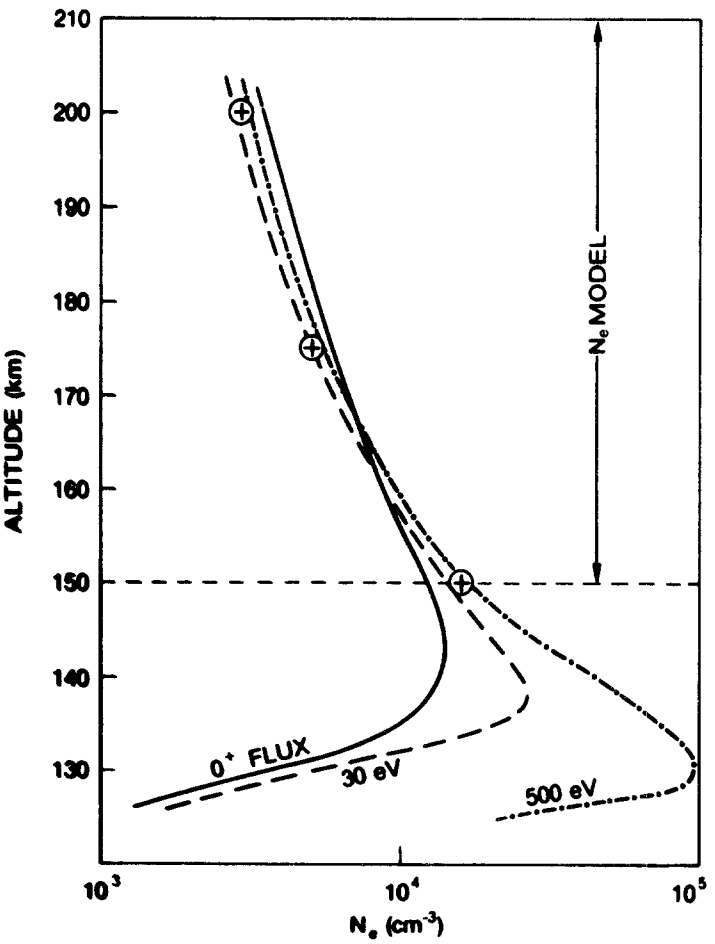

Fig. 45. Comparison of measured and theoretical n_e profiles in the night ionosphere ($z_0 = 140°$). Crosses are experimental data (some are from an empirical model). Continuous line is theoretical model supposing O^+ from the day side (downward flux 6×10^7 cm^{-2} s^{-1}), dashed – model with electron precipitation ($E = 30$ eV, flux 4.4×10^8 cm^{-2} s^{-1}), dash-dotted curve – the same for $E = 500$ eV. Although above 150 km all models are in satisfactory agreement with the in situ measurements of n_e, the last model gives a peak below the altitude of 142 km observed by radio occultations (Brace *et al.*, 1979b).

is necessary). Measurements of the energy spectrum of electrons on P-O (Intriligator *et al.*, 1979) show that an approximate quantitative explanation of night ionization is possible in the frame of precipitation mechanism. However, the equality of the altitudes of day and night ionospherical maxima and the stability of this altitude can be evaluated as an argument in favor of ionization transport because it is connected with the day photochemistry and must be stable enough. Both processes may be effective in supporting the night ionosphere. The other sources can also give some contribution to night ionization, for example, solar He 584 Å emission, scattered by interplanetary medium and meteor ionization (Krasnopolsky, 1979b).

A model of the interaction of the solar wind with the atmosphere of a non-magnetic planet evidently describing well enough the cases of Venus and Mars was presented by Clautier and Daniel (1972, 1979). There is more detailed bibliography in these papers. Some induced magnetosphere arises which works as an obstacle streamlined by the solar wind. The magnetic field of the solar wind compressed and forced behind the bowshock boundary leads to the generation of an electric field $[\mathbf{v}\times\mathbf{B}]$ which accelerates the atmospheric ions and electrons. There is a dynamo mechanism creating electrical currents which strongly decrease the magnetic field strength below the ionopause.

The position of the ionopause is defined by the balance of magnetic pressure and the pressure of the ionized gas ($B^2/8+p=\text{const}$). Knudsen *et al.* (1979a) found the empirical bound of B, n_e, T_e, and T_i in the form

$$\left(\frac{B}{48\gamma}\right)^2+\left(\frac{n_e}{10^4\ \text{cm}^{-3}}\right)\frac{T_e+T_i}{6500}=1\,. \tag{8.11}$$

By the interaction of the ionopause n_e increases from 10 to $10^4\ \text{cm}^{-3}$, B decreases from tens to a few γ, and temperatures T_e and T_i do not change.

Although some of the solar wind particles can penetrate the dayside ionosphere owing to the inhomogeneity of the magnetic field they have essentially no influence on the ionospheric structure (Gombosi *et al.*, 1980). Plasma instabilities inside the ionopause were proposed as a qualitative explanation of the rise of magnetic ropes observed below (Breus, 1979; Johnson and Hanson, 1979; Dubinin *et al.*, 1980). There are a few reviews specially devoted to the Venus solar wind interaction (Bauer *et al.*, 1977; Breus, 1979; Breus and Gringauz, 1980).

The escape of gases on Venus cannot be the essential factor in the evolution of the atmosphere by the contemporary mean exospheric temperature (250–500 K). Even for hydrogen escape the flux is too small in spite of the presence of 'hot' hydrogen atoms (with temperature a few thousands degree) which were mentioned in Section .3. The hydrogen atoms flux caused by the hot component escape (Kumar *et al.*, 1978) is

$$N\simeq 10^7\ \text{cm}^{-2}\,\text{s}^{-1} \tag{8.12}$$

which corresponds to the removal of a liquid water layer of 0.5 m thickness for 5×10^9 years. This is somewhat more than is contained in the contemporary atmosphere of Venus but it cannot explain why the Venusian atmosphere is so poor in water as compared with the Earth's.

9. Origin and Evolution of the Atmosphere

According to modern ideas the planets arose as a result of the condensation of protoplanetary nebula matter. Atmospheric gases came to the planets from the protoplanetary nebula also, however there are two different versions of this process:

(a) The direct capture of gases from the protoplanetary nebula in the period of condensation with the formation of a so-called primary atmosphere.

(b) The capture of gases by dust particles (physical or chemical adsorption) with subsequent release in the planetary outgassing process – either quick (in the beginning of the evolution of the planet) or gradual.

The comparative analysis of the atmospheric composition on the planets will probably permit us to make a choice between these versions. It is also not excluded that in colder parts of the solar system the condensation of gases with the formation of small bodies (nuclei of comets, meteorites) took place; then these bodies bombarded the surface of the inner planets already formed (but poor in volatiles) and made a significant contribution to the formation of the atmosphere. The process of solar wind substance capture was able to make some contribution also.

Data on the abundance of the so-called volatiles on Earth, Venus and Mars are presented in Table XXV. Abundances in carbonaceous chondrites and in the Sun are indicated for comparison. Two versions are given in the cases of Earth and Mars – abundance in the atmosphere and the total amount of outgassing products including the atmosphere, hydrosphere (cryosphere) and sedimentary rocks.

It is clear from Table XXV that, in the total amount of CO_2 and N_2, the difference between Venus and Earth is not large if we take into account the carbon dioxide connected to the earthly sedimentary rocks. The difference in the free oxygen amount is explained by the fact that this gas is supplied by the biosphere on the Earth continuously. The difference in H_2O amount is much more important. Water vapour is the main component of volcanic gases. Cameron (1963) and Fesenkov (1967) expressed an opinion that if the amount of H_2O in the Venusian atmosphere is small it means that it isn't of volcanic origin, but is captured from the protoplanetary nebula. The logic of this reasoning isn't irreproachable, however we shall see further, that the idea of Venusian atmosphere initially found confirmation in the data on the amount of noble gases. On Mars the main products of outgassing (CO_2, N_2, and H_2O) are there approximately in the same proportion as on the Earth, however its entrails were apparently subjected to outgassing to a lesser degree.

Very important criteria in the problem of the origin of the atmosphere's absolute and relative abundances are the unradiogenic ('relict') noble gases isotopes. On the basis of Table XXV data it is possible to come to the following conclusions:

TABLE XXV

Volatile constituents of Venus, Earth and Mars

	Venus	Earth		Mars[a]		Carbonaceous chondrites[b]	Sun[c]
		Contemporary atmosphere	Supposed full mass of the outgassing product	Contemporary atmosphere	Supposed full mass of the outgassing product		
Main constituents g/g							
CO_2	9.3×10^{-5}	4.0×10^{-10}	4.3×10^{-5}	3.6×10^{-3}	4.5×10^{-7}	—	—
N_2	2×10^{-6}	6.8×10^{-7}	6.8×10^{-7}	5.6×10^{-10}	1.1×10^{-8}	—	—
O_2	$\leq1\times10^{-4}$	1.7×10^{-7}	1.7×10^{-7}	4.5×10^{-10}	4.5×10^{-10}	—	—
H_2O	8×10^{-10}	8.5×10^{-10}	2.8×10^{-4}	2.2×10^{-12}	$\sim4.4\times10^{-6}$	—	—
Elemental composition for the main constituents g/g							
H	8×10^{-11}	1×10^{-10}	3.1×10^{-5}	2×10^{-13}	5×10^{-7}	$\sim2\times10^{-2}$	0.75
O	0.8×10^{-5}	1.7×10^{-7}	3.2×10^{-4}	2.6×10^{-8}	5×10^{-6}	0.4	8×10^{-3}
C	2.5×10^{-5}	1.1×10^{-10}	1.2×10^{-5}	1.0×10^{-8}	1.2×10^{-7}	$\sim4\times10^{-2}$	3×10^{-3}
N	2×10^{-6}	6.8×10^{-7}	6.8×10^{-7}	5.6×10^{-10}	1.1×10^{-8}	$\sim3\times10^{-3}$	1×10^{-3}
Noble gases, g/g							
^{20}Ne	5×10^{-10}		1.1×10^{-11}		4×10^{-14}	$\sim3\times10^{-10}$	$\sim1\times10^{-3}$
^{36}Ar	4×10^{-9}		3.8×10^{-11}		2×10^{-13}	$\sim1\times10^{-9}$	$\sim2\times10^{-4}$
^{84}Kr	1×10^{-10}		2.8×10^{-12}		2×10^{-14}	$\sim3\times10^{-11}$	$\sim1\times10^{-7}$
^{132}Xe	—		1.6×10^{-11}		1×10^{-14}	$\sim3\times10^{-11}$	$\sim1\times10^{-8}$
^{40}Ar	6×10^{-9}		1.1×10^{-8}		6×10^{-10}	?	?
Relation of numbers of atoms							
$^{36}Ar/^{20}Ne$	5		2		3	2	0.1
$^{36}Ar/^{84}Kr$	~10		32		20	80	5×10^{3}
$^{36}Ar/^{132}Xe$	—		87		70	120	7×10^{4}
$^{36}Ar/^{40}Ar$	0.8		3.8×10^{-3}		4×10^{-4}		
$^{36}Ar/^{12}C$	5×10^{-5}	1.2×10^{-1}	1.0×10^{-6}	7×10^{-6}	6×10^{-7}	10^{-8}	2×10^{-2}
C/N	15	2×10^{-4}	20	20	15	15	3

(1) The absolute abundances of three relict gases ^{20}Ne, ^{36}Ar ^{84}Kr on Venus and in carbonaceous chondrites are approximately equal.

(2) Absolute abundances of these gases decrease in the transition from Venus to the Earth and then to Mars.

(3) Relative abundances of ^{20}Ne, ^{36}Ar and ^{84}Kr are approximately equal on all three planets and carbonaceous chondrites.

(4) The abundance ratios for relict gases distinguish themselves strongly from the solar ones; the difference decreases with the atom mass increasing.

(5) Ratios $^{36}Ar/N$ and $^{36}Ar/^{40}Ar$ decrease with the transition from Venus to the Earth and then to Mars.

The regularities listed here might be explained quite simply if we suppose that carbonaceous chondrites were the primary material forming the Venusian entrails and their proportion decreases gradually with the transition to the Earth and then to Mars. However this hypothesis doesn't appear to be accceptable, because carbonaceous chondrites were formed in conditions of comparatively low temperature somewhere inside the asteroid belt. From this point of view it is not understandable how it could happen that such material's contribution to the inner planets' entrails was distributed between them in such proportions.

Izakov (1979, 1980) considered the possibility that a large part of the atmospheric gases of Venus is captured from the protoplanet nebula, and its atmosphere is primary in general (mechanism (a)). The proportion of primary component decreases from Venus to the Earth and to Mars. If this hypothesis is correct the relative abundance of the noble gases on all three planets and in the chondrites is the same as in the protoplanetary nebula. It differs sharply from the solar one and therefore it is necessary to propose that protoplanetary nebula composition at the stage of formation didn't correspond to the solar one also. It is a definite difficulty, however it isn't excluded, that the escape mechanism responsible for this difference acted in the protoplanetary nebula.

Pollack and Black (1979) analyzed the other possibility – accretion of gases with the dust matter particles (mechanism (b)). So far as adsorbing processes' speed depends on the temperature exponentially they had to suppose that in the protoplanetary nebula it doesn't depend on the distance from the Sun practically. It explains the relative composition constancy. On the other hand to explain the differences in the absolute amount it is necessary to suppose a strong change of pressure with the distance. These assumptions seem to be unlikely. It is not excluded that both mechanisms worked but for noble and chemically active components their relative role was different (for example, mechanism (a) predominated for the first, and for the second – 8.2.).

Chemically active main components (CO_2, H_2O, and N_2) came to the Venusian atmosphere (as to the atmosphere of the Earth and Mars) most probably by means of process (b) – adsorption by particles with subsequent outgassing. Further the question on the outgassing rate arises: whether it was approximately constant in the course of the planetary life (gradual outgassing) or whether the greater part

of the modern atmosphere formed somewhere in the very beginning (catastrophic outgassing). Most probably the processes of both types took place, only their relative role is questionable.

Rasool and de Bergh (1970) considered the phenomenon of the 'runaway greenhouse' effect which can explain how the modern atmosphere and climate were formed on Venus. Because of the nearness to the Sun and higher temperatures than on the Earth all the water picking out in the process of outgassing (the rate isn't very essential) enters the atmosphere and the temperature increases because of the greenhouse effect. For this in the case of Venus (but not the Earth!) the temperature of saturation remains lower than the temperature of the atmosphere, the liquid phase doesn't occur and all the water picked out appears in the atmosphere. High temperatures shift the vollastonite equilibrium (7.1) in the direction of the gaseous phase and a considerable part of the CO_2 goes away to the atmosphere (unlike the Earth, where it dissolves in the liquid water and transforms into sedimentary rocks). Then water leaves the atmosphere because of the escape of hydrogen.

The scenario described above creates a number of difficulties at more detailed consideration (Pollack, 1971, 1979; Walker, 1975; Moroz and Mukhin, 1977). One of them is that the rotation axis of Venus is almost perpendicular to the ecliptic so in the polar regions liquid water must be stable and this leads to CO_2 tied in the crust; besides which the luminosity of the young Sun was less than that of the modern Sun. In one of the works (Moroz and Mukhin, 1977) the conclusion is that global differences of the atmospheric and climatic characteristics of the both planets (Venus and Earth) may be explained easily if Venus was formed with much less amount of water in its entrails than the Earth. Holland (1964) put forward the hypothesis for explanation of the water deficiency that at the accretion stage at the origin of Venus ice particles were absent (because of the higher temperature). However a significant part of the H_2O was probably contained in hydrated silicates during the period of accretion (Gold, 1964).

The modern rate of hydrogen escape (8.12) is too insignificant to have created the H_2O deficiency on Venus, however it is not excluded that it was essentially higher at the early stages of the atmosphere's evolution.

For the present it is not clear what happened indeed: water deficiency in the protoplanetary matter (at a distance of 0.7 AU from the Sun) or quick escape of hydrogen in the primitive atmosphere. It is impossible to neglect the third possibility – that a significant part of the water ($\approx$10% of the terrestrial quantity was able to remain tied in the rocks, see Section 7).

10. Problems for Future Studies

Investigations of Venus by means of the interplanetary automatic probes carried out in the period from 1967 to 1978 gave much valuable actual information on the planetary atmosphere. We obtained answers for many questions; however at the same time new problems have arisen. We shall enumerate some tasks which await decision.

(1) A more accurate definition of noble gases content. Nothing is known about xenon; there are discrepancies in argon abundances; isotopic ratios of neon and crypton are known only approximately.

(2) It is necessary to have new measurements of sulfuric compounds (a detailed profile of SO_2, H_2S, COS from the surface to the clouds).

(3) Free oxygen abundance in the lower atmosphere.

(4) H_2O vertical profile – data obtained are preliminary and contradictory.

(5) Exact vertical profiles of thermodynamical parameters (T, P, ρ) in the region of the subsolar point.

(6) Horizontal fields of temperature and pressure higher than 45 km and their variations.

(7) Chemical content of the clouds especially of type 3 particles.

(8) The nature of the ultraviolet absorption in the clouds.

(9) Structure of the clouds in the polar regions.

(10) Speeds of wind field at the different heights especially vertical speeds.

(11) The nature of superrotation.

(12) The dynamics of the undercloud atmosphere.

(13) H_2O abundance in the rocks; mineral and elementary content of the rocks.

(14) The nature of low night temperatures of the upper atmosphere.

(15) Source of the ionization at night.

(16) The relative role of different processes in the formation of the atmosphere.

(17) The evolution of the atmosphere.

Some of these problems may be decided by means of separate experiments – for example, 1 is the task for a highly sensitive mass-spectrometer on a descent probe. The other ones require complex studies. For example, the problems of dynamics may be decided by means of a balloon launch in the planetary atmosphere and a set of remote sensing experiments on the orbiter. It is difficult to solve the problem of the chemical interaction of the atmosphere and the rocks without data on the contents of rocks. It is obvious that we are very far from the possibility to put the point in the investigations of the Venusian atmosphere and not a few expeditions of different types will be needed later on including descent probes, orbiters and balloons.

Investigations of the planets by means of space probes cost a great deal. However it is a hope that their results will permit us some time to understand the processes controlling the atmosphere and climate so well that mankind can busy himself with the improvement of his own planet and perhaps with the accommodation of the other planets of the solar system for his needs.

References

Abramovich, S. K., Ageeva, G. D. m Akim, E. L. *et al.*: 1976, *Kosmich. Issled.* **14**, 667 (Russian).
Adamchik, J. A. and Draper, A. L.: 1963, *Planetary Space Sci.* **11**, 1303.
Adams and Dunham: 1932, *Publ. Astron. Soc. Pacific* **44**, 380.
Ainsworth, J. E. and Herman, J. R.: 1977, *Icarus* **30**, 314.
Aleksandrov, Yu. N. *et al.*· 1976a, *Kosmich. Issled.* **14**, 819 (Russian).

Aleksandrov, Yu. N. *et al.*: 1976b, *Kosmich. Issled.* **14**, 824 (Russian).
Allen, C. W.: 1973, *Astrophysical Quantities*, Univ. of London, The Athlone Press.
Anderson, J. D. *et al.*: 1968, *Astron. J.* **73**, 162.
Anderson, R. C., Pipes, J. G., Broadfoot, A. L., and Wallace, L.: 1969, *J. Atm. Sci.* **26**, 874.
Andreev, B. N. *et al.*: 1974, *Kosmich. Issled.* **12**, 419 (Russian).
Andrejchikov, B. M.: 1978, *Geokhimiya* **1**, 11 (Russian).
Antsibor, Ya. M. *et al.*: 1976, *Kosmich. Issled.* **14**, 714 (Russian).
Apt, J. and Goody, R.: 1979, *Science* **203**, 785.
Arking, A. and Potter, J.: 1968, *J. Atm. Sci.* **25**, 617.
Aumann, H. H. and Orton, G. S.: 1979, *Icarus* **38**, 251.
Avduevsky, V. S., Golovin, Yu. M., and Zavelevich, F. S. *et al.*: 1976, *Kosmich. Issled.* **14**, 735 (Russian).
Avduevsky, V. S. *et al.*: 1968, *Dokl. Akad. Nauk SSSR* **179**, 310 (Russian).
Avduevsky, V. S., Marov, M. Ya., and Rozhdestvensky, M. K.: 1969, *Kosmich. Issled.* **7**, 233 (Russian).
Avduevsky, V. S., Marov, M. Ya., and Rozhdestvensky, M. K.: 1970, *Kosmich. Issled.* **8**, 871 (Russian).
Avduevsky, V. S., Marov, M. Ya., Moshkin, B. E., and Ekonomov, A. P.: 1973, *Dokl. Akad. Nauk SSSR* **210**, 799 (Russian).
Avduevsky, V. S., Marov, M. Ya., Moshkin, B. E., and Ekonomov, A. P.: 1974, *J. Atm. Sci.* **30**, 1215.
Avduevsky, V. S. *et al.*: 1976a, *Kosmich. Issled.* **14**, 665 (Russian).
Avduevsky, V. S. *et al.*: 1976b, *Kosmich. Issled.* **14**, 710 (Russian).
Avduevsky, V. S. *et al.*: 1976c, *Kosmich. Issled.* **14**, 735 (Russian).
Avduevsky, V. S. *et al.*: 1979, *Kosmich. Issled.* **17**, 655 (Russian).
Barker, E. S.: 1975, *Icarus* **25**, 268.
Barker, E. S.: 1979, *Geophys. Res. Letters* **6**, 117.
Barker, E. S. and Macy, W. W.: 1977, *Icarus* **30**, 551.
Barker, E. S. and Perry, M. S.: 1975, *Icarus* **25**, 282.
Barker, E. S., Woodman, J. H. and Perry, M. A.: 1975, *J. Atm. Sci.* **32**, 1205.
Barth, G. A.: 1968a, *J. Atm. Sci.* **25**, 564.
Barth, C. A. *et al.*: 1968b, *J. Geophys. Res.* **73**, 2541.
Bauer, S. J. *et al.*: 1979, *Science* **205**, 109.
Belton, M. J. S.: 1968, *J. Atm. Sci.* **25**, 596.
Belton and Hunten: 1966, *Astrophys. J.* **146**, 307.
Belton, M. J. S., Smith, G. R., Elliott, D. A., Klassen, K., and Danielson, G. E.: 1976a, *J. Atm. Sci.* **33**, 1383.
Belton, M. J. S., Smith, G. R., Schubert, G., and Del Genio, A. D.: 1976b, *J. Atm. Sci.* **33**, 1394.
Belyaev, V. P. *et al.*: 1977, *Kosmich. Issled.* **15**, 677.
Bertaux, J. L. *et al.*: 1976, *Kosmich. Issled.* **14**, 799 (Russian).
Bertaux, J. L. *et al.*: 1978, *Planetary Space Sci.* **26**, 817.
Betz, A. L. *et al.*: 1976, *Astrophys. J.* **208**, L141.
Betz, A. L. *et al.*: 1977, *Proc. Symposium on Planetary Atmospheres*, Ottava, p. 29.
Bigourd, C. *et al.*: 1975, *Icarus* **26**, 73.
Blamont, J. and Ragent, B.: 1979, *Science* **205**, 67.
Boyer, C.: 1973, *Planetary Space Sci.* **21**, 1559.
Boyer, Ch. and Camichel, H.: 1961, *Ann. d'Astrophys.* **24**, 531.
Boyer, C. and Camichel, H.: 1965, *Compt. Rend. Acad. Sci.* **260**, 809.
Boyer and Guerin: 1969, *Icarus* **11**, 338.
Boese, R. W., Pollack, J. B., and Silvaggio, P. M.: 1979, *Science* **203**, 797.
Bottema, M., Plummer, W., and Strong, J.: 1965, *Ann. Astrophys.* **28**, 225.
Brace, L. H.: 1979a, *Science* **203**, 763.
Brace, L. H.: 1979b, *Science* **205**, 102.
Brace, L. H. *et al.*: 1979c, *J. Geophys. Res. Letters* **6**, 346.
Breus, T. K.: 1979, *Report for XVIII JUGGIYAGA Gen. Assembly*, Canberra, Dec. 3–14.
Breus, T. K.: 1979, *Space Sci. Rev.* **23**, 253.
Breus, T. K. and Gzingaur, K. I.: 1980, *Kosmich. Issled.* **18**, 587 (Russian).
Bridge, H. S. *et al.*: 1967, *Science* **153**, 1669.
Bridge, H. S. *et al.*: 1974, *Science* **183**, 1293.
Brinton, H. C. *et al.*: 1979, *Bull. Am. Astron. Soc.* **11**, 538.

Broadfoot, A. L., Kumar, S., Belton, M. J. S., and McElroy, M. B.: 1974, *Science* **183**, 1315.
Brown, R. A. and Goody, R. M.: 1978, *Icarus* **35**, 189.
Burangulov, N. I. *et al.*: 1974, *Gynamics of the Venus Atmosphere*, Nauka, Leningrad (Russian).
Camezon, A. G. W.: 1963, *Icarus* **2**, 249.
Chalikov, D. V. *et al.*: 1975, *Icarus* **26**, 178.
Chamberlain, J. W.: 1970, *Astrophys. J.* **159**,
Chamberlain, J. W.: 1975, *Astrophys. J.* **195**, 815.
Chamberlain, J. W. and Kuiper, G. P.: 1956, *Astrophys. J.* **124**,
Chamberlain, J. W. and Smith, C. R.: 1970, *Astrophys. J.* **160**, 755.
Chandrasekhar, S.: 1950, *Radiative Transfer*, Oxford University Press.
Chase, S. C., Kaplan, L. D., and Neugebaurer, G.: 1963, *J. Geophys. Res.* **68**, 6157.
Chase, S. C., Miner, E. D., and Morrison, D. *et al.*: 1974, *Science* **183**, 1291.
Chen, R. H. and Nagy, A. F.: 1978, *J. Geophys. Res.* **83**, 1133.
Cheremukhina *et al.*: 1974, *Kosmich. Issled.* **12**, 264 (Russian).
Chub, E. V. and Yakovlev, O. I.: 1980, *Kosmich. Issled.* **18**, 435.
Clautier, P. A. and Daniel, R. E.: 1973, *Planetary Space Sci.* **21**, 463.
Clautier, P. A. and Daniel, R. E.: 1979, *Planetary Space Sci.* **27**, 1111.
Cochran, W. D., Trafton, L. M., and Macy, W. W. Jr.: 1977, *Astron. Astrophys.* **58**, 345.
Coffeen, D. L.: 1969, *Astron. J.* **74**, 446.
Coffeen, D. L.: 1971, in C. Sagar, T. C. Owen, and H. J. Smith (eds.), 'Planetary Atmospheres', *IAU Symp.* **40**, 84.
Coffeen, D. L. and Gehrels, T.: 1969, *Astron. J.* **74**, 433.
Coldwell, J.: 1972, *Icarus* **17**, 608.
Colin, L.: 1979a, *Science* **203**, 743; 1979b, *Science* **205**, 740.
Connes, P., Connes, J., Benedict, W. S., and Kaplan, L. D.: 1967, *Astrophys. J.* **147**, 1230.
Connes, P., Connes, J., Kaplan, L. D., and Benedict, W. S.: 1968, *Astrophys. J.* **152**, 731.
Connes, J., Connes, P., and Maillard, J. P.: 1969, *Atlas des Spectres dans le Proche Infrarouge de Venus, Mars, Jupiter et de Saturn*, CNRS, Paris.
Connes, P. and Michel, G.: 1975, *Appl. Opt.* **14**, 2067.
Connes, P., Noxon, J. F., Traub, W. A., and Carlton, N. P.: 1979, *Astrophys. J.* **233**, L29.
Counselman III, C. C. *et al.*: 1979a, *Science* **203**, 805.
Counselman III, C. C. *et al.*: 1979b, *Science* **205**, 85.
Counselman III, C. C., Gourevitch, S. A., King, R. W., Loriot, G. B., and Ginsberg, E. S.: 1980, *J. Geophys. Res.* **85**, 8026.
Cruikchank, D. P.: 1967, *Comm. Lun. Planet. Lab.* **6**, 199.
Cruikshank, D. P. and Sill, G. T.: 1967, *Comm. Lun. Planet. Lab.* **6**, 204.
Danielson, R. E., Moore, D. R., and van de Hulst, H. C.: 1969, *J. Atm. Sci.* **26**, 1078.
Danjon, A.: 1949, *Bull. Astron.* **14**, 315.
Del Genio *et al.*: 1979, *Icarus* **39**, 401.
Devaux, C., Herman, M., and Lenoble, J.: 1975, *J. Atm. Sci.* **32**, 1177.
Dickinson, R. E.: 1971, *J. Atm. Sci.* **28**, 885.
Dickinson, R. E.: 1973, *J. Atm. Sci.* **30**, 296.
Dickinson, R. E.: 1976, *Icarus* **27**, 479.
Dickinson, R. E. and Ridley, E. C.: 1977, *Icarus* **30**, 163.
Diner, D. J., Westphal, J. A., and Schoerb, F. P.: 1976, *Icarus* **27**, 191.
Diner, D. J. and Westphal, J. A.: 1979a, *Icarus* **36**, 119.
Diner, D. J. and Westphal, J. A.: 1979b, *Icarus* **38**, 81.
Dolginov, Sh. Sh., Eroshenko, E. G., and Zhuzgov: 1968, *Kosmich. Issled.* **6**, 561.
Dolginov, Sh. Sh. *et al.*: 1978, *Kosmich. Issled.* **16**, 827.
Dollfus, A.: 1961a, in G. P. Kuiper and B. M. Middlhurst (eds.), *Planets and Satellites*, Univ. of Chicago Press.
Dollfus, A.: 1961b, in G. P. Kuiper and B. M. Middlhurst (eds.), *Planets and Satellites*, Univ. of Chicago Press.
Dollfus, A.: 1963, *Compt. Rend. Acad. Sci.* **256**, 3250.
Dollfus, A.: 1972, *Icarus* **17**, 104.
Dollfus, A.: 1975, *J. Atm. Sci.* **32**, 1060.

Dollfus, A. and Coffeen, D. L.: 1970, *Astron. Astrophys.* **8**, 251.
Dollfus, A. *et al.*: 1975, *Icarus* **26**, 53.
Donahue, T. M.: 1968, *J. Atm. Sci.* **25**, 568.
Donahue, T. M.: 1971, *J. Atm. Sci.* **28**, 895.
Dubinin, E. M. *et al.*: 1978, *Kosmich. Issled.* **16**, 870 (Russian).
Dubinin, E. M. *et al.*: 1980, *Pis'ma v Astron. Zh.* **6**, 253 (Russian).
Ekonomov, A. P., Golovin, Yu. M., and Moshkin, B. E.: 1978, *Kosmich. Issled.* **16**, 901 (Russian).
Ekonomov, A. P., Moshkin, B. E., Golovin, Yu. M., Parfent'ev, N. A., and San'ko, N. F.: 1979, *Kosmich. Issled.* **17**, 714 (Russian).
Elson, L. S.: 1979, *Geophys. Res. Let.* **6**, 720.
Evans, D. C.: 1966, NASA Goddard Space Flight Center Report X-613-66-72.
Fehsenfeld, F. C., Dunkin, D. B., and Ferguson, E. E.: 1970, *Planetary Space Sci.* **18**, 1267.
Fels, S. and Lindzen, R.: 1975, *Geophys. Fluid Dyn.* **6**, 149.
Fesenkov, V. G.: 1967, *Trudy Astrofiz. Inst. Akad. Nauk Kazakhskoj SSR* **9**, 109.
Fink, U., Larson, H. P., Kuiper, G. P., and Poppen, R. F.: 1972, *Icarus* **17**, 617.
Fjeldbo, G., Kliore, A. J., and Eshleman, V. R.: 1971, *Astron. J.* **76**, 123.
Fjeldbo, G., Seidel, B., and Sweetnam, D.: 1975, *J. Atm. Sci.* **32**, 1232.
Florensky, K. P. *et al.*: 1976, *Geokhimiya*, **N.8**, 1135.
Florensky, K. P. *et al.*: 1978, *Icarus* **33**, 537.
Galtzev, A. P. and Safraj, A. C.: 1980, *Kosmich. Issled.* **18**, 464 (Russian).
Gehrels, T. and Samuelsen, R. E.: 1961, *Astrophys. J.* **134**, 1022.
Gel'man, B. G., Zolotukhin, V. G., and Lamonov, N. I. *et al.*: 1979, *Kosmich. Issled.* **17**, 708 (Russian).
Gierash, P.: 1975, *J. Atm. Sci.* **32**, 1038.
Gillet, F. C., Low, F. J., and Stein, W. A.: 1968, *J. Atm. Sci.* **25**, 594.
Ginzburg, A. S. and Feigel'son, E. M.: 1969, *Kosmich. Issled.* **7**, 256 (Russian).
Glushneva, I. N.: 1964, *Astron. J.* **41**, 72 (Russian).
Glushneva, I. N.: 1969, *Astron. Zh.* **46**, 211 (Russian).
Gnedykh, V. I., Zhegulev, V. S., and Zasova, L. V. *et al.*: 1976, *Kosmich. Issled.* **14**, 758.
Gold, T.: 1964, in P. Brancazio and Cameron A. G. W. (eds.), *The Origin and Evolution of Atmospheres and Oceans*, Wiley, New York, p. 86.
Gold, T. and Soter, S.: 1971, *Icarus* **14**, 16.
Golitsyn, G.: 1970a, *Dokl. Akad. Nauk SSSR*, **190**, 323.
Golitsyn, G.: 1970b, *Icarus* **13**, 1.
Golitsyn, G. S.: 1973, *Introduction in Dynamics of Planetary Atmospheres*, Gidrometeoizdat, Leningrad (Russian).
Golitsyn, G. S.: 1978, *Kosmich. Issled.* **16**, 156 (Russian).
Golovin, Yu. M.: 1980, *Kosmich. Issled.* **17**, 471 (Russian).
Gombosi, T. *et al.*: 1979, *Geophys. Res. Letters* **6**, 349.
Gombosi, T. I., Gravens, T. E., Nagy, A. F., and Russell, C. T.: 1980, *J. Geophys. Res.*, in press.
Goody, R.: 1965, *J. Geophys. Res.* **70**, 5471.
Goody, R. M. and Robinson, A. R.: 1966, *Astrophys. J.* **146**, 339.
Gravens, T. E., Nagy, A. F., Chen, R. H., and Stewart, A. I.: 1978, *Geophys. Res. Letters* **5**, 613.
Gravens, T. E. *et al.*: 1979, *Geophys. Res. Letters* **6**, 341.
Gravens, T. E. *et al.*: 1980, *J. Geophys. Res.* **85**, 778.
Gray, L. D.: 1969, *Icarus* **10**, 90.
Gray, L. D. and Schorn, R. A.: 1968, *Icarus* **8**, 400.
Gray, L. D. and Schorn, R. A.: 1969, *AO* **8**, 2087.
Grechnev, K. V., Istomin, V. G., Ozerov, L. N., and Klimovitskij, V. G.: 1979, *Kosmich. Issled.* **17**, 697 (Russian).
ingauz, K. I., Bezrukikh, V. V., Musatov, L. S., and Breus, T. K.: 1968, *Kosmich. Issled.* **6**, 411 (Russian).
Gringauz, K. I., Bezrukikh, V. V., Volkov, G. I., Musatov, L. S., and Breus, T. K.: 1970, *Kosmich. Issled.* **8**, 431 (Russian).
Gringauz, K. I. *et al.*: 1976, *Kosmich. Issled.* **14**, 839 (Russian).
Gringauz, K. I., Verigin, M. J., Breus, T. K., and Gombosi, T.: 1979, *J. Geophys. Res.* **84**, 2123.
Guinot, B.: 1965, *Compt. Rend. Acad. Sci.* **260**, 431.

Guinot, B. and Feissel, M.: 1968, *J. Observateurs* **51**, 13.
Hanel, R., Forman, M., Stambach, G., and Meilleur, T.: 1968, *J. Atm. Sci.* **25**, 586.
Hanel, R. A., Kunde, V. G., Meilleur, T., and Stambach, G.: 1971, in C. Sagan, T. C. Owen, and H. J. Smith (eds.), 'Planetary Atmospheres', *IAU Symp.* **40**, 44.
Hansen, J. E.: 1969, *Astrophys. J.* **158**, 337.
Hansen, J. E. and Hovenier, J. W.: 1974, *J. Atm. Sci.* **31**, 1137.
Hansen and Matzushima: 1967, *Astrophys. J.* **150**, 1139.
Hansen, J. E. and Travis, L. D.: 1974, *Space Sci. Rev.* **16**, 527.
Hapke, B.: 1976, *J. Astronaut. Sci.* **33**, 1803.
Hapke, B. and Nelson, R.: 1975, *J. Atmos. Sci.* **32**, 1212.
Harris, D. L.: 1961, in G. P. Kuipez and B. M. Middlehurst (eds.), *Planets and Satellites*, Univ. Chicago Press.
Herman, M., Devaux, C., and Dollfus, A.: 1979, *Icarus* **37**, 282.
Hetz, A. L., Johnson, M. A., McLahren, R. A., and Sutton, E. C.: 1976, *Astrophys. J.* **208**, L141.
Hoffman, J. F. *et al.*: 1977, *Space Sci. Rev.* **20**, 307.
Hoffman, J. H., Hodges, R. R. Jr., and McElroy, M. B.: 1979a, *Science* **203**, 800.
Hoffman, J. H., Hodges, R. R. Jr., McElroy, M. B., and Donahue, T. M., Kolpin, M.: 1979b, *Science* **205**, 49.
Hoffman, J. H. *et al.*: 1980a, *J. Geophys. Res.* **85**, 7882.
Hoffman, J. H., Oyama, V. I., and von Zahn, U.: 1980b, *J. Geophys. Res.* **85**, 7881.
Holland, H. D.: 1964, in P. Brancazio and Cameron A. G. W. (eds.), *Origin and Evolution of Atmospheres and Oceans*, Wiley, New York, p. 86.
Howard *et al.*: 1974, *Science* **183**, 1297.
Hoyle, F.: 1965, *Frontiers of Astronomy*, New York, 1965.
Hunt, G. E.: 1971, *J. Quant. Spectr. Radiative Transfer* **11**, 655.
Hunten, D. *et al.*: 1977, *Sp. Sci. Res.* **20**, 265.
Ingersoll, P. and Orton, G. S.: 1974, *Icarus* **21**, 121.
Intrilligator, D. S. *et al.*: 1979, *Science* **205**, 116.
Irvine, W. M.: 1968, *J. Atmos. Sci.* **25**, 610.
Irvine, W. M.: 1975, *Icarus* **25**, 175.
Istomin, V. G., Grechnev, K. V., and Kochnev, V. A.: 1979a, *Pis'ma v Astron. Zh.* **5**, 211 (Russian).
Istomin, V. G., Grechnev, K. V., Kochnev, V. A., and Ozerov, L. N.: 1979b, *Kosmich. Issled.* **17**, 703.
Istomin, V. G., Grechnev, K. V., and Kochnev, V. A.: 1980, Preprint D-298 of Space Res. Inst. of Academy of Sciences of USSR, Moscow.
Izakov, M. N.: 1978, *Kosmich. Issled.* **16**, 403.
Izakov, M. N.: 1979, *Kosmich. Issled.* **17**, 602.
Izakov, M. N.: 1980, *Kosmich. Issled.* **18**, 918.
Izakov, M. N. and Morozov, S. K.: 1975, *Kosmich. Issled.* **13**, 404 (Russian).
Izakov, M. N. *et al.*: 1981, *Kosmich. Issled.* **19** (in press).
Jenkins, E. B., Morton, D. C., and Sweigart, A. V.: 1968, 'Rocket Spectra of Venus and Jupiter from 2000 to 3000 Å' (preprint).
Johnson, M. A. *et al.*: 1976, *Astrophys. J.* **208**, L145.
Johnson, F. S. and Hanson, W. B.: 1979, *Geoph. Res. Let.* **6**, 581.
Kalnay de Rivas, E.: 1973, *J. Atm. Sci.* **32**, 1017.
Kalnay de Rivas, E.: 1975, *J. Atm. Sci.* **32**, 1017.
Kattawar, G. W. and Young, L. D. G.: 1977, *Icarus* **30**, 179.
Kattawar, G. W.: 1979, *Icarus* **40**, 60.
Kawabata, K. and Hansen, J. E.: 1975, *J. Atm. Sci.* **32**, 1133.
Kawabata *et al.*: 1980, *J. Geophys. Res.* **85**, No. A13.
Keating, G. M. *et al.*: 1979a, *Science* **203**, 772.
Keating, G. M. *et al.*: 1979b, *Science* **205**, 62.
Kerzhanovich, V. V. *et al.*: 1969, *Kosmich. Issled.* **7**, 592 (Russian).
Kerzhanovich, V. V., Andreev, B. N., and Gotlib, V. M.: 1971, *Kosmich. Issled.* **10**, 261.
Kerzhanovich, V. V., Marov, M. Ya., and Rozhdestvensky, M. K.: 1972, *Icarus* **17**, 659.
Kerzhanovitch, V. V. and Marov, M. Ya.: 1974, *Dokl. Acad. Nauk SSSR* **215**, 554 (Russian).
Kerzhanovich, V. V. and Marov, M. Ya.: 1977, *Icarus* **30**, 320.

Kerzhanovich, V. V. *et al.*: 1979, *Kosmich. Issled.* **17**, 690 (Russian).
Khodakovsky *et al.*: 1978, *Geokhimiya* **12**, 1821.
Khodakovsky *et al.*: 1979, *Icarus* **39**, 352.
Khodakovsky *et al.*: 1979, *Geokhimiya* **12**, 1747.
Kliore, A. J.: 1979a, *Science* **203**, 765.
Kliore, A. J.: 1979b, *Science* **205**, 99.
Kliore, A. J., Levy, G. S., Cain, D. L., Fjeldbo, G., and Rasool, S. I.: 1967, *Science* **158**, 1683.
Kliore, A. J. and Cain, D. L.: 1968, *J. Atm. Sci.* **25**, 549.
Kliore, A. J. *et al.*: 1979, *Icarus* **37**, 51.
Kliore, A. J. and Patel, I. R.: 1980, *J. Geophys. Res.* **85**, No. A13.
Knollenbegr, R. G. and Hunten, D. M.: 1979a, *Science* **203**, 792.
Knollenberg, R. G. and Hunten, D. M.: 1979b, *Science* **205**, 70.
Knollenberg, R. G. and Hunten, D. M.: 1980, *J. Geophys. Res.* **85**, 8039.
Knuckles, C. F., Sinton, M. K., and Sinton, W. M.: 1961, *Lovell Obs. Bull.* **5**, 153.
Knudsen, W. C.: 1979a, *Science* **203**, 757.
Knudsen, W. C.: 1979b, *Science* **205**, 107.
Kolosov, M. A. *et al.*: 1970, *Kosmich. Issled.* **8**, 882 (Russian).
Kolosov, M. A. *et al.*: 1978, *Kosmich. Issled.* **16**, 278 (Russian).
Kondrat'ev, K. Ya. and Moskalenko, N. I.: 1977, *Teplovoje Izluchenije Planet*, Gidrometeoizdat, Leningrad (Russian).
Kondrat'ev, K. Ya. and Timofeev, Yu. M.: 1978, *Meteorologycheskoje Zondirovanije Atmosfery iz Kosmosa*, Gidrometeoizdat, Leningrad (Russian).
Kozyrev, N. A.: 1954, *Izvestiya Krymskoj Astrofizicheskoy obse vatorii* **12**, 169.
Krasnopolsky, V. A.: 1979a, 'Venera-9, 10: Spectroscopy of Scattered Radiation in Overcloud Atmosphere', preprint of Space Res. Institute No. 523, Moscow.
Krasnopolsky, V. A.: 1979b, *Planetary Space Sci.* **27**, 1403.
Krasnopolsky, V. A. *et al.*: 1976, *Kosmich. Issled.* **14**, 789 (Russian).
Krasnopolsky, V. A. and Parshev, V. A.: 1979, *Kosmich. Issled.* **17**, 763.
Krasnopolsky, V. A. and Parshev, V. A.: 1980a, 'Initial Data for Calculation of Venus Atmospheric Photohemistry at Heights Down to 50 km', preprint Pr-590 of Space Res. Institute of Academy of Sciences of U.S.S.R., Moscow.
Krasnopolsky, V. A. and Parshev, V. A.: 1980b, 'Initial Data for Calculation of Venus Atmospheric Photochemistry at Heights Down to 50 km', preprint Pr-591 of Space Res. Institute of Academy of Sciences of U.S.S.R., Moscow.
Krasnopolsky, V. A. and Tomashova, G. V.: 1980, *Kosmich. Issled.* **18**, 766.
Ksanfomality, L. V.: 1977, *Astron. Zh.* **54**, 1110 (Russian).
Ksanfomality, L. V.: 1978, *Kosmich. Issled.* **16**, 422 (Russian).
Ksanfomality, L. V.: 1979a, *Kosmich. Issled.* **14**, 747 (Russian).
Ksanfomality, L. V.: 1979b, *Kosmich. Issled.* **17**, 597 (Russian).
Ksanfomality, L. V.: 1980, *Icarus* **41**, 36.
Ksanfomality, L. V.: 1980, *Nature* **284**, 213.
Ksanfomality, L. V., Dedova, E. B., and Obukhova, L. F. *et al.*: 1976a, *Kosmich. Issled.* **14**, 768 (Russian).
Ksanfomality, L. V. *et al.*: 1976b, *Kosmich. Issled.* **14**, 797 (Russian).
Ksanfomality, L. V. *et al.*: 1977, *Astron. Zh.* **54**, 1110 (Russian).
Ksanfomality, L. V. and Petrova, E. V.: 1978, *Kosmich. Issled.* **15**, 886 (Russian).
Ksanfomality, L. V. and Selivanov, A. S.: 1978, *Kosmich. Issled.* **15**, 959 (Russian).
Ksanfomality, L. V. *et al.*: 1979, *Pis'ma v Astron. Zh.* **5**, 222 (Russian).
Kuiper, G. P.: 1962, *Comm. Lunar Planet. Lab.* **1**, 83.
Kuiper, G. P.: 1969, *Comm. Lunar Planet. Lab.* **6**, 229.
Kumaz, S. *et al.*: 1978, *Planetary Space Sci.* **26**, 1063.
Kunde, V. G., Hanel, R. A., and Herath, L. W.: 1977, *Icarus* **32**, 210.
Kurt, V. G. *et al.*: 1968, *J. Atm. Sci.* **25**, 668.
Kurt, V. G., Moroz, V. I.: 1968, *Kosmich. Issled.* **6**, 577 (Russian).
Kurt, V. G., Romanova, N. N., Smirnov, A. S., Berto, J. L., and Blamon, J. E.: 1979, *Kosmich. Issled.* **5**, 772 (Russian).
Kuzmin, A. D. and Marov, M. Ya.: 1974, *Fizika Planety Venera*, M., Nauka (Russian).

Lacis: 1975, *J. Atm. Sci.* **32**, 1107.
Landau, R.: 1975, *J. Atm. Sci.* **32**, 1157.
Lawrence, G. M., Barth, C. A., and Argabright, V.: 1977, *Science* **195**, 573.
Leovy, C.: 1973, *J. Atm. Sci.* **30**, 1218.
Lestrade, J. P.-: 1979, *Icarus* **39**, 418.
Lewis, J. S.: 1968, *Icarus* **8**, 434.
Lewis, J. S.: 1968, *Astrophys. J.* **152**, 79.
Lewis, J. S.: 1969, *Icarus* **11**, 367.
Lewis, J. S.: 1970, *Earth Planetary Sci. Letters* **10**, 73.
Lewis, J. S.: 1971, *Nature* **230**, 295.
Lewis, J. S. and Kreimendahl, F. A.: 1980, *Icarus* **42**, 330.
Limaye, S. and Suomi, V.: 1977, *J. Atm. Sci.* **34**, 205.
Lindzen, R.: 1973, *Boundary Layer Meteorol.* **4**, 327.
Link, F.: 1969, *Eclipse Phenomena in Astronomy*, Springer-Verlag, Berlin, Heidelberg, New York.
Liu, S. C. and Donahue, T. M.: 1975, *Icarus* **24**, 148.
Logan *et al.*: 1974, AFCRL-TR-74-0573.
Macy, W. Jr. *et al.*: 1977, *Icarus* **32**, 27.
Marov, M. Ya.: 1972, *Icarus* **16**, 415.
Marov, M. Ya., Avduevsky, V. S., and Kerzhanovich, V. V. *et al.*: 1973, *Dokl. Acad. Nauk SSSR* **210**, 559 (Russian).
Marov, M. Ya. and Ryabov, O. L.: 1974, 'Model Atmosfery Venera', Preprint No. 112, IPM AN SSSR, Moscow (Russian).
Marov, M. Ya., Byvshev, B. V., and Manujlov, K. N. *et al.*: 1976, *Kosmich. Issled.* **14**, 729 (Russian).
Marov, M. Ya., Lystsev, V. E., and Lebedev, V. N.: 1978, 'Structure and Microphysical Properties of Venussian Clouds', preprint N.144 of the Applied Mathematical Institute (Russian).
Marov, M. Ya., Byvshev, B. V., and Baranov, Yu. P. *et al.*: 1979, *Kosmich. Issled.* **17**, 743 (Russian).
Martonchik, J. and Beer, R.: 1975, *J. Atm. Sci.* **32**, 1151.
Mauersberger, K. *et al.*: 1979, *Geophys. Res. Let.* **6**, 671.
Mayer, C. H., McCullough, T. P., and Seoanaker, R. M.: 1958, *Astrophys. J.* **127**, 1.
Mayr, H. G. *et al.*: 1978, *J. Geophys. Res.* **83**, 4411.
McElroy, M. B., Sze, N. D. and Young, Y. L.: 1973, *J. Atm. Sci.* **30**, 1437.
Mikhnevich, V. V. and Sokolov, V. A.: 1969, *Kosmich. Issled.* **2**, 220 (Russian).
Mintz, Y.: 1961, in W. W. Kellog and C. Sagan (eds.), *The Atmosphere of Mars and Venus*, Washington, D.C.
Moroz, V. I.: 1963, *Astron. Zh.* **40**, 144 (Russian).
Moroz, V. I.: 1964, *Astron. Zh.* **41**, 711 (Russian).
Moroz, V. I.: 1967, *Fizika Planet*, M., Nauka (Russian).
Moroz, V. I.: 1971a, *Nature* **231**, 36.
Moroz, V. I.: 1971b, *Uspekhi Fiz. Nauk* **104**, 255 (Russian).
Moroz, V. I.: 1973, 'Rabochaya Model Atmosfery venery', Preprint N.162, IKI AN SSSR, Moscow (Russian).
Moroz, V. I.: 1976, *Kosmich. Issled.* **14**, 691 (Russian).
Moroz, V. I.: 1978, *Fizika Planety Mars*, Moscow, Nauka (Russian).
Moroz, V. I., Davydov, V. D., and Zhegulev, V. S.: 1969, *Astron. Zh.* **46**, 136.
Moroz, V. I., Vasilchenko, N. V., Danilyants, L. B., and Kaufman, S. A.: 1968, *Astron. Zh.* **45**, 189 (Russian).
Moroz, V. I., Parfent'ev, N. A., and San'ko, N. F. *et al.*: 1976, *Kosmich. Issled.* **14**, 743 (Russian).
Moroz, V. I. and Mukhin, L. M.: 1977, *Kosmich. Issled.* **15**, 901 (Russian).
Moroz, V. I., Moshkin, B. E., and Ekonomov, A. P. *et al.*: 1979a, *Pis'ma v Astron. Zh.* **5**, 222 (Russian).
Moroz, V. I., Parfent'ev, N. A., and San'ko, N. F.: 1979b, *Kosmich. Issled.* **17**, 727 (Russian).
Moroz, V. I. *et al.*: 1980, *Nature* **284**, 243.
Morozhenko, A. V. and Yanovitskij, E. G.: 1973, *Icarus* **18**, 583.
Morrison, D.: 1976, *Icarus* **28**, 423.
Mueller, R. F.: 1963, *Science* **141**, 1046.
Mueller, R. F.: 1964, *Icarus* **3**, 285.
Mueller, R. F.: *Icarus* **4**, 506, 1965.

Mueller, R. F.: *Nature* **220**, 55, 1968.
Mueller, R. F. and Kridebaugh, J.: 1973, *Icarus* **19**, 531.
Mukai, S. and Mukai, T.: 1979, *Icarus* **38**, 90.
Müller, G.: 1893, Publs. *Potsdam Astrophys. Observ.* **8**, 326.
Murray, B. C., Wildey, R. L., and Westphal, J. A.: 1963, *J. Geophys. Res.* **68**, 4813.
Murray, B. C., Belton, M. S., and Danielson, G. E. *et al.*: 1974, *Science* **183**, 1307.
Nagy, A. F. *et al.*: 1979, *Science* **205**, 106.
Nagy, A. F. *et al.*: 1980, *J. Geophys. Res.* **85**, No. A13.
Ness, N. F. *et al.*: 1974, *Science* **183**, 1301.
Newkirk, C. G.: 1959, *Planetary Space Sci.* **1**, 32.
Newman, W. I.: 1975, *Icarus* **26**, 451.
Niemann, H. B. *et al.*: 1979a, *Science* **203**, 770.
Niemann, H. B. *et al.*: 1979b, *Science* **205**, 54.
Niemann, H. B. *et al.*: 1980, *J. Geophys. Res.* **85**, 7817.
Nikander, J. and Boyer, Ch.: 1970, *Nature* **222**, 477.
O'Leary, B.: 1975, *J. Atm. Sci.* **32**, 1091.
Öpik, E. J.: 1961, *J. Geophys. Res.* **66**, 2807.
Ostriker, J. P.: 1963, *Astrophys. J.* **138**, 281.
Owen, T. C.: 1962, *Comm. Lunar Planet. Obs.* **1**, 29.
Owen, T. and Sagan, C.: 1972, *Icarus* **16**, 557.
Oyama, V. I., Carle, G. C., and Woeller, F.: 1979a, *Science* **203**, 802.
Oyama, V. I. *et al.*: 1979b, *Science* **205**, 52.
Oyama, V. I. *et al.*: 1980, *J. Geophys. Res.* **85**, 7891.
Palmer, K. F. and Williams, D.: 1975, *Appl. Opt.* **14**, 208.
Pechman, J. B. *et al.*: 1979, *Nature* **279**, 618.
Petrova, E. V.: 1979, *Kosmich. Issled.* **16**, 146 (Russian).
Pettengill, G. H. *et al.*: 1980, *J. Geophys. Res.* **85**, 8260.
Pettit, E.: 1961, '*Planets and Satellites*', in G. P. Kuipez and B. M. Middlehurst (eds.), Univ. Chicago Press.
Pettit, E. and Nickolson, S. B.: 1924, *Pop. Astron.* **32**, 614.
Pollack, J. B.: 1971, *Icarus* **14**, 295.
Pollack, J. B. and Sagan, C.: 1965, *J. Geophys. Res.* **70**, 4403.
Pollack, J. B. and Ohring, G.: 1973, *Icarus* **19**, 34.
Pollack, J. B. *et al.*: 1974, *Icarus* **23**, 8.
Pollack, J. B. and Young, R. E.: 1975, *J. Atm. Sci.* **32**, 1025.
Pollack, J. B. *et al.*: 1975, *J. Atm. Sci.* **32**, 1140.
Pollack, J. B. *et al.*: 1978, *Icarus* **34**, 28.
Pollack, J. B.: 1979, *Icarus* **37**, 479.
Pollack, J. B. and Black, D. C.: 1979, *Science* **205**, 56.
Pollack, J. B. *et al.*: 1979, *Science* **205**, 76.
Pollack, J. B. *et al.*: 1980, *J. Geophys. Res.* **85**, 8191.
Polozhentseva, T. A.: 1964, *Izv. Glav. Astron. Obs., Pulkovo* **23** (5), 74.
Potter, F. J.: 1972, *Icarus* **17**, 79.
Prinn, R. G.: 1971, *J. Atm. Sci.* **28**, 1058.
Prinn, R. G.: 1973, *Science* **182**, 1132.
Prinn, R. G.: 1975, *J. Atm. Sci.* **32**, 1237.
Prinn, R. G.: 1979, *Geophys. Res. Letters* **6**, 807.
Prokof'ev, V. K.: 1965, *Izvestiya Krymskoy Astr. Obs.* **34**, 243; 1967, **37**, 3 (Russian).
Prokof'ev, V. K. and Petrova, N. N.: 1963, *Izvestiya Krymskoy Astr. Obs.* **29**, 3.
Ragent, B. and Blamont, J.: 1979, *Science* **203**, 790.
Ragent, B. and Blamont, J.: 1980, *J. Geophys. Res.* **85**, 8089.
Rasool, S. I. and de Bergh, C.: 1970, *Nature* **226**, 1037.
Reed *et al.*: 1978, *Icarus* **33**, 554.
Regas *et al.*: 1975, *Icarus* **24**, 11.
Richardson, R. S.: 1956, *Publ. Astron. Soc. Pacific*, **70**, 251.
Robinson, A. R.: 1970, Paper Presented in IV Arizona Conference, March 2–4, Tucson, 1970.

Ross, F. E.: 1928, *Astrophys. J.* **68**, 57.
Rozenberg, G. V.: 1964, *Dokl. Akad. Nauk SSSR* **145**, 775 (Russian).
Russell, C. T. *et al.*: 1979a, *Science* **203**, 745.
Russell, C. T. and Elphic, R. C.: 1979, *Nature* **279**, 614.
Russell, C. T. and Elphic, R. C.: 1979, *Nature* **279**, 616.
Sagan, C.: 1960, *Astron. J.* **65**, 332.
Sagan, C.: 1962, *Icarus* **1**, 151.
Sagan, C.: 1969, *Icarus* **10**, 290.
Sagan, C.: 1971, in C. Sagan, T. C. Owen, and H. J. Smith (eds.), 'Planetary Atmospheres', *IAU Symp.* **40**.
Samuelson, R. E. and Hanel, R. A. *et al.*: 1975, *Icarus* **25**, 49.
San'ko, N. F.: 1980, *Kosmich. Issled.* **18**, 600 (Russian).
Sasamori, T.: 1971, *J. Atm. Sci.* **28**, 1045.
Sato, M. Kawabata, K. and Hansen, J. E.: 1977, *Astrophys. J.* **216**, 947.
Scarf, F. L. *et al.*: 1979, *Science* **203**, 748.
Schorn, R. A. and Shawl, S.: 1966, *Astrophys. J.* **146**, 328.
Schorn, R. A., Barker, E. S., Grey, L. D., and Moore, R. C.: 1969a, *Icarus* **10**, 98.
Schorn, R. A., Grey, L. D., and Barker, E. S.: 1969b, *Icarus* **10**, 241.
Schorn, R. A., Young, L. D. G., and Barker, E. S.: 1971, *Icarus* **14**, 21.
Schorn, R. A. *et al.*: 1975, *Icarus* **25**, 64.
Schorn, R. A. J. *et al.*: 1979, *Icarus* **38**, 420.
Schubert, G. and Whitehead, J. A.: 1969, *Science* **163**, 71.
Schubert, G. *et al.*: 1977, *Space Sci. Rev.* **20**, 357.
Schubert, G. *et al.*: 1980, *J. Geophys. Res.* **85**, 8007.
Scott, A. H. and Resse, E. J.: 1972, *Icarus* **17**, 589.
Seiff, A. *et al.*: 1979a, *Science* **203**, 787.
Seiff, A. *et al.*: 1979b, *Science* **205**, 46.
Seiff, A. *et al.*: 1980, *J. Geophys. Res.* **85**, 7903.
Selivanov, A. S. *et al.*: 1978, *Kosmich. Issled.* **16**, 877 (Russian).
Serkowsky, K., Frecker, J. E., Heacox, W. P., Ken Knight, C. E., and Roland, E. H.: 1979, *Astrophys. J.* **228**, 630.
Shapiro, I. I., Campbell, D. B., and De Campli, W. M.: 1979a, *Astrophys. J.* **230**, L123.
Shapiro, I. I. *et al.*: 1979b, *Science* **203**, 775.
Shari, V. P.: 1975, 'Mathematical Simulation of Heat Radiative Transfer in the Low Atmosphere of Venus', preprint No. 34 of Applied Math. Inst. of Acad. of Sci. U.S.S.R. (Russian).
Shari, V. P.: 1976, *Kosmich. Issled.* **14**, 97 (Russian).
Sharonov, V. V.: 1965, *Planeta Veneza*, M., Nauka (Russian).
Shutko, A. M.: 1978, *Radiophysical Studies of Planets*, Moscow (Russian).
Sidi, S.: 1976, *Icarus* **28**, 359.
Sill, G. T.: 1972, *Comm. Lunar Planet. Lab.* **9**, 191.
Sill, G. T.: 1975, *J. Atm. Sci.* **32**, 1201.
Sinton, W. M.: 1961, in G. P. Kuiper and B. M. Middlehurst (eds.). *Planets and Satellites*, Univ. Chicago Press.
Sinton, W. M.: 1963, *Mem. Soc. Roy. Sci. Liege* **7**, 300.
Sinton, W. M. and Strong, J.: 1960, *Astrophys. J.* **131**, 470.
Smith, B. A.: 1967, *Science* **158**, 114.
Smirnova, T. V. and Kuzmin, A. D.: 1974, *Astron. Zh.* **51**, N. 3 (Russian).
Sobolev, V. V.: 1944, *Astron. Zh.* **41**, 97 (Russian).
Sobolev, V. V.: 1956, *Perenoss Luchistoj Energii v Atmosferakh Zvezd i Planet*, Gos. izdat. tekh.-teor. lit., Moskwa.
Sobolev, V. V.: 1968, *Astron. Zh.* **45**, 169 (Russian).
Sobolev, V. V.: 1972, *Rasseyanie Sveta v Atmosferakh Planet*, Nauka, Moskwa (Russian).
Spinrad, H.: 1962, *Publ. Astron. Soc. Pacific* **74**, 187.
Spinrad, H. and Shawl, S. J.: 1966, *Astrophys. J.* **146**, 328.
Stewart, A. I. *et al.*: 1979, *Science* **203**, 777.
Stewart, A. I. and Barth, C. A.: 1979, *Science* **205**, 59.

Stone, P.: 1968, *J. Atm. Sci.* **25**, 644.
Stone, P. H.: 1975, *J. Atm. Sci.* **32**, 1005.
Strelkov, G. M. and Kukharskaya, N. F.: 1969, *Kosmich. Issled.* **7**, 247.
Suomi, V.: 1974, in J. E. Hansen (ed.), *The Atmosphere of Venus*, p. 42.
Suomi, V. E., Sromovsky, L. A., and Revercomb, H. E.: 1979, *Science* **205**, 83.
Suomi, V. E., Sromovsky, L. A., and Revercomb, H. E.: 1980, *J. Geophys. Res.* **85**, 8200.
Surkov, Yu. A., Andrejchikov, B. M., and Kalinkina, O. M.: 1973, *Dokl. Akad. Nauk SSSR* **213**, 296.
Surkov, Yu. A. *et al.*: 1978, *Geokhimiya*, **4**, 506.
Surkov, Yu. A.: 1979a, *Pis'ma v Astron. Zh.* **5**, 7 (Russian).
Surkov, Yu. A.: 1979b, *COSPAR 22 Plenary Meeting*, (abstracts), p. 264.
Sze, N. D. and McElroy, M. B.: 1975, *Planetary Space Sci.* **23**, 763.
Taranova, O. G.: 1977, *Astron. Tsirkulyar* **950**, 1 (Russian).
Taylor, F. W.: 1975, *J. Atm. Sci.* **32**, 1101.
Taylor, F. W., Diner, D. J., and Elson, L. S. *et al.*: 1979a, *Science* **203**, 779.
Taylor, F. W., Diner, D. J., and Elson, L. S. *et al.*: 1979b, *Science* **205**, 67.
Taylor, F. W. *et al.*: 1979c, *Nature* **279**, 613.
Taylor, F. W. *et al.*: 1980, *J. Geophys. Res.* **85**, 7963.
Taylor, H. A. *et al.*: 1979a, *Science* **203**, 752.
Taylor, H. A. *et al.*: 1979b, *Science* **203**, 755.
Taylor, H. A.: 1979c, *Science* **205**, 96.
Taylor, H. A. *et al.*: 1980, *J. Geophys. Res.* **85**, 7759.
Taylor, W. W. L. *et al.*: 1979a, *Science* **205**, 112.
Taylor, W. W. L. *et al.*: 1979b, *Nature* **279**, 614.
Thompson, R.: 1970, *J. Atm. Sci.* **27**, 1107.
Timofeeva, T. S., Yakovlev, O. I., and Efimov, A. I.: 1978, *Kosmich. Issled.* **16**, 285 (Russian).
Timofeeva, T. S. *et al.*: 1980, *Kosmich. Issled.* **5**, 775.
Tomasko, M. G., Doose, L. R., and Palmer, J. *et al.*: 1979a, *Science* **203**, 797.
Tomasko, M. G., Doose, L. R., and Smith, P. H.: 1979b, *Science* **205**, 80.
Traub, W. A. and Carlton, N. P.: 1974, in A. Woszczyk and C. Iwaniszewska (eds.), 'Exploration of the Planetary System', *IAU Symp.* **65**, 223.
Traub, W. A. and Carlton, N. P.: 1975, *J. Atm. Sci.* **32**, 1060.
Traub, W. A. and Carlton, N. P.: 1979, *Astrophys. J.* **227**, 329.
Travis, L. D.: 1975, *J. Atm. Sci.* **32**, 1150.
Travis, L. D., Coffeen, D. L., and Hansen, J. E.: 1979a, *Science* **203**, 781.
Travis, L. D., Coffeen, D. L., and Del Genio, A. D.: 1979b, *Science* **205**, 74.
Urey, H. C.: 1952, *The Planets*, Yale Univ. Press, New Haven.
Ustinov, E. A. and Moroz, V. I.: 1978, *Kosmich. Issled.* **17** (Russian).
Vasin, V. G. and Marov, M. Ya.: 1977, 'About the Circulation Mechanism on Venus', preprint of Appl. Math. Inst. of Acad. Sci. U.S.S.R. N. 6 (Russian).
Vaisberg, O. L. *et al.*: 1976, *Kosmich. Issled.* **14**, 827 (Russian).
Vaucouleur, G. de and Menzel, D. H.: 1960, *Nature* **188**, 28.
Vinogradov, A. P., Surkov, Yu. A., Florensky, K. P., and Andrejchikov, B. M.: 1968a, *Dokl. Akad. Nauk SSSR* **179**, 37 (Russian).
Vinogradov, A. P., Surkov, Yu. A., and Florensky, C. P.: 1968b, *J. Atm. Sci.* **25**, 535.
Vinogradov, A. P., Surkov, Yu. A., and Andrejchikov, B. M.: 1970, *Kosmich. Issled.* **8**, 578 (Russian).
Vinogradov, A. P. and Volkov, V. P.: 1971, *Geopkhimiya* **7**, 755 (Russian).
Vukalowitch, M. P. and Altunin, V. V.: 1965, *Heat Properties of Carbon Dioxide*, Atomizdat, Moscow (Russian).
Wallace, L., Caldwell, J. J., and Savage, B. D.: 1972, *Astrophys. J.* **172**, 755.
Walker, J. C. G.: 1975, *J. Atm. Sci.* **32**, 1248.
Walker, R. C. and Sagan, C.: 1966, *Icarus* **5**, 105.
Watson, A. J. *et al.*: 1979, *Geophys. Res. Letters* **6**, 743.
Wattson, R.: 1968, *Astrophys. J.* **154**, 987.
Westphal, J. A.: 1971, in C. Sagan, T. C. Owen, and H. J. Smith (eds.), 'Planetary Atmospheres', *IAU Symp.* **40**, 48.
Westphal, J. A., Wildey, R. L., and Murray, B. C.: 1965, *Astrophys. J.* **142**, 799.

Wildt, R.: 1966, *Icarus* **5**, 24.
Whitcomb, S. E., Hildebrand, R. H., and Keen, J.: 1979, *Icarus* **38**, 75.
Wolf, R. S., Goldstein, B. E., and Kumar, S.: 1979, *Geophys. Res. Letters* **6**, 353.
Woo, R.: 1975, *J. Atm. Sci.* **32**, 1084.
Woo, R., Armstrong, J. W., and Kendall, W. B.: 1979, *Science* **205**, 87.
Yakovlev, O. I.: 1974, *Rasprostranenije radiovoln v solnechnoj sisteme*, Sovetckoe radio, Moscow (Russian).
Yakovlev, O. I. *et al.*: 1974, *Kosmich. Issled.* **12**, 100.
Yakovlev, O. I. *et al.*: 1976, *Kosmich. Issled.* **14**, 722 (Russian).
Yakovlev, O. I., Efimov, A. I., Matyugov, S. S., Timofeeva, T. S., Chub, E. V., and Yakovleva, G. D.: 1978, *Kosmich. Issled.* **16**, 112 (Russian).
Yanovitskij, E. G.: 1972, *Astron. Zh.* **49**, 845 (Russian).
Young, A. T.: 1973, *Icarus* **18**, 564.
Young, A. T.: 1975, *Icarus* **24**, 1.
Young, A. T.: 1977, *Icarus* **32**, 1.
Young, A. T. and Gray, L. D.: 1968, *Icarus* **9**, 74.
Young, A. T. and Kattawar, G. W.: 1978, *J. Atm. Sci.* **35**, 323.
Young, A. T. *et al.*: 1978, *Icarus* **34**, 46.
Young, A. T. *et al.*: 1979, *Icarus* **38**, 435.
Young, L. D. G.: 1969, *Icarus* **11**, 66.
Young, L. D. G.: 1970, *Icarus* **13**, 449.
Young, L. D. G.: 1972, *Icarus* **17**, 632.
Young, L. D. G., Schorn, R. A., Barker, E. S., and McElroy, M.: 1969, *Icarus* **11**, 390.
Young, L. D. G., Schorn, R. A. J., and Barker, E. S.: 1970a, *Icarus* **13**, 58.
Young, L. D. G., Schorn, R. A., and Smith, H. J.: 1970b, *Icarus* **13**, 74.
Young, L. D. G. and Young, A. T.: 1972, *Astrophys. J.* **176**, 533.
Young, L. D. G. *et al.*: 1975, *Icarus* **25**, 239.
Young, L. D. G. and Kattawar, G. W.: 1976, *Icarus* **29**, 483.
Young, L. D. G. and Kattawar, G. W.: 1977, *Icarus* **30**, 360.
Young, L. D. G. *et al.*: 1979, *Icarus* **30**, 559.
Young, R. E. and Schubert, G.: 1973, *Planetary Space Sci.* **21**, 1563.
Young, R. E. and Pollack, J. B.: 1977, *J. Atm. Sci.* **34**, 1315.
von Zahn, U. *et al.*: 1979a, *Science* **203**, 768.
von Zahn, U. *et al.*: 1979b, *Geophys. Res. Letters* **6**, 337.
von Zahn, U. *et al.*: 1980, *J. Geophys. Res.* **85**, 7829.
Zaitsev, A. V., Karyagin, V. P., and Kovtunenko, V. M. *et al.*: 1979, *Kosmich. Issled.* **17**, 646 (Russian).
Zelmanovich, I. L. and Shifran, K. S.: *Tablizy po Svetorasseyaniyu*, t. III, 'Koeffitsienty Ekstinktsii, Rasseyaniya i Luchevogo Davleniya', Gidrometeoizdat, Leningrad (Russian).